I. INVESTIGATION OF THE EFFECTS OF SURFACE TOPOGRAPHY UPON THE REACTION DYNAMICS OF POLYATOMIC SYSTEMS: THE

$$O_3 + NO \rightarrow O_2 + NO_2^+$$

REACTION

II. QUANTUM MECHANICAL STUDY OF ROTATIONALLY INELASTIC SCATTERING IN THE HF-Ar SYSTEM

By

RAJALAKSHMI VISWANATHAN

Bachelor of Science
University of Madras
Madras, India
1976

Master of Science
University of Madras
Madras, India
1978

Submitted to the Faculty of the Graduate College
of the Oklahoma State University
in partial fulfillment of the requirements
for the Degree of
DOCTOR OF PHILOSOPHY
December, 1981

I. INVESTIGATION OF THE EFFECTS OF SURFACE TOPOGRAPHY UPON THE REACTION DYNAMICS OF POLYATOMIC SYSTEMS: THE $O_3 + NO \rightarrow O_2 + NO_2^+$ REACTION

II. QUANTUM MECHANICAL STUDY OF ROTATIONALLY INELASTIC SCATTERING IN THE HF-Ar SYSTEM

Thesis Approved:

Leonard M. Raff
Thesis Adviser

J. Paul Devlin

N. V. V. J. Swamy

Th G Rockley

Norman N Durham
Dean of the Graduate College

ACKNOWLEDGMENTS

I express my sincere gratitude to Dr. Lionel Raff, for his continued help and encouragement throughout the course of this work. Virtually none of the work presented here could have been accomplished without his most able guidance. I thank Dr. J. P. Devlin, Dr. M. G. Rockley and Dr. N. V. V. J. Swamy for serving as members of my advisory committee.

I thank Dr. David Martin who was happy to discuss the development of my research problem at any time, and Charles B. Smith who was extremely helpful and made my stay in the group a pleasant experience. I thank Dr. D. L. Thompson and Dr. P. M. Agrawal for showing a lot of interest and encouragement in my work. I thank Max Mckee and Bahm Eldean for their valuable assistance in using the university computer. I thank Dr. Chandler and Dr. Burchard for helping me with the various numerical techniques.

I gratefully acknowledge the financial support received from the Department of Chemistry through a teaching assistantship, and the National Science Foundation through a research assistantship.

I thank Sue Heil for typing the final copy of this thesis.

I am grateful to my parents for their endless love and affection and their continued encouragement. Finally, I thank my husband, Viswa, for his love and understanding without which this work would have been an impossible task.

TABLE OF CONTENTS

Chapter		Page
I.	INTRODUCTION	1
	The Study of Collision Dynamics	2
	Polyatomic Reaction Dynamics and the Effect of Surface Topology	6
	Rotational-to-Translational Energy Transfer Processes in the HF-Ar System	14
II.	POTENTIAL-ENERGY SURFACE FOR THE O_3 + NO SYSTEM	18
	Derivatives of the Potential-Energy Surface	65
III.	QUASICLASSICAL TRAJECTORY STUDY OF THE EFFECTS OF SURFACE TOPOGRAPHY UPON THE REACTION DYNAMICS OF POLYATOMIC SYSTEMS	79
	Calculation Methods	79
	Selection of Initial Conditions	89
	Numerical Integration of the Equations of Motion	102
	Analysis of Final State	103
	Statistical Averaging	109
	Results and Discussion	112
	Conclusions	138
IV.	POTENTIAL-ENERGY SURFACE FOR THE HF + Ar RIGID ROTOR SYSTEM	140
	Spline Fitted Ab Initio Surface (SAI)	140
	Lennard Jones Potential-Energy Surface	149
V.	STUDY OF THE ROTATIONALLY INELASTIC SCATTERING IN THE HF-Ar RIGID ROTOR SYSTEM USING THE INFINITE ORDER SUDDEN APPROXIMATION METHOD	152
	Calculational Methods	152
	State-to-State Cross Section	155
	Results and Discussion	159
	Conclusions	173
BIBLIOGRAPHY		178
APPENDIX		184

LIST OF TABLES

Table		Page
I.	Morse Parameters for the Diatomic Molecules	21
II.	Variation of D_{NO} with R_i^a	24
III.	Ionization Potentials and Electron Affinities of the Atoms[a]	27
IV.	Calculated ^3E Values from EQ (II-24) with Z = 3.2	29
V.	Calculated ^3E Values from EQ (II-24) with Z = 3.4	30
VI.	Calculated ^3E Values from EQ (II-24) with Z = 3.8	31
VII.	Triplet-State Energy Parameters for Z = 3.2	32
VIII.	Singlet-State Energy Parameters	32
IX.	Triplet-State Energy Parameters for Z = 3.4	33
X.	Triplet-State Energy Parameters for Z = 3.8	33
XI.	Fundamental Vibrational Wavenumbers of O_3 Calculated by a Variational Method	35
XII.	INDO Computed Variation of O-N-O Bending Force Constant as a Function of R_{N-O}	37
XIII.	INDO Computations of the Variations of the Equilibrium Angle in NO_2 as a Function of R_{N-O}	38
XIV.	The Three-Body Interaction Potential, V_I, for O_3 -NO. Energies are in EV, Distances Are in Å and Angles Are in Radians	42
XV.	Saddle-Point Geometries	64
XVI.	Spectroscopic Constants of O_3 and NO	92
XVII.	Rotation Matrices	100
XVIII.	Units Used in the O_3-NO Quasiclassical Trajectory Computer Code	104

Table		Page
XIX.	Arrhenius Parameters for the Ground State Reactants . .	114
XX.	Arrhenius Parameters for the Vibrationally Excited (0010) Reactants	115
XXI.	Cross Sections $(\text{Å})^2$ Obtained on Surface S3	116
XXII.	Rate Constants Computed on Surface S4	117
XXIII.	Effectiveness of Vibration Over Relative Translation in Promoting the Reaction	118
XXIV.	Cross Sections $(\text{Å})^2$ Obtained on Surface S5	124
XXV.	Comparison of Thermal Rate Constants and Those Obtained with Vibrationally Excited NO	128
XXVI.	Rate Constants Obtained with Vibrationally Excited Ozone (n_1 n_2 n_3) on Surface S5	132
XXVII.	Analysis of Normal Mode Energies of Ozone	133
XXVIII.	Fraction (%) of the Available Energy Deposited in the Product Molecules on Surface S5 at T = 400K . . .	133
XXIX.	Fraction (%) of the Available Energy Deposited in the Product Molecules at T = 400K	134
XXX.	Scattering Distribution of the Product Molecules for the Ground State Reactants on Surface S5	136
XXXI.	Average Scattering Angles on Surfaces S1, S2, S3 and S5	137
XXXII.	Scattering Angles for Various Initial States of Reactants on Surface S5	137
XXXIII.	Comparison of Times and Accuracies of the Different Basis Sets for Argon and HF	143
XXXIV.	Ab initio Intermolecular Potential for the Rigid Rotor HF-Ar System. Energies are Measured in eV from the Energy of HF and Ar at Infinite Separation. R is in Å	145
XXXV.	Lennard-Jones Parameters	150
XXXVI.	IOSAM Results for the State-to-State Integral Cross Sections on the LJ(12,6) Potential Surface[a] . .	162
XXXVII.	IOSAM Results for the State-to-State Integral Cross Sections on the LJ(12,6) Potential Surface[a] . .	163

Table		Page
XXXVIII.	IOSAM Results for the State-to-State Integral Cross Sections on the LJ(12,6) Potential Surface[a] . .	164
XXXIX.	IOSAM Results for the State-to-State Integral Cross Sections as a Function of the Well-Depth of the Potential Surface[a]	170
XL.	IOSAM Results for the State-to-State Integral Cross Sections as a Function of the Well-Depth of the Potential Surface[a]	171
XLI.	Total Inelastic Integral Cross Section on the LJ(12,6) Surface[a]	172
XLII.	Total Inelastic Integral Cross Section as a Function of the Well-Depth of the Potential[a]	172
XLIII.	Comparison of IOSAM and IOSA Cross Section Ratios $\{\sigma(J' \leftarrow 2)/\sigma(4 \leftarrow 2)\}$ on the SAI Surface to the Measured Ratios	176
XLIV.	Basis Set Components	186

LIST OF FIGURES

Figure		Page
1.	The O_3-NO Systme	19
2.	Variation of the Equilibrium Angle in NO_2 with R_{N-O}	39
3.	Contour Plot of Surface S1 for α = 2.09 Radians	56
4.	Contour Plot of Surface S1 for α = 1.60 Radians	57
5.	Contour Plot of Surface S2 for α = 1.90 Radians	58
6.	Contour Plot of Surface S3 for α = 1.90 Radians	59
7.	Contour Plot of Surface S4 for α = 1.90 Radians	60
8.	Contour Plot of Surface S5 for α = 1.90 Radians	61
9.	Saddle-Point Region of Surface S3	62
10.	Saddle-Point Region of Surface S5	63
11.	Coordinate Systems for the O_3-NO System	81
12.	Cartesian Coordinats and Conjugate Momenta for the O_3-NO System	82
13.	Approximate Normal Modes for O_3	84
14.	Course of a Reactive Trajectory on Surface S5 for the Ground State Reactants	120
15.	Total Reactive Cross Section Versus Relative Translational Energy on Surface S5 for (0000) State of Reactants	122
16.	Total Reactive Cross Section Versus Relative Translational Energy on Surface S5 for (0010) State of Reactants	123
17.	Arrhenius Fit to the Rate Constants for the O_3-NO System Obtained on Surface S5 for the (0000) State of Reactants	125

Figure Page

18. Arrhenius Fit to the Rate Constants for the O_3-NO System Obtained on Surface S5 for the (0010) State of Reactants 126

19. O-O^i and O^i-N Bond Distances as a Function of Time for a Reactive Trajectory on Surface S5 for the (0000) State of Reactants 129

20. O-O^i and O^i-N Bond Distances as a Function of Time for a Reactive Trajectory on Surface S5 for the (0010) State of Reactants 130

21. The HF-Ar Rigid Rotor System 141

22. Plot of ln V Versus r for $\Gamma = 90^o$ 151

23. HF-Ar Phase Shifts (in Radians) on the LJ(12,6) Surface for $\Gamma = 100^o$ Versus Partial Wave 160

24. HF-Ar Phase Shifts (in Radians) on the SAI Surface for $\Gamma = 100^o$ Versus Partial Wave 161

25. Comparison of Computed IOSAM Cross Section Ratios $[\sigma(j'-1)/\sigma(3-1)]$ with Experimental Ratios at T_i = 4 Kcal/mole 165

26. Comparison of Computed IOSAM Cross Section Ratios $[\sigma(j'-2)/\sigma(4-2)]$ with Experimental Ratios at T_i = 4 Kcal/mole 166

27. Log-Log Plot of $[\frac{\sigma(j'-1)}{\sigma(3-1)} (\frac{T_i}{T_f}) (2j'+1)^{-1}]$ Versus $|\Delta E_{jj'}|$ on the LJ(12,6) Surface 168

28. Comparison of IOSAM and IOSA Cross Section Ratios $[\sigma(j'-1)/\sigma(3-1)]$ on the LJ(12,6) Surface to the Measured Ratios at T_i = 4 Kcal/mole 174

29. Comparison of IOSAM and IOSA Cross Sections Ratios $\sigma(j'-2)/\sigma(4-2)$ on the LJ(12,6) Surface to the Measured Ratios at T_i = 5 Kcal/mole 175

CHAPTER I

INTRODUCTION

With the availability of nozzle sources, lasers for selective excitation, and sensitive spectroscopic techniques for identifying molecular states, the experimental reaction dynamicist can now control the energies of chemical reagents and observe the states of reaction products to an extent only imagined two decades ago. Already one can foresee the day when state-to-state cross sections, like those for spectroscopic transitions, will become available for chemical reactions. Although state-to-state cross sections are the ultimate goal, they are currently available for very few reactions.

The desire to improve our fundamental understanding of reactive processes has not been the only stimulus to studies in reaction dynamics. The development of laser sources has been another. The search for new laser systems has inspired many experiments on chemical excitation, and existing lasers have served as photochemical sources for selective excitation. An important objective of dynamical theories is the elucidation of the connection between the form of the potential-energy surface and the way in which the energy released passes into the products of reaction. An experimental study of energy distributions, combined with a dynamical treatment for a variety of hypothetical potential-energy surfaces, can lead to valuable conclusions about the actual topography of potential-energy surfaces.

The Study of Collision Dynamics

The theoretical study of any chemical problem which falls within the domain of the Born-Oppenheimer approximation involves two basic steps:

1. The evaluation of the potential-energy surface by solving the electronic Schrodinger's equation over the range of nuclear configurations demanded by the problem.

2. Solution of the nuclear scattering problem on the potential-energy surface thus obtained.

The most accurate type of potential-energy surface is a converged CI ab initio surface. In an ab initio calculation of the potential-energy surface, the electronic Schrodinger equation is solved by employing different levels of approximations. The most widely used are the Hartree-Fock and Linear Combination of Atomic Orbitals-Molecular Orbital-Self Consistent Field (ICAO-MO-SCF) calculations. Due to the enormous amount of computer time required, these calculations are extremely difficult for many-electron systems. Considerable progress is being made, however, and complete potential surfaces with an accuracy acceptable for scattering studies for systems with up to 30 electrons and four nuclei now lie within the present bound of accomplishment (1).

In many scattering calculations the ab initio results cannot be employed directly and hence a suitable interpolation of the computed values is necessary. Ab initio results for the CO_2-H_2 (2) and CO_2-He (3) systems have been computed and the potential-energy surface generated by a three-dimensional cubic spline interpolation technique (4). Classical trajectory calculations on such a spline fitted ab initio surface of the CO_2-H_2 (2) and CO_2-He (3) systems and a quantum

mechanical scattering study on the latter system (5) have been shown to yield reliable results.

Unfortunately, the Hartree-Fock calculation is inexact, and the energy obtained differs considerably from the true energy due to the correlation error. This arises due to the inaccurate description of the pair probability function for electrons of opposite spin. This error is especially large if the number of electron pairs predicted by the orbital model of the system changes during the course of the reaction or if the reaction does not involve closed-shell reactants and products. The method of configuration interaction, CI, first discussed by Hylleraas (6), is one of the oldest techniques used to surmount this problem. In a standard CI calculation, the excited state determinants are formed by systematically promoting electrons from the occupied orbitals of the ground state determinant to the vacant or virtual orbitals. The number of configurations which can be formed in this way from N electrons and n basis functions (7) is of the order of n^N. Thus, even with today's high speed computers, a 'full' CI is possible only for very small systems.

In order to overcome such difficulties while dealing with many-electron systems, we resort to semi-empirical methods. Semi-empirical surfaces have the advantage of being simple and fast to compute and can be used to describe a much wider variety of systems than ab initio surfaces presently are able to do. Here, a simplified expression is used to represent the surface, and experimental results are either directly incorporated into it or fitted by adjustable parameters within the expression. Numerous three- and four-body investigations have shown that the simple valence-bond surfaces can correctly predict

diatomic bond energies and lengths and fundamental vibration frequencies. Moreover, Porter and Raff (8) have shown that the simple valence bond minimal basis wavefunction contains a significant amount of configuration mixing. Recently, such methods have been used to obtain a representation for the potential-energy surface for the six-body $CH_4 + T^*$ system. Equilibrium thermodynamic and spectroscopic data for reactants and products, the results of all-valence electron INDO and all-electron ab initio SCF and CI quantum calculations, and previously formulated three and four-body valence-bond potential surfaces were used to obtain this surface, and an unadjusted computation of the reaction dynamics was reported (9). These semi-empirical procedures are especially useful if we seek to assess the role played by various reactant properties and surface topological features rather than to accurately represent any specific system. The effect and relative importance of different topological features of these surfaces may then be systematically studied by numerically varying the surface in any desired manner.

The second phase in the study of collision dynamics is the scattering calculation which involves the solution of the nuclear equations of motion on the potential-energy surface computed. This can be done either quantum mechanically by solving the Schrodinger equation or classically by solving the Hamilton's equations of motion. In most calculations quantum conditions have been imposed as far as the initial states are concerned, but the actual motion over the potential energy barrier has been treated classically in the majority of studies. It is considerably easier to do this than to carry out a purely quantum-mechanical treatment. The two main sources of error inherent in a

classical mechanical calculation are the neglect of energy quantization and quantum mechanical tunneling. However for reactions involving a large number of available quantum states, the classical treatment may be expected to be completely adequate.

The first classical calculations were made for the $H + H_2$ system by Eyring and Polanyi (10) and further work was done by Hirschfelder, Eyring and Topley (11). The first computer calculations of reaction dynamics were performed by Wall, Hiller and Mazur (12), for the $H + H_2$ system. It is now feasible to carry out complete cross section calculations by trajectory integrations for a system of three or more atoms (13). An unadjusted computation of the reaction dynamics in the $CH_4 + T^*$ and $CD_4 + T^*$ systems have been carried out by Raff (9). Similar calculations with an unrestricted potential for CH_5 have been carried out by Valencich and Bunker (30). The isomerization of CH_3NC molecule to CH_3CN has been studied in great detail by Bunker and Hase (14) by the classical trajectory procedure. They used an empirical potential energy function for treating this six-body system and these authors used the results of approximately 6000 trajectories to calculate energy dependent isomerization rate constants at excitations of 70, 100 and 200 Kcal/mole. The hot-atom displacement reactions

$$T^* + CH_3NC \longrightarrow CH_2TNC$$
$$T^* + CH_3CN \longrightarrow CH_2TCN$$

have been studied by Harris and Bunker (14). These are a few examples that elucidate the feasibility of trajectory calculations on many-atom systems.

Polyatomic Reaction Dynamics and the Effect of Surface Topology

The role played by vibrational excitation in atom-diatomic molecule reactions is now reasonably well understood. Experimental studies using microwave (15), chemical (16) and IR laser (17) excitation methods have shown that such excitation can produce a factor of 100 or more increase in the measured reaction cross sections. Several theoretical investigations using model semi-empirical potential-energy surfaces have clearly related the effect to various topological features of the surface. Some of these features which will have an effect upon the computed reaction dynamics are the following:

1. The magnitude of the energy barrier to reaction.

2. Position of the barrier: The location of the barrier is found to determine what kind of energy is needed by the reagents in order to react at all. If the barrier is located deep in the entrance channel relative translation is found to be more effective in surmounting the barrier whereas if the barrier is located in the exit channel vibrational energy is found to be more effective (18). However, the Chapman-Bunker (19) study suggests that this may not be true in the case of polyatomic reactions. It is important to determine to what extent this result is an artifact of their surface and to what extent it is generally true.

3. The curvature of the reaction path near the saddle point and the position of maximum curvature relative to the point of energy release. If most of the energy is released before the maximum curvature region, the product will be vibrationally excited. On the other hand if the point of energy release occurs after the maximum curvature region, most of the energy will go to enhance the relative motion producing products with little vibration. Polanyi and Sathyamurthy (20) have found that gradual curvature of the reaction coordinate at the saddle point significantly reduces the effect of vibrational excitation and Duff and Truhlar (21) have shown that the relative positions of maximum curvature and energy release can be important in an atom-diatomic reaction.

4. Nature of the inner repulsive wall of the potential-

energy surface: This has been shown to be a feature of critical importance for some atom-diatomic reactions (22).

5. Formation of collision complex: The formation of a long-lived collision complex in the case of polyatomic reactions may be the cause for the absence of a marked dependence of the rate constant on the specification of initial vibrational modes of excitation since an efficient energy transfer to the reaction coordinate occurs via the collision complex (23).

The effect of these features of the potential-energy surface on the collision dynamics is well understood, at least for the atom-diatomic molecule reactions. The insight these studies have produced has been extremely important in the development of an understanding of the basic nature of atom-diatomic molecule reactions.

Unfortunately, such a complete study is unavailable for the case of polyatomic reactions. Not only are the effects of the various surface features on the observed reaction dynamics unknown, but sometimes even a qualitative prediction of the effect of vibrational excitation of the reactants upon the reaction dynamics cannot be made. This is obviously due to the complexity of the problem. The dynamics of atom-diatomic molecule reactions are complex functions of the potential-energy surface features, and it is natural to expect such a relation to be more complex for polyatomic reactions.

The reactions of C_2H_4 and OCS with O_2 were studied by Manning, Braun and Kurylo (24) and no significant increase in the reaction rate was observed when either C_2H_4 or OCS were vibrationally excited (24). Similar effects were observed by Riley, Shatas and Arkle (25) in the reactions of diborane to yield various B_nH_m molecules. They carried out the reaction with vibrationally excited diborane molecules produced by multipole photon absorption and observed that the reaction did not

proceed more rapidly than with the reagents in the ground state. Weston and Ting (26) and Tsao and Root (27) have interpreted the results of their photolysis experiments on (CH_3Br, H_2) and (CD_3Br, H_2) systems to suggest that the reaction rate for

$$CH_3 + H_2 \longrightarrow CH_4 + H \qquad (R1)$$

is significantly enhanced by excitation of the out-of-plane bending mode of CH_3. However, contradictory results were obtained from the theoretical studies of reaction R1 by Bunker and Chapman (19). Bunker and Chapman studied the effect of vibrational excitation of CH_3 on reaction R1 by using their previously obtained (CH_5) potential-energy surface (28-30). They not only observed the absence of reaction rate enhancement on vibrational excitation but a significant decrease in the reaction rate. Excitation of the CH_3 bending mode to $v_2 = 6$ decreased the cross section by a factor of five. Similar computations were carried out by Raff (31) by using the unadjusted six-body potential-energy surface (9) and the results agreed with those of Bunker and Chapman (19). It was observed by Raff (31) that at a relative translational energy of 30 Kcal/mole, excitation of the CH_3 bending mode to the $v_2 = 4$ state reduces the reaction cross section by 17% from that obtained with all reactants in the ground vibrational state.

On the other hand, Lussier, Reiser, Jensen and Steinfeld (32) have reported vibrationally induced dehydrohalogenation of chlorinated ethylenes. Cross (33) has found that the reaction cross section for the chemionization reaction

$$SbF_5 + RX \longrightarrow SbF_5X^- + R^+,$$

with R an alkyl, acyl or inorganic halide, is very sensitive to vibrational excitation but is completely independent of translational energy.

Finally, in those cases where vibrational excitation enhances the reaction rate, a mode selective enhancement is not observed. In the reaction of O_3 + NO, Kurylo et al. (37) observed that all three modes make comparable contributions to the reaction rate enhancement. Thus it is clear that the effect of vibrational energy on polyatomic systems has not been well understood and has been the subject of a number of recent experiments. It is clear that the microscopic effects that produce the observed results are not well understood. A thorough theoretical study of appropriate model systems has not yet become available. The present investigation consists of initiating such a study on the O_3 + NO system.

The reaction of NO with O_3 produces visible (34, 35) and infrared (36, 37) emission from electronically and vibrationally excited NO_2. The thermal rate constants for these reactions are (35)

$$O_3 + NO \longrightarrow O_2 + NO_2^+ (^2A_1) \qquad \text{(I-1)}$$

$$k(T) = (4.3 \pm 1.0) \times 10^{11} \exp(-2330 \pm 150/RT)$$

$$O_3 + NO \longrightarrow O_2 + NO_2^* (^2B_1) \qquad \text{(I-2)}$$

$$k(T) = (7.6 \pm 1.5) \times 10^{11} \exp(-4180 \pm 300/RT)$$

Electronically excited O_2, although energetically accessible, is not observed (38). Clough and Thrush (35) argue that the different activation energies of the two reactions suggest that they take place on different potential-energy surfaces.

Recently, lasers have been used to produce vibrationally excited

ozone and the enhancement of the chemiluminescence due to vibrational excitation has been studied in great detail. Pioneering work in the study of vibrationally excited reactions was carried out by groups at the National Bureau of Standards (43-46, 23) and at Cornell (47, 48). It has been found that laser excitation of O_3 increases the reaction rate. Hui and Cool (47) and Gordon and coworkers (42) have observed that when the stretching modes (ν_1 and ν_3) of ozone were excited, the activation energies of both reactions (I-1) and (I-2) decreased by about 50%. Enhancement in reaction rate of the same order was observed even when the bending mode of ozone was excited. It was therefore concluded that mode selective enhancement was not observed. Stephenson and Freund (23) studied the effect of vibrational excitation of NO on the rate of these reactions. They observed comparable enhancement of the reaction rate. The interpretation of these bulk experiments is seriously complicated and it has not been possible to determine independently the contributions of the individual modes to the reaction rate.

Another class of experiments on the O_3 + NO system, pioneered by Menzinger and coworkers (51, 52), are molecular beam studies. More recent beam experiments have been carried out by Van den Ende and Stolte (49, 50), by Valentini, Cross and Kwei (53), by Kahler, Kowalczyk and Lee (54) and by Brooks and Anderson (55). In these experiments the kinetic energy dependence of both the electronic and vibrational chemiluminescence of the O_3 + NO reaction has been studied. The vibrational chemiluminescence exhibits no threshold and a finite signal is measured even at the lowest collision energy (1 Kcal/mole). In addition, the vibrational emission rises considerably slower with

increasing kinetic energy than the electronic emission. The electronic emission was found to be enhanced by raising the NO internal temperature. This has been shown to be due to the enhanced reactivity of the $NO(^2\pi_{3/2})$ fine structure component. Vibrational IR emission from NO_2^+ was thus observed to exhibit an energy dependence different from electronic NO_2^* emission, confirming that the emitters are formed predominantly in distinct reaction channels rather than via a common precursor.

Van Den Ende and Stolte (49) have studied the influence of internal (rotational and electronic fine structure states of NO) and translational energy upon the chemiluminescence. The chemiluminescent cross section was found to increase rapidly with increasing translational energy up to E(trans) = 1.2 ev. At very high translational energies (E(trans) > 1.4 ev) some levelling off begins to set in. A strong increase of an exothermal reaction cross section with translational energy is uncommon (57). For chemiluminescent exothermic reactions it may occur as a consequence of the branching processes where the chemiluminescent channel competes with the reaction channel leading to electronic ground state products.

Valentini, Cross and Kwei (53) have carried out crossed-beam studies of the reaction using mass spectrometric detection. They are able to distinguish two peaks in the angular distribution of the NO_2 product. Backscattered (with respect to the direction of the incoming NO molecule) is a signal attributed to the ground electronic state product, while a peak scattered to the side is attributed to the excited electronic state product. Interestingly, in preliminary studies they observe that different nozzle temperatures leave the ratio of the two

signals unchanged. This suggests, contrary to earlier statements, that the reactions giving rise to the different electronic states of the products should not be viewed as taking place on separate adiabatic potential-energy surfaces, but rather that nonadiabatic effects play an important role.

Brooks and Anderson (55) in very recent work have controlled the NO beam by focussing with inhomogeneous magnetic fields. In this way, they observe the difference in reactivity of the NO fine structure components. They conclude that the NO electronic state has little to do with the chemiluminescent yield, but that for low J, chemiluminescence depends strongly on rotation.

Among the striking features of the reaction is the fact that electronically excited nitrogen dioxide, NO_2^*, is formed whereas electronically excited oxygen, O_2^*, is not formed though energetically accessible. For any process involving several electronic states, a correlation diagram provides basic information about energetically accessible states and their interactions. In a minimal state correlation diagram one simply draws straight lines connecting states arising from reactants with states arising from products, in such a way that lines representing states of the same symmetry do not cross.

Redpath, Menzinger and Carrington (52) explain the observed features of the O_3 + NO reaction by making use of the minimal state correlation diagrams. If the reaction is viewed to proceed through a planar transition state in which the NO approaches an end atom of the O_3 molecule and abstracts that atom, ground state reactants correlate to ground state products as well as to $NO_2(^2A_1) + O_2(^1\Delta_g)$ which is not observed experimentally. However, if the NO approaches O_3 in the plane

which bisects the O_3 bond angle, the excited states of O_2 are not adiabatically accessible. Other examples of reactions involving the center atom of a triatomic molecule have been seen (56).

It was suggested that the excitation of the asymmetric stretch mode might be expected to increase the rate constant (23). However, within the accuracy of presently available data, comparable enhancement of the rate constant was observed by excitation of either the stretching or bending modes of O_3 (48). Stephenson and Freund (23) observed enhancement in reaction rate of the same order when NO was vibrationally excited. The absence of a marked dependence of the rate constant on the specification of the initial vibrational modes of excitation lends support to the hypothesis of an efficient energy transfer to the reaction coordinate via a collision complex or an efficient intramolecular energy transfer.

In the present study, a theoretical investigation of the reaction,

$$O_3 + NO \longrightarrow NO_2^+ + O_2,$$

where NO_2^+ denotes vibrationally excited NO_2, has been carried out. We have attempted to assess the role played by various reactant properties and surface topological features rather than to accurately represent the system. The potential energy hypersurface for the system has been obtained by semi-empirical procedures making use of all available data relating to the equilibrium thermodynamics and spectroscopy of the reactants and products of reaction. A part of the potential-energy surface has been spline fitted. This enabled us to study the effect and relative importance of different topological features of these surfaces by numerically varying the surface in any desired manner. The

collision dynamic study has been performed on such a surface using quasiclassical trajectory analysis. This involves solving Hamilton's equations of motion:

$$\partial H/\partial q_i = -\dot{p}_i \quad \text{and} \quad \partial H/\partial p_i = \dot{q}_i$$

Here the q's denote the coordinates, p's the conjugate momenta, the dotted variables are the derivatives with respect to time. H is the classical Hamiltonian and for a conservative system, H = T + V, the total energy of the system; T is the kinetic energy, $T = 1/2 m_i \dot{q}_i^2$, and V the potential energy. Hamilton's equations were solved by a predictor-corrector method. The initial states of the trajectories were chosen randomly from the proper distribution functions for the phase angle, rotational quantum numbers, etc. The results from these trajectories were then averaged over these variables by the Monte Carlo procedure to calculate cross sections, rate coefficients, etc. The details of these procedures have been described elsewhere (58).

Rotational-to-Translational Energy Transfer Processes in the HF-Ar System

Molecular energy transfer is the study of the acquisition, transfer, and disposal of energy from the microscopic point of view. The bulk, macroscopic processes are traced to changes at the moelcular level. Until recently, most of our knowledge about inelastic scattering processes came from bulk experiments, such as ultrasonic dispersion (59) and microwave line-broadening. Following the stimulating experiments of Blythe, Grosser and Bernstein on $K + D_2$ (60), the crossed molecular beam method has been employed with increasing frequency in

the investigation of inelastic processes. The availability of sophisticated experimental techniques points to the need for the development of more efficient theoretical procedures for the treatment of the inelastic scattering processes.

A technological device in which the energy transfer processes play an important role is the gas-phase laser. Lasers operate by the excitation of rotational-vibrational or electronic modes of the molecule. The power of the laser radiation output depends upon the population of the excited state. The energy transfer processes accompanying the bimolecular collision events decrease the lifetime of the excited state and thereby act as performance limiting factors in the operation of lasers. In certain cases, like the He-Ne laser, the excitation of Ne atoms is brought about by resonant energy transfer collisions between 2's excited He and ground state Ne atoms. This excitation path is more efficient than the direct excitation of Ne by an electrical discharge. Hence it is necessary to understand these energy transfer processes in great detail in order to develop lasers with better performance. Because HF is an integral part of several laser systems, understanding the vibrational and rotational excitations and relaxations that occur in the molecule is vital to the improvement of the efficiency of HF lasers.

The most accurate theoretical treatment of the scattering processes involves the use of the close coupling (CC) method of Arthurs and Dalgarno (61). However, the CC equations become very difficult to solve when there are a large number of scattering channels involved. Consequently, a variety of decoupling approximations have been developed to simplify the close-coupling formulation. Recently, Parker and Pack

(62) have employed the Infinite Order Sudden Approximation (IOSA) method for the treatment of rotationally inelastic scattering. In the IOS approximation, the internal states (rotational states, especially) of the molecule and also the centrifugal potentials are assumed to be degenerate. The former is referred to as the "Energy Sudden" (ES) approximation and the latter is known as the "Centrifugal Sudden" (CS) approximation. Integral and differential cross sections for the (CO_2-He) system obtained from the IOSA method were found to be in good agreement with experimental results. Agrawal and Raff (63) have investigated the effect of potential surface topography upon elastic and inelastic scattering in the (CO_2-He) system using the IOSA method. The results were in good to excellent agreement with the quasiclassical trajectory results (64), and with experiment (65). However, a condition for the validity of the IOSA approximation is that the fraction of the total translational energy transferred to internal modes during a collision be small. Consequently, difficulties arise if the IOS approximation is employed to examine processes in which large multiple quantum excitations of internal modes play an important role.

Recently, a simple modification of the IOSA equations has been suggested that incorporates an explicit exit-channel velocity dependence into the scattering cross section (66). It has been shown that the resulting modified formalism (IOSAM) properly closes those channels required to be closed by energy considerations. In addition, a comparison of IOSAM and IOSA results with quasiclassical trajectory calculations in the rigid rotor (CO_2-He) system showed the IOSAM cross sections to be in significantly better accord with the trajectory

results (66). The simplicity and accuracy of the IOSAM method make it a viable method for routine analysis of the experimental results.

The present study reports an investigation of rotationally inelastic scattering processes in the HF + Ar system using the modified IOSA method. This particular system was chosen because of its simplicity and because experimental data are available. Barnes et al. (67) have measured the state-to-state cross sections for rotational-to-translational energy transfer in HF + Ar, as a function of collision energy. The data reported by these investigators exhibit several interesting features. For instance, the relative R $\leftrightarrow$ T cross sections are found to be unaffected by increasing the center of mass collision energy from 4 to 16 Kcal/mole (67). In the present study, the results of the IOSA (62) and IOSAM (66) formulations are compared with the experimental data (67). Both ab initio and semi-empirical potential-energy surfaces have been employed in the calculations.

CHAPTER II

POTENTIAL-ENERGY SURFACE FOR THE O_3 + NO SYSTEM

The formulation of an unrestricted potential-energy surface for the O_3 + NO system requires the computation of the potential energy as a function of the ten internuclear distances (see Figure 1). Thus, such evaluation by ab initio procedures is almost an impossible task. However, since the major point of current interest is the investigation of the effects of various topographical features of the surface upon the observed reaction dynamics of polyatomic systems, a formulation with maximum flexibility is favored over a more accurate representation with a reduced flexibility.

Simple valence-bond type surfaces have been employed in numerous three- and four-body investigations. Raff (68) has carried out an unadjusted computation of the reaction dynamics in the (CH_4 + T^*) and (CD_4 + T^*) systems, using a valence-bond formulation of the six-body potential-energy surface that was a summation of three-body type terms. Following this example, a semi-empirical potential-energy surface has been formulated for the O_3 + NO system by making full use of the available data related to the equilibrium thermodynamics and spectroscopy of the reactants and products. The mathematical form of the surface is given by,

$$V_{NO_4}(R_i,\theta_i) = V_I(R_1,R_2,R_3) + V_I(R_4,R_6,R_3) + V_{O_3}(R_1,R_4,R_5)$$

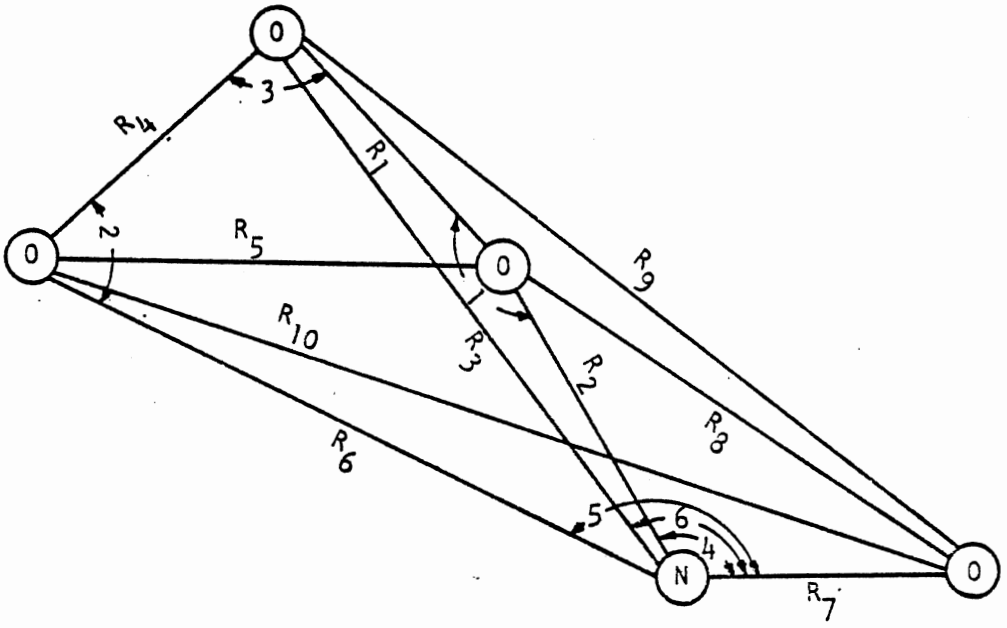

Figure 1. The O_3-NO System; the Interbond Angles are: (1) α_1; (2) α_2; (3) β; (4) θ_1; (5) θ_2; (6) θ_3

$$+ V_{O_2}(R_5) + V_{NO}(R_7) + V_{NO_2}(\theta_i) + V_{OO}(R_9)$$

$$+ V_{OO}(R_{10}) + V_{att}(R_i,R_3) \qquad \text{(II-1)}$$

where,

V_I are three-body interaction potentials operating between two oxygen atoms and the nitrogen atom. V_{O_3} is the ozone three-body interaction potential. V_{O_2} and V_{NO} are the Morse potentials for the diatomic interactions. $V_{NO_2}(\theta_i)$ is the bending potential for the NO_2 product molecule. V_{OO} are the repulsive interactions operating among pairs of oxygen atoms between which no bond formation takes place and V_{att} is an attenuation term. The variables, $R_i (1 \leq i \leq 10)$ and the bond angles are defined in Figure 1. The detailed description and the functional forms of each of these terms are considered below:

The function $V_I(R_i,R_j,R_k)$ in Eq (II-1) is the three-body valence-bond potential given by (69),

$$V_I(R_i,R_j,R_k) = Q_{AB} + Q_{BC} + Q_{CA} - \{0.5\{(J_{AB} - J_{BC})^2 + (J_{BC} - J_{CA})^2 + (J_{CA} - J_{AB})^2\}\}^{\frac{1}{2}} \qquad \text{(II-2)}$$

where the Q's are the coulomb integrals given by,

$$Q_{\alpha\beta} = ({}^1E_{\alpha\beta} + {}^3E_{\alpha\beta})/2 \qquad \text{(II-3)}$$

and J's are the exchange integrals given by,

$$J_{\alpha\beta} = ({}^1E_{\alpha\beta} - {}^3E_{\alpha\beta})/2 \qquad \text{(II-4)}$$

${}^1E_{\alpha\beta}$ and ${}^3E_{\alpha\beta}$ are the singlet and triplet state energies

respectively, for the αβ diatomic system. The singlet state energies have been represented by a Morse function,

$$^1E_{\alpha\beta}(R_i) = D\{\exp\{-2\alpha(R_i - R_e)\} - 2\exp\{-\alpha(R_i - R_e)\}\} \qquad \text{(II-5)}$$

where D is the bond-dissociation energy plus the zero point energy; R_e is the equilibrium separation of the diatomic molecule; and

$$\alpha = \pi\nu_o(2\mu/D)^{\frac{1}{2}} \qquad \text{(II-6)}$$

where μ is the reduced mass of the diatomic α-β system. The values of these parameters for O_2 and NO molecules are given in Table I.

TABLE I

MORSE PARAMETERS FOR THE DIATOMIC MOLECULES

Parameter	NO[b]	O_2[a]
D/ev	6.6	5.21
α/au^{-1}	1.45327	1.40478
R_e/au	2.1747	2.2816

(a) Spectra of diatomic molecules, G. Herzberg, Vol. I, p. 560.
(b) Reference 95.

The Morse parameters for the N-O bond have been made to vary

smoothly as the reaction proceeds. In order to represent the physical situation more accurately, some semi-empirical quantum mechanical calculations have been carried out for a few configurations of the NO_2 molecule. The experimentally observed exothermicity for the reaction

$$NO_2 \longrightarrow NO + O$$

is 3.11 ev (70). INDO open shell methods (71) have been used to calculate the energies of NO_2 in its equilibrium configuration, and the separated NO molecule and oxygen atom. The computed endothermicity of the reaction is

$$(\Delta E)_{INDO} = E_{NO_2} - (E_{NO} + E_O) = 13.9171 \text{ ev} \qquad \text{(II-7)}$$

$$\delta = (\Delta E)_{INDO}/(\Delta E)_{expt.} = 4.2211 \qquad \text{(II-8)}$$

INDO calculations were carried out for a few intermediate configurations. The change in energy from the NO_2 equilibrium configuration, $(E_{NO_2} - E^{eq}_{NO_2})_{INDO}$, were scaled using the δ parameter obtained as indicated above. The NO_2 potential is represented by the sum of the Morse potentials for the two N-O bonds if the interbond angle, θ, is equal to the equilibrium angle, θ_e, for each configuration. The potential of NO_2 at equilibrium, $(V_{NO_2})_{eq}$, is -9.91ev (70), with the zero of the potential corresponding to the separated atom limit. By knowing $(V_{NO_2})_{eq}$ and $(E_{NO_2} - E^{eq}_{NO_2})_{INDO}/\delta$, V_{NO_2} for the various configurations have been calculated as follows:

$$V_{NO_2} = (V_{NO_2})_{eq} + (E_{NO_2} - E^{eq}_{NO_2})_{INDO}/\delta \qquad \text{(II-9)}$$

By equating V_{NO_2} to the sum of the Morse potentials, the value of the Morse parameter, D_{NO}, can be calculated as a function of the N-O bond distance. The values of $(E_{NO_2} - E^{eq}_{NO_2})_{INDO}$ and D_{NO} as a function of the N-O bond distance are given in Table II. These results have been fitted to a fourth degree polynomial by using a non-linear least squares procedure as follows:

$$D_{NO} = 6.6 - \Delta D \qquad \text{(II-10)}$$

where,

$$\Delta D = 1.65 \qquad R_i \leq 2.21$$

$$\Delta D = a_0 + a_1 R_i + a_2 R_i^2 + a_3 R_i^3 + a_4 R_i^4, \quad 2.21 \leq R_i \leq 3.3$$

$$\Delta D = 0 \qquad R_i > 3.3 \qquad \text{(II-11)}$$

where R_i is the N-O bond that is being formed. The values of the constants[a] that have been employed in the calculation are,

$$a_0 = 0.04 \quad \text{ev}$$
$$a_1 = 0.968394 \ \text{ev}\cdot\text{au}^{-1}$$
$$a_2 = 0.232423 \ \text{ev}\cdot\text{au}^{-2}$$
$$a_3 = -0.1378116 \ \text{ev}\cdot\text{au}^{-3}$$
$$a_4 = -0.0078416 \ \text{ev}\cdot\text{au}^{-4} \qquad \text{(II-12)}$$

(a) R_i are in au.

The equilibrium distance of the N-O bond also changes as the reaction proceeds. This feature has been incorporated into the potential energy hypersurface formulation as follows:

$$R_e = 2.1747 \text{ au} \qquad R_i > 3.3$$

$$R_e = 2.1747 + 21723.2\{\exp(-0.049376\ R_i^5)\} \qquad 3.0 \leq R_i \leq 3.3$$

$$R_e = 2.2575 \qquad R_i < 3.0 \qquad \text{(II-13)}$$

This functional form produces a smooth and rapid change of the equilibrium distance as the reaction proceeds.

TABLE II

VARIATION OF D_{NO} WITH R_i[a]

R_i/au	θeq/deg	$(E_{NO_2} - E^{eq}_{NO_2})_{INDO}/\delta$[b]	$\Delta D = 6.6 - D_{NO}$
2.2575	138	0.0	1.58037
2.3810	136	0.10166	1.49136
2.4188	133.8	0.16407	1.46476
2.4566	132	0.23537	1.43757

(a) The other N-O bond distance in NO was fixed at the Equilibrium value = 2.2575 au.
(b) All energies are in eV.

By varying the Morse parameters as indicated above, we were able to obtain a potential-energy surface which approached the proper asymptotic limits, reproduced the experimental exothermicity, and the

equilibrium geometries of reactants and products.

Unfortunately, the triplet-state energies required in Eq (II-3) and (II-4) are much more difficult to obtain than is the case for the ground-state singlet. Hence, in order to obtain the triplet-state potential energies for O_2 and NO, semi-empirical calculations of the type previously reported by Pohl, Rein and Appel (72) and by Pohl and Raff (73) have been employed. Similar procedures have also been employed by Raff, Stivers, Porter, Thompson and Sims (69) for evaluating the triplet-state energies of HI and I_2.

The triplet-state energies are given by,

$$^3E = \langle {}^3\Psi \mid H \mid {}^3\Psi \rangle \qquad \text{(II-14)}$$

where H is the Hamiltonian for the diatomic system given by,

$$H = -\tfrac{1}{2}\nabla_1^2 - \tfrac{1}{2}\nabla_2^2 + r_{12}^{-1} + V_A(1) + V_A(2) + V_B(1) + V_B(2) \qquad \text{(II-15)}$$

where V_A and V_B represent core potentials. The triplet-state wavefunction is given by,

$$^3\Psi = (2 - 2S_{AB}^2)^{-\frac{1}{2}} (\phi_A(1)\phi_B(2) - \phi_A(2)\phi_B(1)) \times \alpha(1)\,\alpha(2) \qquad \text{(II-16)}$$

where S_{AB} represents the overlap integral $\langle \phi_A \mid \phi_B \rangle$. ϕ_A and ϕ_B are the 2pσ Slater-type orbitals for the O and N atoms given by (74),

$$\phi_O = 4.4040\ r \exp(-2.275\ r)\cos\theta$$

$$\phi_N = 2.9956\ r \exp(-1.950\ r)\cos\theta \qquad \text{(II-17)}$$

The triplet-state energy is now given by,

$$^3E = (1 - S_{AB}^2)^{-1} (X_1 - X_2) \qquad \text{(II-18)}$$

with

$$X_1 = \langle \phi_A(1)\phi_B(2) \mid H \mid \phi_A(1)\phi_B(2) \rangle \qquad \text{(II-19)}$$

and

$$X_2 = \langle \phi_A(1)\phi_B(2) \mid H \mid \phi_A(2)\phi_B(1) \rangle \qquad \text{(II-20)}$$

The integrals in Eq (II-19) and (II-20) have been evaluated by using the semi-empirical approximations previously employed (72, 73). This results in the following expression for the triplet-state energies.

$$^3E = (1 - S_{AB}^2)^{-1} (-I_A - I_B - R_{12}^{-1} + S_{AB}^2(I_A + I_B + 0.5\ Z_A + 0.5\ Z_B + R_{12}^{-1}) - S_{AB}^2(I_A + A_A + I_B + A_B + 2\ R_{12}^{-1})/4) \qquad \text{(II-21)}$$

The total energy, ^3E_T, relative to separated atoms A + B in the ground state is given by (72, 73),

$$^3E_T = I_A + I_B + R_{12}^{-1} + {}^3E \qquad \text{(II-22)}$$

where I's are the ionization potentials of the atoms, R_{12} is the inter-particle separation and A's are the electron affinities and

$$Z_A = \langle \phi_A(1) \mid V_A(1) \mid \phi_A(1) \rangle$$
$$= \langle \phi_A(1) \mid -Z/r_A \mid \phi_A(1) \rangle \qquad \text{(II-23)}$$

The parameters employed for the evaluation of the triplet-state energies

for O_2 and NO are given in Table III. The overlap integrals and the integral in Eq (II-23) have been evaluated analytically, using 2pσ Slater-type orbitals for the O and N atoms (74). Thus, the triplet-state energies are completely known, once the value of Z in Eq (II-23) has been fixed. However, because of the approximate nature of the treatment, the values cannot be expected to be accurate. By carrying out similar calculations on H_2 (69), for which a functional representation for ^3E was available (75), it was observed that,

$$^3E_{true} \approx 0.38871\ ^3E_T \qquad \text{(II-24)}$$

In the present case, the ^3E_T values have therefore been corrected by using the above expression.

TABLE III

IONIZATION POTENTIALS AND ELECTRON AFFINITIES OF THE ATOMS[a]

Atom	I(au)	A(au)
N	0.5082	-0.0312
O	0.6350	-0.0992

(a) Reference 96.

It was observed that the barrier height of the resulting potential-

energy surface was dependent upon the value of Z employed in Eq (II-23). Thus, potential-energy surfaces with different barrier heights have been generated by using various values of Z ranging from 3.2 to 3.8.

The triplet-state energies for O_2 and NO computed for the various Z-values are given in Tables IV-VI. The triplet-state energies have been fitted to the following functional forms by making use of a non-linear least squares procedure;

$$^3E_{\alpha\beta} = D_3\{\exp\{-2\beta(R_n - R_e)\} + 2\exp\{-\beta(R_n - R_e)\}\}, \quad R_n \leq R^* \qquad \text{(II-25)}$$

and

$$^3E_{\alpha\beta} = C\{R_n + A\}\exp(-\sigma R_n), \quad R_n > R^* \qquad \text{(II-26)}$$

The values of the various parameters, obtained by a non-linear least squares fit of the semi-empirical triplet-state energies, for the different Z-values, and the parameters employed in evaluating the singlet-state energies are given in Tables VII-X. As can be seen, the values for the extensive energy parameters, D, D_3 and C, for the $N\text{-}O^3$ bond are 50% of those for the $N\text{-}O^1$ or $N\text{-}O^2$ bonds. This is to compensate for the fact that the $N\text{-}O^3$ interaction is counted twice by the functional form of Eq (II-1).

$V_{O_3}(R_1,R_4,R_5)$ is the three-body interaction potential between the oxygen atoms in the ozone molecule. This potential has been defined in terms of the three internuclear distances R_1, R_4 and R_5 by Murrel and Farantos (76). In the reactant limit, the potential for the O_3 molecule is given by a sum of the three two-body terms and the three-body term

TABLE IV

CALCULATED ^3E VALUES FROM EQ (II-24) WITH Z = 3.2

R_{ab}(au)	^3E from Eq (II-24) (eV)	
	O_2	NO
2.5	2.7423	3.0494
2.6	2.3815	2.7615
2.8	1.7251	2.1645
3.0	1.1956	1.6159
3.1	0.9815	1.3754
3.5	0.4125	0.6662
4.0	0.1212	0.2335
5.0	0.0074	0.0204
6.0	0.0003	----

TABLE V

CALCULATED ^3E VALUES FROM EQ (II-24) WITH Z = 3.4

R_{ab}(au)	^3E from Eq (II-24) (eV)	
	O_2	NO
2.5	2.9390	3.2695
2.6	2.5519	2.9603
2.7	2.1851	2.6385
2.8	1.8480	2.3196
2.9	1.5459	2.0147
3.0	1.2804	1.7312
3.5	0.4416	0.7134
4.0	0.1297	0.2499
4.5	0.0337	0.0776
5.0	0.0079	0.0219

TABLE VI

CALCULATED ^3E VALUES FROM EQ (II-24) WITH Z = 3.8

R_{ab}(au)	^3E from Eq (II-24) (eV)	
	O_2	NO
2.4	3.7778	4.0243
2.5	3.3324	3.7097
2.6	2.8927	3.3579
2.7	2.4762	2.9921
2.8	2.0938	2.6297
2.9	1.7511	2.2836
3.0	1.4501	1.9619
3.2	0.9686	1.4081
3.5	0.4997	0.8077
4.5	0.0380	0.0877

TABLE VII

TRIPLET-STATE ENERGY PARAMETERS FOR Z = 3.2

Parameter	Diatomic pair		
	O-O	O-N	^{3}O-N
D_3/eV	1.28355	1.66056	0.83028
β/au^{-1}	1.23508	1.09662	1.09662
A/au	-2.13074	-2.48169	-2.48169
C/eV·au^{-1}	12586.7147	16649.8124	8324.906
σ/au^{-1}	3.04081	2.89868	2.89868
R*/au	3.0	3.2	3.2

TABLE VIII

SINGLET-STATE ENERGY PARAMETERS

Parameter	Diatomic pair		
	O-O	O-N	^{3}O-N
D/eV	5.21	Eq (II-10)	D_{NO}/2 Eq (II-10)
α/au	1.40478	1.45327	1.45327
R_e/au	2.2816	Eq (II-13)	Eq (II-13)

TABLE IX

TRIPLET-STATE ENERGY PARAMETERS FOR Z = 3.4

Parameter	Diatomic pair		
	O-O	O-N	^{3}O-N
D_3/eV	1.38512	1.55799	0.77900
β/au^{-1}	1.24345	0.88657	0.88657
A/au	-2.14125	-2.17002	-2.17002
C/eV·au^{-1}	14027.628	7250.1161	3625.0581
σ/au^{-1}	3.05018	2.71840	2.71840
R*/au	3.0	3.0	3.0

TABLE X

TRIPLET-STATE ENERGY PARAMETERS FOR Z = 3.8

Parameter	Diatomic pair		
	O-O	O-N	^{3}O-N
D_3/eV	1.56728	1.80137	0.90068
β/au^{-1}	1.24965	0.94574	0.94574
A/au	-2.10705	-2.28416	-2.28416
C/eV·au^{-1}	14076.5935	11331.6366	5665.818
σ/au^{-1}	3.02263	2.78394	2.78394
R*/au	3.0	3.0	3.0

V_{O_3}.

$$V_{ozone}(R_1,R_4,R_5) = V_{O_2}(R_1) + V_{O_2}(R_4) + V_{O_2}(R_5) + V_{O_3}(R_1,R_4,R_5) \quad \text{(II-27)}$$

The three two-body terms are described by the V_I terms and $V_{O_2}(R_5)$ terms in Eq (II-1). The functional form used here is the one given by these authors (76). The Murrel-Farantos potential is defined in terms of the symmetry coordinates, Q_1, Q_2 and Q_3 which are in turn defined by the transformation

$$\begin{bmatrix} Q_1 \\ Q_2 \\ Q_3 \end{bmatrix} = \begin{bmatrix} 1/\sqrt{3} & 1/\sqrt{3} & 1/\sqrt{3} \\ 0 & 1/\sqrt{2} & -1/\sqrt{2} \\ 2/\sqrt{6} & -1/\sqrt{6} & -1/\sqrt{6} \end{bmatrix} \begin{bmatrix} R_4 - R_0 \\ R_1 - R_0 \\ R_5 - R_0 \end{bmatrix} \quad \text{(II-28)}$$

with $R_o = 1.5698$ Å. The three-body term is given by,

$$V_{O_3}(Q_1,Q_2,Q_3) = (P + Q)(1 - \tanh\ 2.3\ Q_1) \quad \text{(II-29)}$$

with

$$P = 8.7066 + 6.5822\ Q_1 + 13.9106\ Q_1^2 - 17.1931(Q_2^2 + Q_3^2) - 3.1421\ Q_1(Q_2^2 + Q_3^2) + 2.6323\ Q_3(Q_3^2 - 3.0\ Q_2^2) + 13.9659(Q_2^2 + Q_3^2)^2 \quad \text{(II-30)}$$

and

$$G = -3.0\{\exp\{-7.5(Q_2^2 + Q_3^2)\}\} \quad \text{(II-31)}$$

with the restriction

$$\lim_{R_1 \to \infty} V_{O_3} = 0; \quad i = 1, 4, \text{ or } 5 \qquad \text{(II-32)}$$

This potential function for O_3 reproduces the harmonic force constants, equilibrium bond lengths and dissociation energy of the molecule. The fundamental vibration wavenumbers of O_3 have been calculated by a variational method (77) and the results are compared with experiment in Table XI (76). The agreement between calculated and experimental values is very good. However, it must be remembered that the potential is based on a quadratic force-field assumption for the molecule and exact agreement is not expected. The good agreement with the known experimental features of the O_3 potential makes it suitable for a dynamical study.

TABLE XI

FUNDAMENTAL VIBRATIONAL WAVENUMBERS OF O_3
CALCULATED BY A VARIATIONAL METHOD

	Sym. st. cm^{-1}	Bend cm^{-1}	Asym. st. cm^{-1}
Theoretical (Ref. 76)	1098	707	1043
Experiment[a]	1103	701	1042

(a) Reference (82).

$V_{O_2}(R_5)$ and $V_{NO}(R_7)$ are simple Morse functions for the corresponding diatomic species given by

$$V_{AB}(R_i) = D_{AB} \{\exp(-2\alpha_{AB}(R_i - R_e)) - 2.0 \exp(-\alpha_{AB}(R_i - R_e))\} \quad \text{(II-33)}$$

In the case of the N-O bond, both D_{AB} and R_e are variables and are functions of the N-O bond distance that is being formed or broken as the reaction proceeds. The functional forms for these parameters have been given earlier in Eq (II-10) to (II-13).

The bending potential, $V_{NO_2}(\theta_i)$ of the NO_2 molecule has been assumed to have a harmonic form,

$$V_{NO_2}(\theta_i) = 0.5\ k_{bi}(\theta_i - \theta_e)^2 \quad \text{(II-34)}$$

where θ_i is the O-N-O angle in the NO_2 molecule. k_{bi} is not a constant, but attenuates as the N-O bond in the NO_2 molecule is being stretched. It should be noted that the nature of the attenuation will have a strong influence on the calculated cross sections. In order to obtain information about the attenuation of the bending forces, semi-empirical quantum mechanical calculations have been carried out.

The force constant k_{bi} has been computed under the assumption of a harmonic potential between the bonds. That is, for a given finite angular displacement, $\Delta\theta = \theta_i - \theta_e$, we define

$$\Delta E = 0.5\ k_{bi}(\theta_i - \theta_e)^2 \quad \text{(II-35)}$$

For various asymmetrically stretched configurations of the NO_2 molecule, the ΔE values have been computed as a function of the displacement from the equilibrium angle using INDO open shell methods. The k_{bi}'s were

then evaluated from Eq (II-35) for every $\Delta\theta$ value. The results were then extrapolated to $\Delta\theta \rightarrow 0$ to obtain k_{bi} as a function of R_i. For the equilibrium configuration of NO_2(R_i = 2.25754 au), this yielded a value of 1.646 mdyne $\mathring{A}$/rad^2 for the force constant, k^o_{bi}, which compares very well with the valence force field value of 1.624 mdyne $\mathring{A}$/rad^2 (78). The values of k_{bi}/k^o_{bi} evaluated by these procedures are given in Table XII. These were fitted to the following functional form by using a non-linear least squares technique.

TABLE XII

INDO COMPUTED VARIATION OF O-N-O BENDING FORCE CONSTANT AS A FUNCTION OF R_{N-O}

R_{NO}/au[a]	k_{bi}/mdyne $\mathring{A}$/rad^2	k_{bi}/k^o_{bi}
2.2583	1.646	1.0
2.3818	0.82	0.4982
2.4575	0.7156	0.4347

(a) The other N-O bond in NO_2 was fixed at the equilibrium value.

$$k_{bi}/k^o_{bi} = 4.32629\{\exp\{-0.95627(R_i - 2.25754)\}\} \qquad \text{(II-36)}$$

where R_i is the shorter of R_2, R_6 and R_3, which is the newly formed N-O bond.

The equilibrium angle, θ_e, has been computed for the NO_2 molecule as a function of R_i. It has been observed that θ_e decreases linearly as one of the N-O bonds in NO_2 is stretched. The results are shown in Table XIII and Figure 2. These results have been fitted to the following functional form by a linear least squares procedure.

$$\theta_e = 2.40855 - 0.458367(R_i - 2.2583),$$
$$i = 2, 3 \text{ or } 6 \qquad \text{(II-37)}$$

R_i are in au and θ_e is given in radians.

TABLE XIII

INDO COMPUTATIONS OF THE VARIATION OF THE EQUILIBRIUM ANGLE IN NO_2 AS A FUNCTION OF R_{N-O}

R_{N-O}/au[a]	θ_e/deg
2.2583	138
2.3818	136
2.4575	132

(a) The other N-O bond in NO_2 was fixed at the equilibrium value.

$V_{oo}(R_i)$ are the short-range repulsive interactions operating between pairs of oxygen atoms, among which no bond formation occurs.

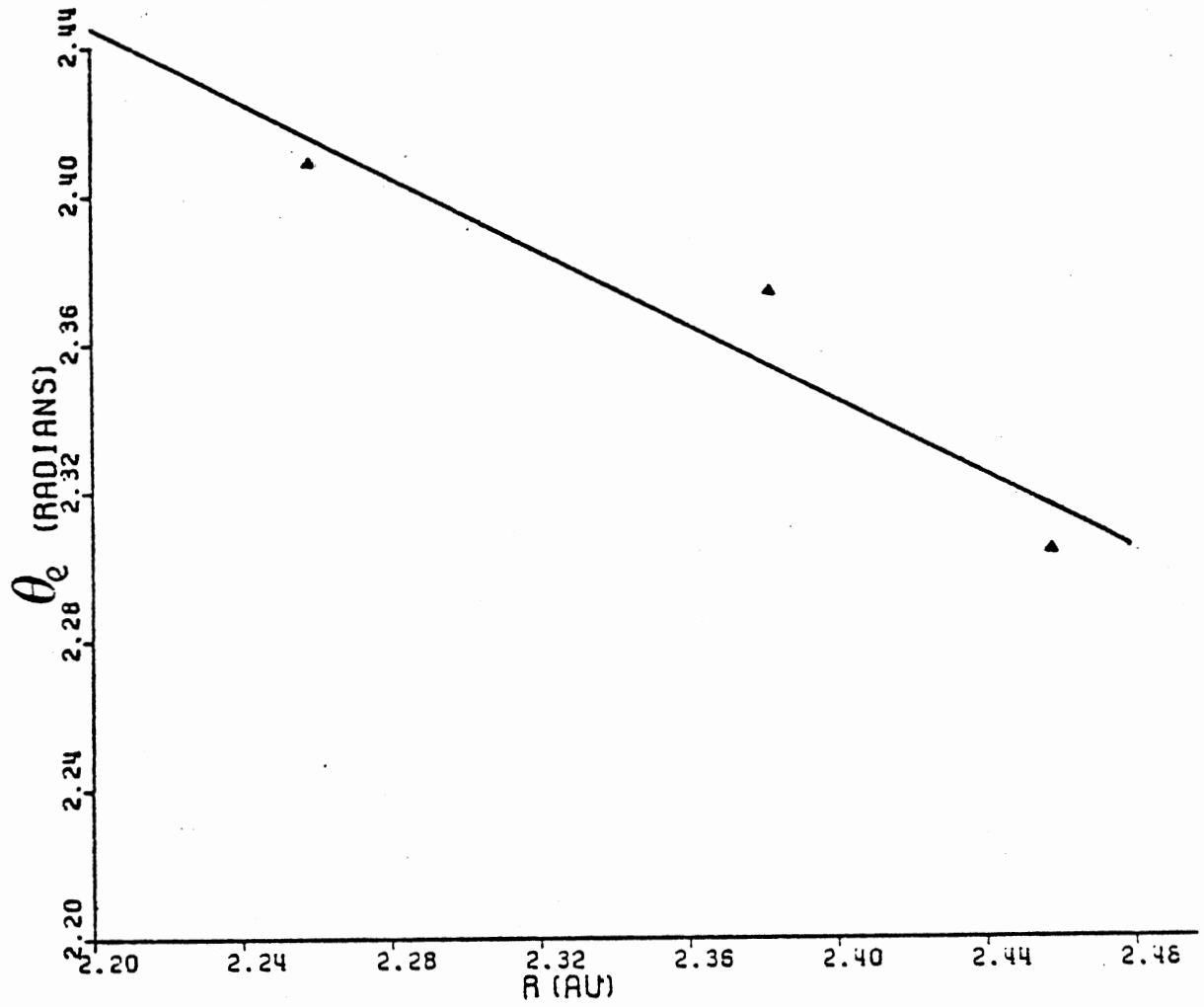

Figure 2. Variation of the Equilibrium Angle in NO_2 with R_{N-O}.

These have been assumed to be of the following form:

$$V_{oo}(R_i) = \exp(-1.8511\ R_i^2), \quad i = 8,\ 9 \text{ and } 10 \qquad \text{(II-38)}$$

where R_i is the internuclear distance in $\mathring{A}$.

$V_{att}(R_i, R_3)$ is an attenuation term described by,

$$V_{att}(R_i, R_3) = V_{O_2}(R_i)\{\tanh\ \ 2.0(R_3 - R_3^0) - 1\} \qquad \text{(II-39)}$$

where R_i is the shorter of the two O-O bonds in ozone. This term operates whenever the N atom approaches the central oxygen atom in O_3 ($R_3 \approx R_3^0$). When the N atom approaches the central oxygen atom, one of the O-O bonds in O_3 is stretched (since the V_I term becomes highly repulsive whenever all three atoms are close to one another), while the other O-O bond is not significantly affected. This will eventually lead to the formation of NO_3 + O, which is not desired. The V_{att} (R_i, R_3) term functions by attenuating the interaction between the shorter of the two O-O bonds in ozone, which would require a bond formation between ^1O and ^2O. This term enables us to leave open the channel leading to reaction through attack of N on the central oxygen atom.

In order to study the effect of changing the barrier height of the potential-energy surface on the observed reaction dynamics, four different surfaces have been employed. These have been denoted S1, S2, S3 and S4. These surfaces show a marked difference in the barrier heights, without a significant alteration of other surface features. Surface S1 has been obtained by using a value of Z = 3.2 with $V_{att}(R_i, R_3)$ set equal to zero. The three-body interaction potentials,

V_I, have been interpolated using a three-dimensional cubic-spline technique (79), while carrying out classical trajectory calculations on this surface, S1. Surfaces S2, S3 and S4 have been obtained by using Eq (II-1) for the total potential, and with Z values 3.2, 3.4 and 3.8, respectively.

It has been observed that the position of the saddle point plays a major role in determining the reaction dynamics, at least in the case of atom-diatomic molecule reactions (18). In order to study the effect of changing the saddle-point position on polyatomic reaction dynamics, a surface, S5, has been formulated which has approximately the same barrier height as S3 but differs in the location of the barrier. To obtain surface S5, the potential V_I has been replaced by a numerical grid of values that have been interpolated by using a three-dimensional cubic spline technique (79). The numerical grid of node values employed is given in Table XIV.

Contour maps of two-dimensional sections of these multi-dimensional hypersurfaces have been drawn by imposing suitable constraints on the coordinates. Representative maps of each of these surfaces are shown in Figures 3 to 10. The angles β, θ (see Figure 1) and the bond distances R_4 and R_7 have been fixed at their respective equilibrium values.

The contour lines have been plotted as a function of R_1 and R_2 for various α values. The maps shown correspond to the α values for the minimum energy path. The maps of the surfaces not shown are quite similar in appearance. Reactants enter from the top of the figure and products exit from the right. The saddle point geometries have been determined correct to $\pm$ 0.01 au, using a two-dimensional spline

TABLE XIV

THE THREE-BODY INTERACTION POTENTIAL, V_I, FOR O_3 -NO. ENERGIES ARE IN EV, DISTANCES ARE IN Å AND ANGLES ARE IN RADIANS

$R_2(R_6)$	α = 0.34	α = 0.69	α = 1.04	α = 1.39	α = 1.57
		A. $R_1(R_4)$ = 1.50			
1.50	51.6813	40.2296	33.4288	26.1775	25.3337
2.34	22.8973	17.1424	12.8334	12.0923	11.9955
2.62	19.9985	15.1877	12.7973	12.5362	12.4360
2.90	17.9111	14.0795	13.2957	13.2023	13.1475
3.18	15.7087	14.0038	14.1110	14.1335	14.0699
3.36	14.6161	14.1335	14.5237	14.5651	14.4938
3.64	14.1672	14.5047	15.1924	15.1410	15.0588
4.20	14.6702	15.2366	15.5580	15.4869	15.4617
4.76	15.3234	15.4993	15.5319	15.5305	15.5309
5.32	15.5176	15.5409	15.5524	15.5601	15.5629
6.10	15.5646	15.5719	15.5791	15.5840	15.5855
7.50	15.5928	15.5945	15.5959	15.5968	15.5971
12.00	15.5990	15.5990	15.5990	15.5990	15.5990
25.00	15.5990	15.5990	15.5990	15.5990	15.5990

$R_2(R_6)$	α = 1.74	α = 1.90	α = 2.44	α = 2.79	α = 3.14
		A. $R_1(R_4)$ = 1.50			
1.50	25.1620	25.1767	25.5346	25.6649	25.7068
2.34	11.9360	11.8645	11.7091	11.6811	11.6737
2.62	12.3816	12.3340	12.2321	12.2153	12.2111
2.90	13.0884	13.0453	12.9822	12.9723	12.9700
3.18	14.0159	13.9806	13.9332	13.9261	13.9244
3.36	14.4423	14.4108	14.3696	14.3634	14.3619
3.64	15.0107	14.9832	14.9496	14.9444	14.9431
4.20	15.4482	15.4406	15.4331	15.4321	15.4319
4.76	15.5319	15.5329	15.5352	15.5359	15.5361
5.32	15.5649	15.5663	15.5687	15.5693	15.5694
6.10	15.5865	15.5872	15.5882	15.5885	15.5885
7.50	15.5972	15.5973	15.5975	15.5975	15.5975
12.00	15.5990	15.5990	15.5990	15.5990	15.5990
25.00	15.5990	15.5990	15.5990	15.5990	15.5990

TABLE XIV (Continued)

$R_2(R_6)$	α = 0.34	α = 0.69	α = 1.04	α = 1.39	α = 1.57
		B. $R_1(R_4)$ = 2.34			
1.50	20.2301	12.1733	6.6849	6.0943	6.1119
2.34	8.6607	-0.8370	-3.7363	-4.7627	-5.1824
2.62	7.0484	-1.4464	-4.0203	-4.9831	-5.2665
2.90	4.8584	-2.2252	-4.2403	-5.0099	-5.2021
3.18	2.9225	-3.2042	-4.4071	-4.9347	-5.0403
3.36	1.6502	-3.7112	-4.5084	-4.9217	-4.9889
3.64	-0.7848	-4.3163	-4.7776	-4.9982	-5.0264
4.20	-4.1830	-4.7174	-4.9382	-4.9878	-4.9869
4.76	-4.7587	-4.9183	-4.9974	-4.9949	-4.9895
5.32	-4.9601	-5.0430	-5.0529	-5.0408	-5.0366
6.10	-5.2105	-5.2122	-5.2000	-5.1921	-5.1901
7.50	-5.1913	-5.1855	-5.1815	-5.1799	-5.1796
12.00	-5.1778	-5.1778	-5.1778	-5.1778	-5.1778
25.00	-5.1778	-5.1778	-5.1778	-5.1778	-5.1778

$R_2(R_6)$	α = 1.74	α = 1.90	α = 2.44	α = 2.79	α = 3.14
		B. $R_1(R_4)$ = 2.34			
1.50	6.1481	6.1785	6.2422	6.2636	6.2703
2.34	-5.3902	-5.5014	-5.6431	-5.6632	-5.6682
2.62	-5.4147	-5.4917	-5.5752	-5.5863	-5.5889
2.90	-5.2944	-5.3398	-5.0836	-5.0888	-5.0899
3.18	-5.0863	-5.1078	-4.8229	-4.8240	-4.8242
3.36	-5.0157	-5.0278	-4.7323	-4.6521	-4.6521
3.64	-5.0347	-5.0374	-4.7340	-4.7329	-4.7326
4.20	-4.9836	-4.9808	-4.6754	-4.6743	-4.6740
4.76	-4.9857	-4.9832	-4.8797	-4.7791	-4.6789
5.32	-5.0342	-5.0327	-5.0308	-5.0305	-5.0304
6.10	-5.1891	-5.1885	-5.1878	-5.1877	-5.1876
7.50	-5.1794	-5.1793	-5.1792	-5.1792	-5.1792
12.00	-5.1778	-5.1778	-5.1778	-5.1778	-5.1778
25.00	-5.1778	-5.1778	-5.1778	-5.1778	-5.1788

TABLE XIV (Continued)

$R_2(R_6)$	α = 0.34	α = 0.69	α = 1.04	α = 1.39	α = 1.57
		C. $R_1(R_4)$ = 2.62			
1.50	16.7270	9.2149	6.6349	6.6144	6.6603
2.34	6.6448	-1.8762	-4.4596	-5.4088	-5.6894
2.62	6.7594	-1.9584	-4.3456	-5.3032	-5.5368
2.90	5.6974	-2.1950	-4.2420	-5.0922	-5.2616
3.18	4.5022	-2.6835	-3.9230	-4.5258	-4.6243
3.36	3.3516	-3.2419	-4.0952	-4.5034	-4.5667
3.64	1.5760	-3.7544	-4.1956	-4.4184	-4.4444
4.20	-3.1266	-4.2564	-4.4398	-4.4882	-4.4866
4.76	-4.3020	-4.4009	-4.4887	-4.4849	-4.4795
5.32	-4.3567	-4.4483	-4.4629	-4.4498	-4.4456
6.10	-4.4901	-4.5010	-4.4872	-4.4785	-4.4765
7.50	-4.4819	-4.4737	-4.4685	-4.4666	-4.4663
12.00	-4.4646	-4.4646	-4.4645	-4.4645	-4.4645
25.00	-4.4645	-4.4645	-4.4645	-4.4645	-4.4645

$R_2(R_6)$	α = 1.74	α = 1.90	α = 2.44	α = 2.79	α = 3.14
		C. $R_1(R_4)$ = 2.62			
1.50	6.7592	6.8213	6.9024	6.9274	6.9350
2.34	-5.8362	-5.9124	-5.9952	-6.0062	-6.0086
2.62	-5.6480	-5.7030	-5.9566	-5.9634	-5.9648
2.90	-5.3362	-5.3719	-5.3026	-5.3062	-5.3070
3.18	-4.6643	-4.6832	-4.3447	-4.3958	-4.3960
3.36	-4.5904	-4.6012	-4.2550	-4.3051	-4.3050
3.64	-4.4516	-4.4546	-4.1516	-4.1508	-4.1506
4.20	-4.4834	-4.4812	-4.1766	-4.1758	-4.1756
4.76	-4.4760	-4.4738	-4.3710	-4.2705	-4.1704
5.32	-4.4433	-4.4420	-4.4405	-4.4403	-4.4402
6.10	-4.4756	-4.4751	-4.4745	-4.4744	-4.4743
7.50	-4.4661	-4.4660	-4.4660	-4.4660	-4.4660
12.00	-4.4645	-4.4645	-4.4645	-4.4645	-4.4645
25.00	-4.4645	-4.4645	-4.4645	-4.4645	-4.4645

TABLE XIV (Continued)

$R_2(R_6)$	α = 0.34	α = 0.69	α = 1.04	α = 1.39	α = 1.57
		D. $R_1(R_4)$ = 2.90			
1.50	12.8988	7.9284	7.2422	7.4493	7.5968
2.34	4.5900	-2.7032	-4.6820	-5.3922	-5.5728
2.62	5.7050	-2.4667	-4.4151	-5.1941	-5.3531
2.90	6.0033	-2.0413	-3.9247	-4.7351	-4.8633
3.18	5.4700	-2.3598	-3.5515	-4.1704	-4.2575
3.36	4.8995	-2.6290	-3.3281	-3.7868	-3.8462
3.64	3.5379	-3.0520	-3.3323	-3.5681	-3.5935
4.20	-0.9039	-3.4252	-3.4950	-3.5418	-3.5403
4.76	-3.4835	-3.4547	-3.5201	-3.5150	-3.5098
5.32	-3.5355	-3.4914	-3.5033	-3.4892	-3.4853
6.10	-3.4813	-3.4931	-3.4776	-3.4682	-3.4663
7.50	-3.4763	-3.4654	-3.4587	-3.4567	-3.4563
12.00	-3.4547	-3.4547	-3.4546	-3.4546	-3.4546
25.00	-3.4546	-3.4546	-3.4546	-3.4546	-3.4546

$R_2(R_6)$	α = 1.74	α = 1.90	α = 2.44	α = 2.79	α = 3.14
		D. $R_1(R_4)$ = 2.90			
1.50	7.6880	7.7459	7.8480	7.8732	7.8807
2.34	-5.6594	-5.7018	-5.7422	-5.7468	-5.7478
2.62	-5.4231	-5.4564	-5.6843	-5.6875	-5.6881
2.90	-4.9159	-4.9407	-4.8587	-4.8607	-4.8611
3.18	-4.2909	-4.3070	-4.1156	-4.1366	-4.1368
3.36	-3.8676	-3.8783	-3.5814	-3.5818	-3.5818
3.64	-3.6008	-3.6048	-3.6025	-3.6021	-3.6020
4.20	-3.5376	-3.5363	-3.5325	-3.5319	-3.5318
4.76	-3.5066	-3.5047	-3.5026	-3.5023	-3.5022
5.32	-3.4832	-3.4821	-3.4809	-3.4807	-3.4807
6.10	-3.4654	-3.4650	-3.4645	-3.4644	-3.4644
7.50	-3.4562	-3.4562	-3.4560	-3.4560	-3.4560
12.00	-3.4546	-3.4546	-3.4546	-3.4546	-3.4546
25.00	-3.4546	-3.4546	-3.4546	-3.4546	-3.4546

TABLE XIV (Continued)

$R_2(R_6)$	α = 0.34	α = 0.69	α = 1.04	α = 1.39	α = 1.57
		E. $R_1(R_4)$ = 3.18			
1.50	9.4871	7.7917	7.9337	8.2960	8.4382
2.34	2.9122	-3.4345	-4.5708	-5.0498	-5.1465
2.62	4.3522	-3.1819	-4.3190	-4.8437	-4.9305
2.90	5.4938	-2.7398	-3.7814	-4.3005	-4.3765
3.18	5.8964	-2.4700	-3.0528	-3.6007	-3.6654
3.36	5.8757	-2.3762	-2.5890	-3.0654	-3.1167
3.64	4.9910	-2.6052	-2.4699	-2.7415	-2.7681
4.20	1.9120	-2.7744	-2.5809	-2.6297	-2.6295
4.76	-2.7025	-2.6496	-2.5987	-2.5927	-2.5881
5.32	-3.0055	-2.5936	-2.5809	-2.5662	-2.5626
6.10	-2.6305	-2.5746	-2.5555	-2.5456	-2.5438
7.50	-2.5594	-2.5449	-2.5367	-2.5344	-2.5341
12.00	-2.5325	-2.5325	-2.5324	-2.5324	-2.5324
25.00	-2.5324	-2.5324	-2.5324	-2.5324	-2.5324

$R_2(R_6)$	α = 1.74	α = 1.90	α = 2.44	α = 2.79	α = 3.14
		E. $R_1(R_4)$ = 3.18			
1.50	8.5266	8.5841	8.6829	8.7063	8.7131
2.34	-5.1882	-5.2075	-5.2199	-5.2206	-5.2207
2.62	-4.9652	-4.9813	-4.9897	-4.9902	-4.9903
2.90	-4.4051	-4.4187	-4.4247	-4.4253	-4.4254
3.18	-3.6887	-3.7013	-3.7049	-3.7055	-3.7056
3.36	-3.1345	-3.1450	-3.1463	-3.1467	-3.1468
3.64	-2.7762	-2.7821	-2.7801	-2.7801	-2.7801
4.20	-2.6278	-2.6281	-2.6245	-2.6241	-2.6241
4.76	-2.5855	-2.5841	-2.5824	-2.5822	-2.5821
5.32	-2.5608	-2.5598	-2.5590	-2.5588	-2.5588
6.10	-2.5430	-2.5426	-2.5423	-2.5422	-2.5422
7.50	-2.5340	-2.5340	-2.5338	-2.5338	-2.5338
12.00	-2.5324	-2.5324	-2.5324	-2.5324	-2.5324
25.00	-2.5324	-2.5324	-2.5324	-2.5324	-2.5324

TABLE XIV (Continued)

$R_2(R_6)$	α = 0.34	α = 0.69	α = 1.04	α = 1.39	α = 1.57
		F. $R_1(R_4)$ = 3.36			
1.50	8.5357	7.9987	8.3510	8.7598	8.8909
2.34	1.5565	-3.9855	-4.7203	-5.0926	-5.1530
2.62	3.3092	-3.5857	-4.3631	-4.7116	-4.7653
2.90	4.8830	-2.9894	-3.6336	-4.0054	-4.0532
3.18	5.7722	-2.6191	-2.8493	-3.2545	-3.2998
3.36	5.9722	-2.4927	-2.3850	-2.7919	-2.8322
3.64	5.5547	-2.5147	-2.0520	-2.3440	-2.3698
4.20	3.2100	-2.5273	-2.0937	-2.1474	-2.1484
4.76	-2.0485	-2.3035	-2.1058	-2.0999	-2.0959
5.32	-2.8735	-2.1370	-2.0873	-2.0724	-2.0691
6.10	-2.2523	-2.0857	-2.0620	-2.0520	-2.0503
7.50	-2.0704	-2.0528	-2.0434	-2.0410	-2.0407
12.00	-2.0392	-2.0391	-2.0391	-2.0391	-2.0391
25.00	-2.0391	-2.0391	-2.0391	-2.0391	-2.0391

$R_2(R_6)$	α = 1.74	α = 1.90	α - 2.44	α = 2.79	α = 3.14
		F. $R_1(R_4)$ = 3.36			
1.50	8.9736	9.0279	9.1190	9.1401	9.1462
2.34	-5.1763	-5.1866	-5.1890	-5.1885	-5.1883
2.62	-4.7845	-4.7930	-4.7941	-4.7938	-4.7937
2.90	-4.0695	-4.0776	-4.0780	-4.0779	-4.0779
3.18	-3.3152	-3.3242	-3.3245	-3.3248	-3.3248
3.36	-2.8456	-2.8546	-2.8540	-2.8542	-2.8543
3.64	-2.3778	-2.3846	-2.3822	-2.3823	-2.3823
4.20	-2.1475	-2.1490	-2.1453	-2.1451	-2.1451
4.76	-2.0936	-2.0928	-2.0911	-2.0909	-2.0909
5.32	-2.0675	-2.0665	-2.0659	-2.0658	-2.0658
6.10	-2.0496	-2.0493	-2.0489	-2.0489	-2.0489
7.50	-2.0406	-2.0405	-2.0405	-2.0405	-2.0405
12.00	-2.0391	-2.0391	-2.0391	-2.0391	-2.0391
25.00	-2.0391	-2.0391	-2.0391	-2.0391	-2.0391

TABLE XIV (Continued)

$R_2(R_6)$	α = 0.34	α = 0.69	α = 1.04	α = 1.39	α = 1.57
		G. $R_1(R_4)$ = 3.64			
1.50	8.2769	8.4751	8.9901	9.3424	9.4519
2.34	-0.9245	-4.4999	-4.9222	-5.1254	-5.1506
2.62	1.4791	-3.9707	-4.3836	-4.5797	-4.6011
2.90	3.4464	-3.3253	-3.6332	-3.8257	-3.8444
3.18	4.9809	-2.7212	-2.6808	-2.8913	-2.9110
3.36	5.5227	-2.5767	-2.2468	-2.4742	-2.4944
3.64	5.7743	-2.4790	-1.7010	-1.9465	-1.9653
4.20	4.3933	-2.3207	-1.4998	-1.5692	-1.5725
4.76	-0.5447	-2.0008	-1.4984	-1.4945	-1.4916
5.32	-2.7566	-1.6386	-1.4788	-1.4641	-1.4613
6.10	-2.1474	-1.4923	-1.4539	-1.4437	-1.4423
7.50	-1.4748	-1.4470	-1.4356	-1.4331	-1.4328
12.00	-1.4314	-1.4313	-1.4312	-1.4312	-1.4312
25.00	-1.4312	-1.4312	-1.4312	-1.4312	-1.4312

$R_2(R_6)$	α = 1.74	α = 1.90	α = 2.44	α = 2.79	α = 3.14
		G. $R_1(R_4)$ = 3.64			
1.50	9.5217	9.5673	9.6427	9.6597	9.6646
2.34	-5.1574	-5.1594	-5.1550	-5.1537	-5.1534
2.62	-4.6062	-4.6080	-4.6037	-4.6028	-4.6025
2.90	-3.8487	-3.8511	-3.8472	-3.8467	-3.8465
3.18	-2.9162	-2.9203	-2.9173	-2.9171	-2.9170
3.36	-2.5001	-2.5053	-2.5024	-2.5023	-2.5023
3.64	-1.9709	-1.9771	-1.9739	-1.9739	-1.9739
4.20	-1.5728	-1.5759	-1.5722	-1.5721	-1.5721
4.76	-1.4900	-1.4903	-1.4883	-1.4882	-1.4882
5.32	-1.4600	-1.4594	-1.4588	-1.4588	-1.4588
6.10	-1.4417	-1.4413	-1.4412	-1.4411	-1.4411
7.50	-1.4327	-1.4327	-1.4326	-1.4326	-1.4326
12.00	-1.4312	-1.4312	-1.4312	-1.4312	-1.4312
25.00	-1.4312	-1.4312	-1.4312	-1.4312	-1.4312

TABLE XIV (Continued)

$R_2(R_6)$	α = 0.34	α = 0.69	α = 1.04	α = 1.39	α = 1.57
		H. $R_1(R_4)$ = 4.20			
1.50	9.0298	9.4693	9.8645	10.0919	10.1569
2.34	-4.3196	-4.8413	-5.0518	-5.0988	-5.0974
2.62	-3.1573	-4.3038	-4.4886	-4.5331	-4.5308
2.90	-1.0746	-3.6019	-3.7127	-3.7532	-3.7505
3.18	1.7621	-2.8364	-2.7297	-2.7685	-2.7667
3.36	3.0883	-2.5672	-2.2640	-2.3039	-2.3029
3.64	4.3694	-2.2968	-1.6026	-1.6518	-1.6529
4.20	5.0445	-2.0456	-0.8753	-0.9543	-0.9580
4.76	3.2774	-1.6429	-0.7497	-0.7605	-0.7602
5.32	-1.8574	-1.2353	-0.7253	-0.7141	-0.7124
6.10	-2.4250	-0.8325	-0.7017	-0.6921	-0.6911
7.50	-0.8829	-0.7016	-0.6845	-0.6820	-0.6817
12.00	-0.6804	-0.6802	-0.6802	-0.6802	-0.6802
25.00	-0.6802	-0.6802	-0.6802	-0.6802	-0.6802

$R_2(R_6)$	α = 1.74	α = 1.98	α = 2.44	α = 2.79	α = 3.14
		H. $R_1(R_4)$ = 4.20			
1.50	10.1984	10.2254	10.2687	10.2782	10.2808
2.34	-5.0939	-5.0909	-5.0855	-5.0844	-5.0841
2.62	-4.5272	-4.5247	-4.5201	-4.5192	-4.5190
2.90	-3.7473	-3.7456	-3.7415	-3.7409	-3.7408
3.18	-2.7643	-2.7641	-2.7603	-2.7599	-2.7598
3.36	-2.3011	-2.3019	-2.2981	-2.2979	-2.2978
3.64	-1.6524	-1.6548	-1.6510	-1.6509	-1.6509
4.20	-0.9589	-0.9631	-0.9593	-0.9593	-0.9593
4.76	-0.7599	-0.7624	-0.7595	-0.7595	-0.7595
5.32	-0.7117	-0.7120	-0.7112	-0.7111	-0.7111
6.10	-0.6906	-0.6902	-0.6904	-0.6903	-0.6903
7.50	-0.6816	-0.6816	-0.6816	-0.6816	-0.6816
12.00	-0.6802	-0.6802	-0.6802	-0.6802	-0.6802
25.00	-0.6802	-0.6802	-0.6802	-0.6802	-0.6802

TABLE XIV (Continued)

$R_2(R_6)$	α = 0.34	α = 0.69	α = 1.04	α = 1.39	α = 1.57
		I. $R_1(R_4)$ = 4.76			
1.50	9.8705	10.1422	10.3564	10.4742	10.5082
2.34	-4.8139	-4.9683	-5.0458	-5.0430	-5.0376
2.62	-4.2680	-4.3883	-4.4787	-4.4746	-4.4691
2.90	-3.5392	-3.6143	-3.6971	-3.6913	-3.6860
3.18	-2.6362	-2.7173	-2.7073	-2.7002	-2.6954
3.36	-1.9837	-2.3629	-2.2369	-2.2293	-2.2250
3.64	-0.4712	-1.9743	-1.5664	-1.5599	-1.5566
4.20	3.2928	-1.6129	-0.7684	-0.7741	-0.7733
4.76	3.4434	-1.3718	-0.4255	-0.4486	-0.4493
5.32	-0.2584	-1.0500	-0.3584	-0.3563	-0.3559
6.10	-2.5687	-0.6323	-0.3352	-0.3276	-0.3269
7.50	-1.0940	-0.3495	-0.3197	-0.3173	-0.3171
12.00	-0.3162	-0.3157	-0.3156	-0.3156	-0.3156
25.00	-0.3156	-0.3156	-013156	-013156	-0.3156

$R_2(R_6)$	α = 1.74	α = 1.90	α = 2.44	α = 2.79	α = 3.14
		I. $R_1(R_4)$ = 4.76			
1.50	10.5298	10.5437	10.5657	10.5704	10.5717
2.34	-5.0338	-5.0313	-5.0278	-5.0271	-5.0270
2.62	-4.4655	-4.4633	-4.4604	-4.4599	-4.4598
2.90	-3.6827	-3.6807	-3.6786	-3.6783	-3.6782
3.18	-2.6926	-2.6912	-2.6894	-2.6892	-2.6891
3.36	-2.2226	-2.2217	-2.2200	-2.2198	-2.2197
3.64	-1.5548	-1.5549	-1.5530	-1.5529	-1.5528
4.20	-0.7728	-0.7751	-0.7723	-0.7723	-0.7723
4.76	-0.4495	-0.4523	-0.4495	-0.4495	-0.4495
5.31	-0.3557	-0.3569	-0.3555	-0.3555	-0.3555
6.10	-0.3267	-0.3266	-0.3265	-0.3265	-0.3265
7.50	-0.3171	-0.3169	-0.3170	-0.3170	-0.3170
12.00	-0.3156	-0.3156	-0.3156	-0.3156	-0.3156
25.00	-0.3156	-0.3156	-0.3156	-0.3156	-0.3156

TABLE XIV (Continued)

$R_2(R_6)$	α = 0.34	α = 0.69	α = 1.04	α = 1.39	α = 1.57
		J. $R_1(R_4)$ = 5.32			
1.50	10.3726	10.4989	10.6018	10.6594	10.6761
2.34	-4.9232	-5.0051	-5.0149	-5.0028	-4.9986
2.62	-4.3309	-4.4322	-4.4478	-4.4346	-4.4304
2.90	-3.6371	-3.6490	-3.6655	-3.6514	-3.6475
3.18	-2.9719	-2.6761	-2.6747	-2.6599	-2.6563
3.36	-2.8155	-2.2321	-2.2035	-2.1885	-2.1851
3.64	-2.6596	-1.6528	-1.5319	-1.5171	-1.5142
4.20	-1.8072	-1.1999	-0.7305	-0.7190	-0.7172
4.76	-0.2440	-1.0363	-0.3557	-0.3531	-0.3526
5.32	-0.3273	-0.8392	-0.2002	-0.2065	-0.2066
6.10	-2.3022	-0.5404	-0.1625	-0.1581	-0.1578
7.50	-1.5670	-0.2112	-0.1487	-0.1466	-0.1464
12.00	-0.1460	-0.1451	-0.1450	-0.1449	-0.1449
25.00	-0.1449	-0.1449	-0.1449	-0.1449	-0.1449

$R_2(R_6)$	α = 1.74	α = 1.90	α = 2.44	α = 2.79	α = 3.14
		J. $R_1(R_4)$ = 5.32			
1.50	10.6866	10.6933	10.7039	10.7061	10.7067
2.34	-4.9961	-4.9947	-4.9928	-4.9925	-4.9924
2.62	-4.4281	-4.4268	-4.4253	-4.4251	-4.4250
2.90	-3.6454	-3.6442	-3.6430	-3.6429	-3.6428
3.18	-2.6545	-2.6535	-2.6526	-2.6525	-2.6524
3.36	-2.1835	-2.1826	-2.1819	-2.1818	-2.1818
3.64	-1.5129	-1.5122	-1.5117	-1.5116	-1.5116
4.20	-0.7165	-0.7167	-0.7159	-0.7159	-0.7159
4.76	-0.3524	-0.3536	-0.3522	-0.3522	-0.3522
5.32	-0.2066	-0.2078	-0.2066	-0.2066	-0.2066
6.10	-0.1577	-0.1578	-0.1576	-0.1576	-0.1576
7.50	-0.1464	-0.1462	-0.1464	-0.1464	-0.1464
12.00	-0.1449	-0.1449	-0.1449	-0.1449	-0.1449
25.00	-0.1449	-0.1449	-0.1449	-0.1449	-0.1449

TABLE XIV (Continued)

$R_2(R_6)$	α = 0.34	α = 0.69	α = 1.04	α = 1.39	α = 1.57
		K. $R_1(R_4)$ = 6.10			
1.50	10.6678	10.7105	10.7461	10.7663	10.7721
2.34	-4.9931	-4.9948	-4.9825	-4.9746	-4.9727
2.62	-4.4175	-4.4293	-4.4157	-4.4069	-4.4050
2.90	-3.6297	-3.6487	-3.6338	-3.6243	-3.6225
3.18	-2.6898	-2.6610	-2.6432	-2.6333	-2.6316
3.36	-2.3011	-2.1934	-2.1722	-2.1622	-2.1605
3.64	-2.0873	-1.5342	-1.5010	-1.4909	-1.4894
4.20	-2.3709	-0.8168	-0.7008	-0.6914	-0.6903
4.76	-2.5483	-0.6146	-0.3264	-0.3189	-0.3182
5.32	-2.2961	-0.5340	-0.1557	-0.1517	-0.1514
6.10	-2.2354	-0.3973	-0.0680	-0.0689	-0.0689
7.50	-2.1222	-0.1627	-0.0518	-0.0503	-0.0502
12.00	-0.0518	-0.0489	-0.0487	-0.0487	-0.0487
25.00	-0.0487	-0.0487	-0.0487	-0.0487	-0.0487

$R_2(R_6)$	α = 1.74	α = 1.90	α = 2.44	α = 2.79	α = 3.14
		K. $R_1(R_4)$ = 6.10			
1.50	10.7758	10.7781	10.7818	10.7825	10.7827
2.34	-4.9716	-4.9710	-4.9703	-4.9702	-4.9702
2.62	-4.4040	-4.4035	-4.4029	-4.4028	-4.4028
2.90	-3.6216	-3.6212	-3.6207	-3.6206	-3.6206
3.18	-2.6308	-2.6304	-2.6300	-2.6300	-2.6300
3.36	-2.1598	-2.1595	-2.1591	-2.1591	-2.1591
3.64	-1.4888	-1.4884	-1.4883	-1.4883	-1.4882
4.20	-0.6899	-0.6895	-0.6896	-0.6896	-0.6896
4.76	-0.3180	-0.3179	-0.3178	-0.3178	-0.3178
5.32	-0.1513	-0.1514	-0.1513	-0.1513	-0.1513
6.10	-0.0689	-0.0690	-0.0689	-0.0689	-0.0689
7.50	-0.0502	-0.0499	-0.0502	-0.0502	-0.0502
12.00	-0.0487	-0.0487	-0.0487	-0.0487	-0.0487
25.00	-0.0487	-0.0487	-0.0487	-0.0487	-0.0487

TABLE XIV (Continued)

$R_2(R_6)$	α = 0.34	α = 0.69	α = 1.04	α = 1.39	α = 1.57
		L. $R_1(R_4)$ = 7.50			
1.50	10.7999	10.8056	10.8106	10.8134	10.8142
2.34	-4.9720	-4.9662	-4.9622	-4.9606	-4.9602
2.62	-4.4084	-4.4003	-4.3951	-4.3932	-4.3929
2.90	-3.6305	-3.6197	-3.6130	-3.6110	-3.6106
3.18	-2.6449	-2.6308	-2.6225	-2.6203	-2.6199
3.36	-2.1779	-2.1611	-2.1517	-2.1493	-2.1490
3.64	-1.5175	-1.4922	-1.4808	-1.4784	-1.4781
4.20	-0.8608	-0.6986	-0.6818	-0.6793	-0.6791
4.76	-1.0729	-0.3380	-0.3090	-0.3066	-0.3064
5.32	-1.5590	-0.2025	-0.1399	-0.1378	-0.1377
6.10	-2.1203	-0.1604	-0.0473	-0.0459	-0.0458
7.50	-2.3047	-0.1002	-0.0094	-0.0094	-0.0094
12.00	-0.0522	-0.0074	-0.0068	-0.0068	-0.0068
25.00	-0.0068	-0.0068	-0.0068	-0.0068	-0.0068

$R_2(R_6)$	α = 1.74	α = 1.90	α = 2.44	α = 2.79	α = 3.14
		L. $R_1(R_4)$ = 7.50			
1.50	10.8147	10.8150	10.8156	10.8157	10.8157
2.34	-4.9601	-4.9600	-4.9599	-4.9599	-4.9598
2.62	-4.3927	-4.3926	-4.3926	-4.3925	-4.3925
2.90	-3.6105	-3.6105	-3.6103	-3.6103	-3.6103
3.18	-2.6198	-2.6198	-2.6197	-2.6197	-2.6197
3.36	-2.1489	-2.1488	-2.1488	-2.1488	-2.1488
3.64	-1.4780	-1.4779	-1.4779	-1.4779	-1.4779
4.20	-0.6790	-0.6789	-0.6789	-0.6789	-0.6789
4.76	-0.3064	-0.3063	-0.3064	-0.3064	-0.3064
5.32	-0.1377	-0.1374	-0.1376	-0.1376	-0.1376
6.10	-0.0458	-0.0455	-0.0458	-0.0458	-0.0458
7.50	-0.0094	-0.0090	-0.0094	-0.0094	-0.0094
12.00	-0.0068	-0.0068	-0.0068	-0.0068	-0.0068
25.00	-0.0068	-0.0068	-0.0068	-0.0068	-0.0068

TABLE XIV (Continued)

$R_2(R_6)$	α = 0.34	α = 0.69	α = 1.04	α = 1.39	α = 1.57
		M. $R_1(R_4)$ = 12.00			
1.50	10.8210	10.8210	10.8211	10.8211	10.8211
2.34	-4.9582	-4.9581	-4.9581	-4.9581	-4.9581
2.62	-4.3909	-4.3908	-4.3908	-4.3908	-4.3908
2.90	-3.6087	-3.6086	-3.6086	-3.6086	-3.6086
3.18	-2.6180	-2.6180	-2.6180	-2.6180	-2.6180
3.36	-2.1472	-2.1471	-2.1471	-2.1471	-2.1471
3.64	-1.4763	-1.4762	-1.4762	-1.4762	-1.4762
4.20	-0.6775	-0.6773	-0.6772	-0.6772	-0.6772
4.76	-0.3052	-0.3047	-0.3046	-0.3046	-0.3046
5.32	-0.1370	-0.1360	-0.1359	-0.1359	-0.1359
6.10	-0.0470	-0.0441	-0.0439	-0.0439	-0.0439
7.50	-0.0518	-0.0063	-0.0058	-0.0058	-0.0057
12.00	-0.4123	-0.0012	0.0000	0.0000	0.0000
25.00	0.0000	0.0000	0.0000	0.0000	0.0000

$R_2(R_6)$	α = 1.74	α = 1.90	α = 2.44	α = 2.79	α = 3.14
		M. $R_1(R_4)$ = 12.00			
1.50	10.8211	10.8211	10.8211	10.8211	10.8211
2.34	-4.9581	-4.9581	-4.9581	-4.9581	-4.9581
2.62	-4.3908	-4.3908	-4.3908	-4.3908	-4.3908
2.90	-3.6086	-3.6086	-3.6086	-3.6086	-3.6086
3.18	-2.6180	-2.6180	-2.6180	-2.6180	-2.6180
3.36	-2.1471	-2.1471	-2.1471	-2.1471	-2.1471
3.64	-1.4762	-1.4762	-1.4762	-1.4762	-1.4762
4.20	-0.6772	-0.6772	-0.6772	-0.6772	-0.6772
4.76	-0.3046	-0.3046	-0.3046	-0.3046	-0.3046
5.32	-0.1359	-0.1359	-0.1359	-0.1359	-0.1359
6.10	-0.0439	-0.0439	-0.0439	-0.0439	-0.0439
7.50	-0.0057	-0.0057	-0.0057	-0.0057	-0.0057
12.00	0.0000	0.0001	0.0000	0.0000	0.0000
25.00	0.0000	0.0000	0.0000	0.0000	0.0000

TABLE XIV (Continued)

$R_2(R_6)$	α = 0.34	α = 0.69	α = 1.04	α = 1.39	α = 1.57
		N. $R_1(R_4)$ = 25.00			
1.50	10.8211	10.8211	10.8211	10.8211	10.8211
2.34	-4.9581	-4.9581	-4.9581	-4.9581	-4.9581
2.62	-4.3908	-4.3908	-4.3908	-4.3908	-4.3908
2.90	-3.6086	-3.6086	-3.6086	-3.6086	-3.6086
3.18	-2.6180	-2.6180	-2.6180	-2.6180	-2.6180
3.36	-2.1471	-2.1471	-2.1471	-2.1471	-2.1471
3.64	-1.4762	-1.4762	-1.4762	-1.4762	-1.4762
4.20	-0.6772	-0.6772	-0.6772	-0.6772	-0.6772
4.76	-0.3046	-0.3046	-0.3046	-0.3046	-0.3046
5.32	-0.1359	-0.1359	-0.1359	-0.1359	-0.1359
6.10	-0.0439	-0.0439	-0.0439	-0.0439	-0.0439
7.50	-0.0057	-0.0057	-0.0057	-0.0057	-0.0057
12.00	0.0000	0.0000	0.0000	0.0000	0.0000
25.00	-0.0007	0.0000	0.0000	0.0000	0.0000

$R_2(R_6)$	α = 1.74	α = 1.90	α = 2.44	α = 2.79	α = 3.14
		N. $R_1(R_4)$ = 25.00			
1.50	10.8211	10.8211	10.8211	10.8211	10.8211
2.34	-4.9581	-4.9581	-4.9581	-4.9581	-4.9581
2.62	-4.3908	-4.3908	-4.3908	-4.3908	-4.3908
2.90	-3.6086	-3.6086	-3.6086	-3.6086	-3.6086
3.18	-2.6180	-2.6180	-2.6180	-2.6180	-2.6180
3.36	-2.1471	-2.1471	-2.1471	-2.1471	-2.1471
3.64	-1.4762	-1.4762	-1.4762	-1.4762	-1.4762
4.20	-0.6772	-0.6772	-0.6772	-0.6772	-0.6772
4.76	-0.3046	-0.3046	-0.3046	-0.3046	-0.3046
5.32	-0.1359	-0.1359	-0.1359	-0.1359	-0.1359
6.10	-0.0439	-0.0439	-0.0439	-0.0439	-0.0439
7.50	-0.0057	-0.0057	-0.0057	-0.0057	-0.0057
12.00	0.0000	0.0000	0.0000	0.0000	0.0000
25.00	0.0000	0.0000	0.0000	0.0000	0.0000

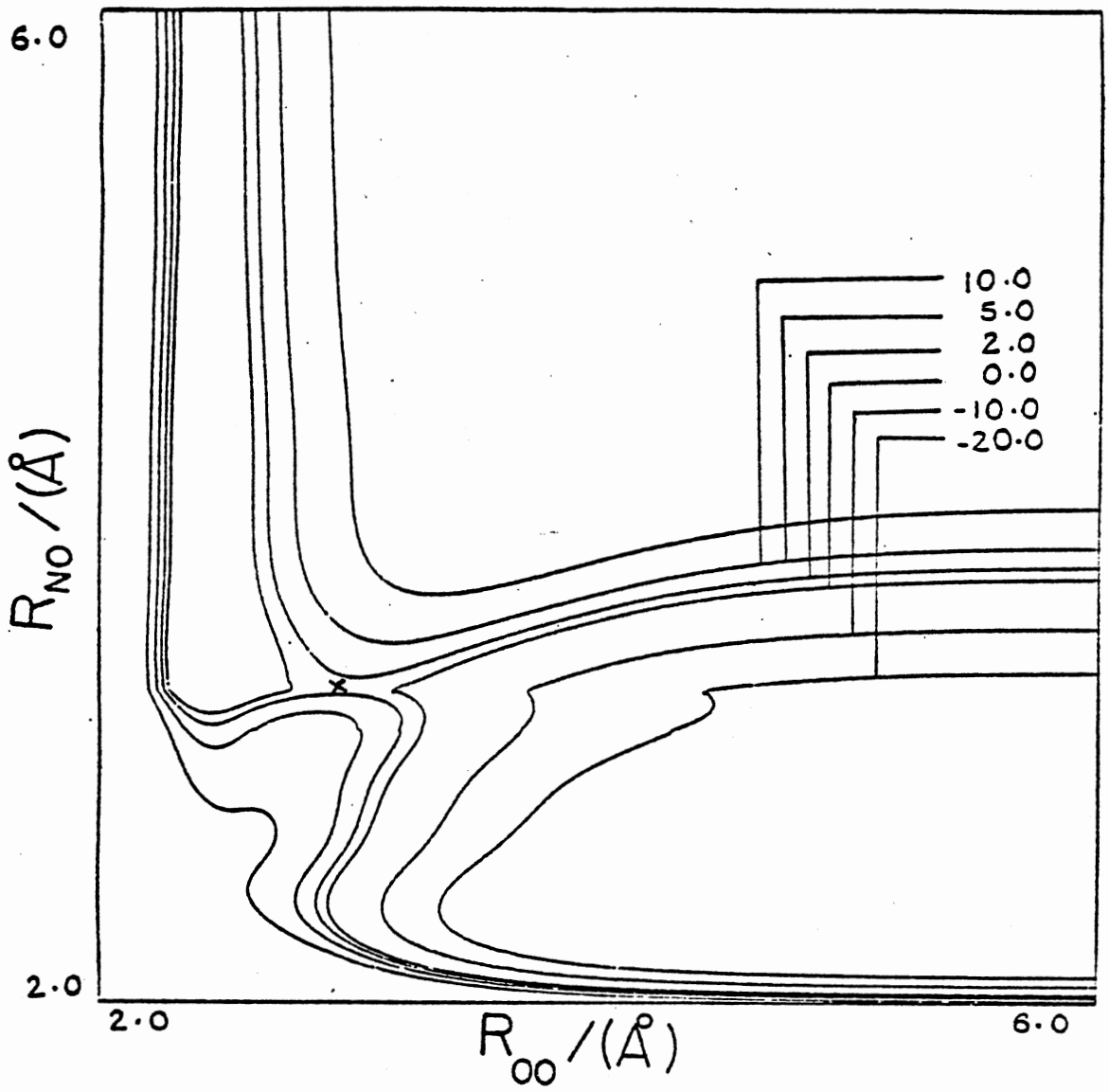

Figure 3. Contour Plot of Surface S1 for α = 2.09 Radians. Contours are in Kcal/mole. X designates the saddle-point. Barrier = 0.71 Kcal/mole.

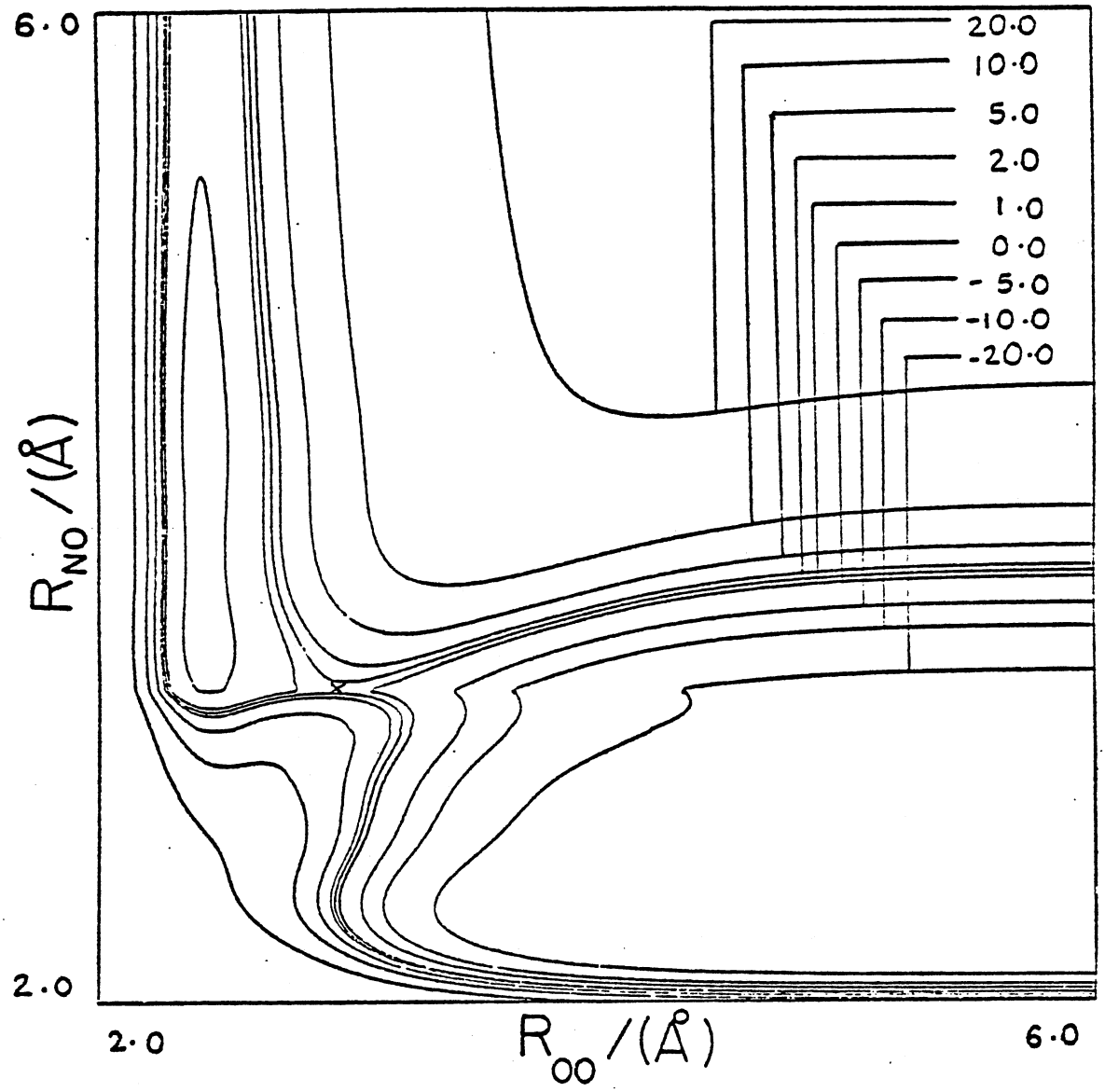

Figure 4. Contour Plot of Surface S1 for α = 1.60 Radians. Contours are in Kcal/mole. X designates the saddle-point. Barrier = 0.71 Kcal/mole.

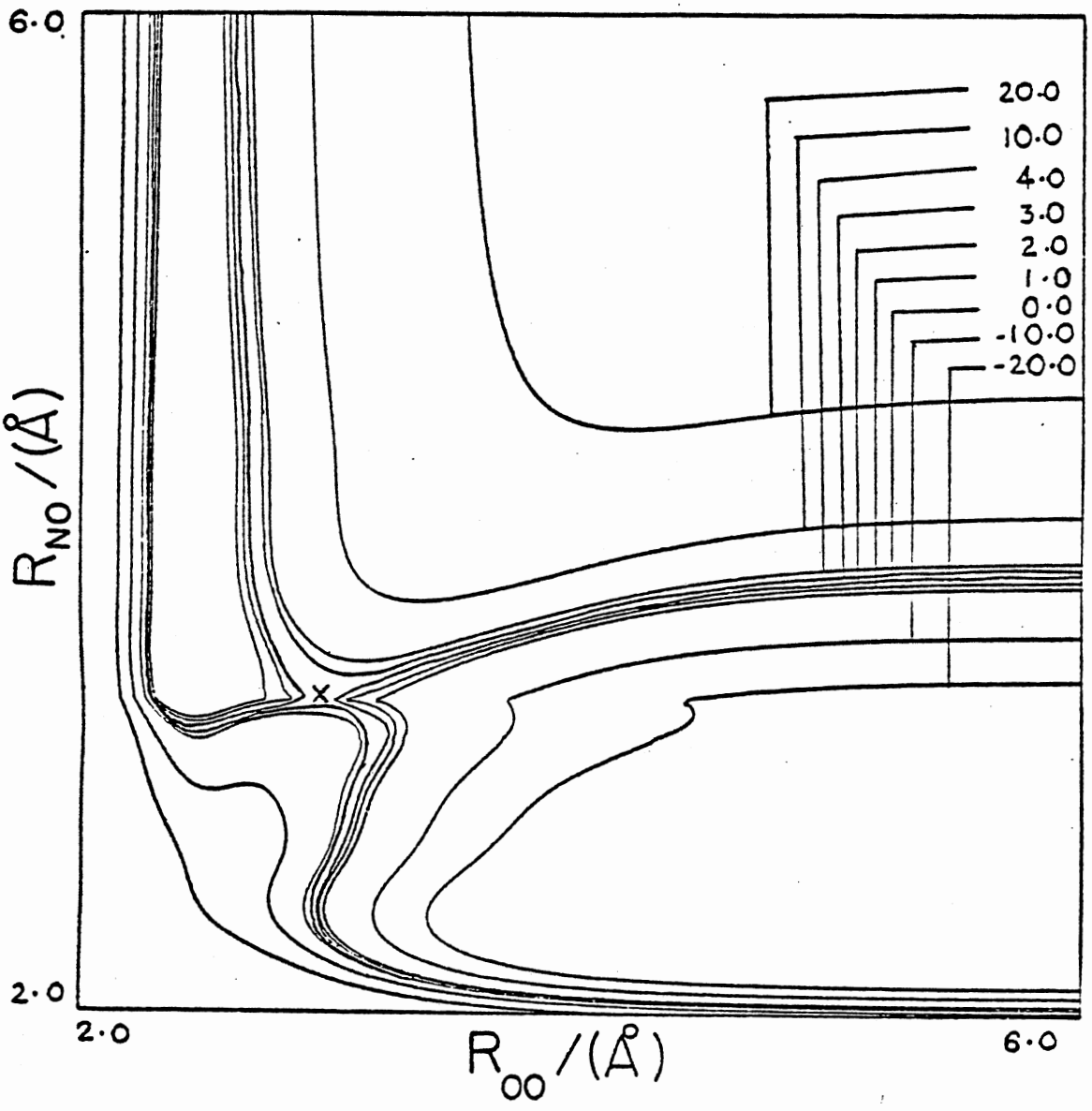

Figure 5. Contour Plot of Surface S2 for α = 1.90 Radians. Contours are in Kcal/mole. X designates the saddle-point. Barrier = 2.35 Kcal/mole.

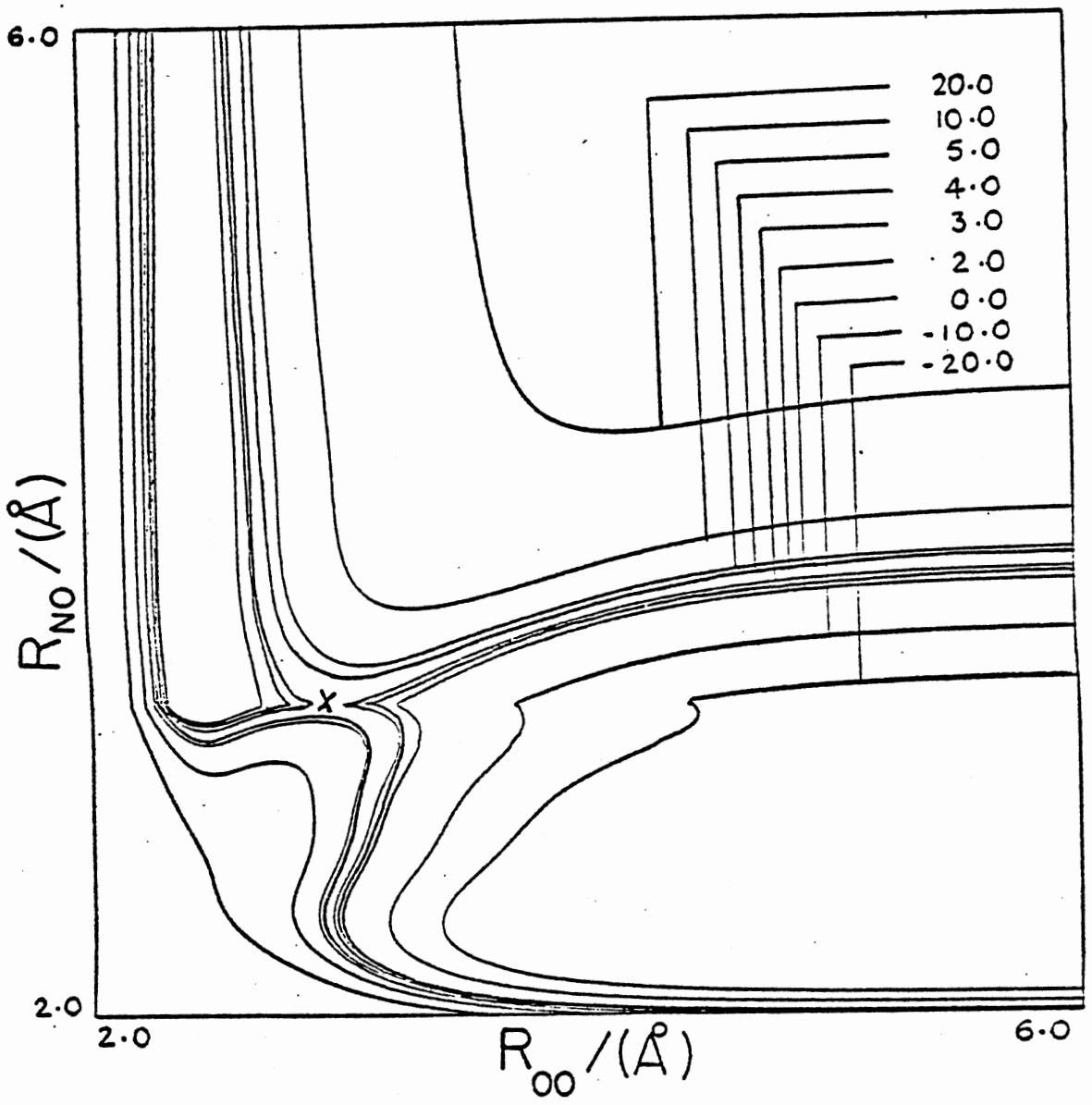

Figure 6. Contour Plot of Surface S3 for α = 1.90 Radians. Contours are in Kcal/mole. X designates the saddle-point. Barrier = 3.57 Kcal/mole.

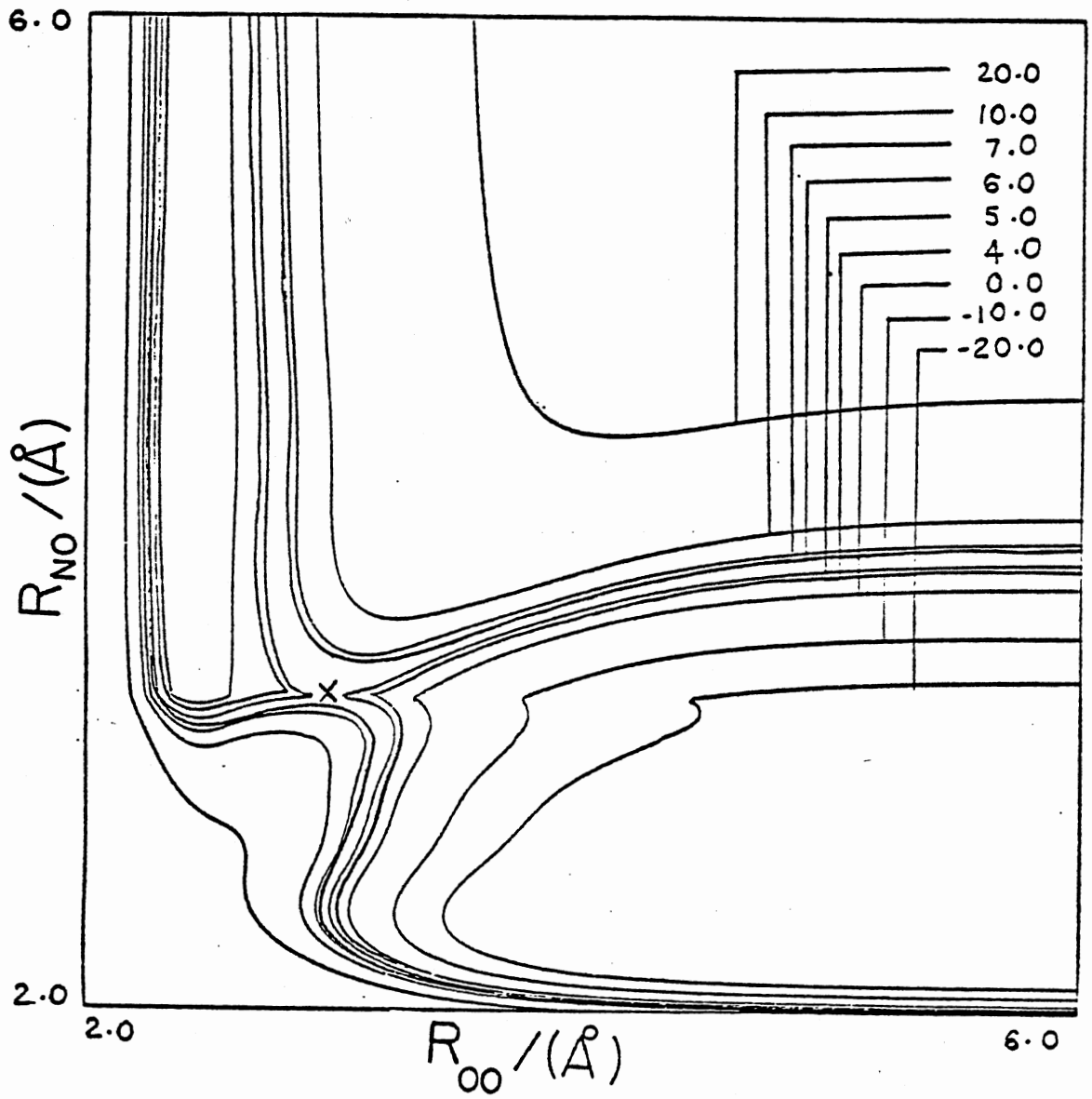

Figure 7. Contour Plot of Surface S4 for α = 1.90 Radians. Contours are in Kcal/mole. X designates the saddle-point. Barrier = 5.4 Kcal/mole.

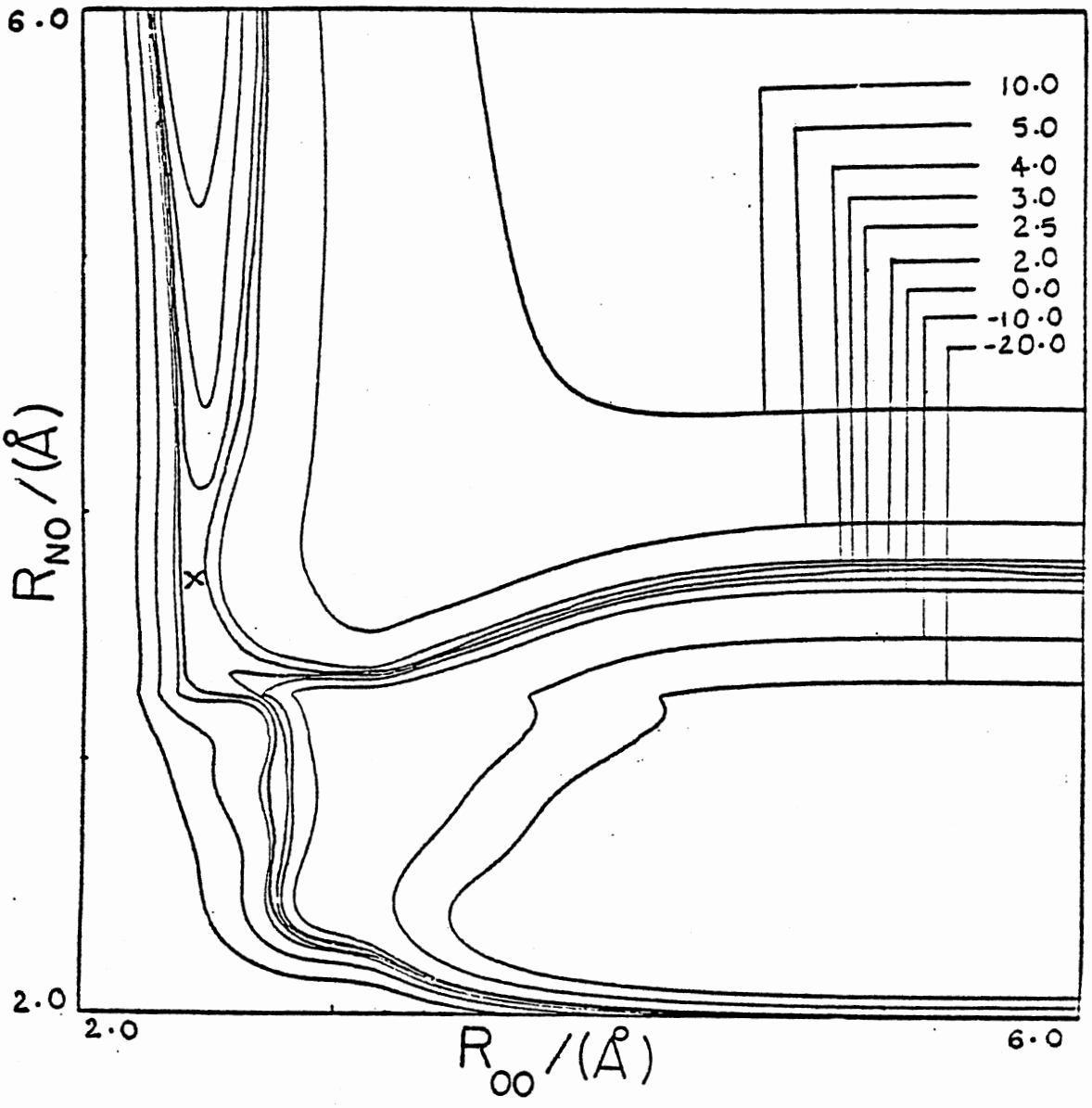

Figure 8. Contour Plot of Surface S5 for α = 1.90 Radians. Contours are in Kcal/mole. X designates the saddle-point. Barrier = 3.5 Kcal/mole.

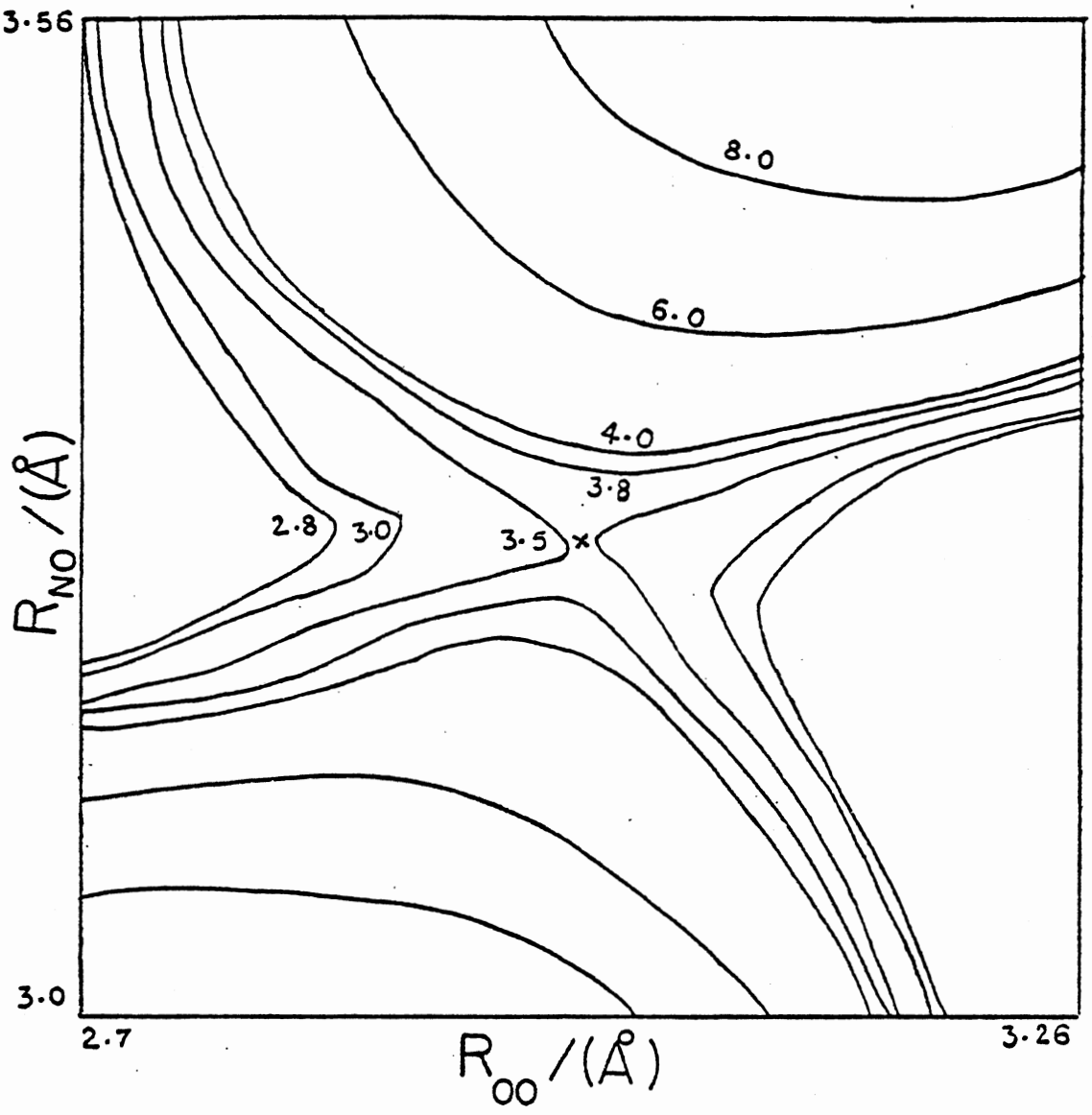

Figure 9. Saddle-Point Region of Surface S3. Contours are in Kcal/mole. X designates the saddle-point. Barrier = 3.57 Kcal/mole.

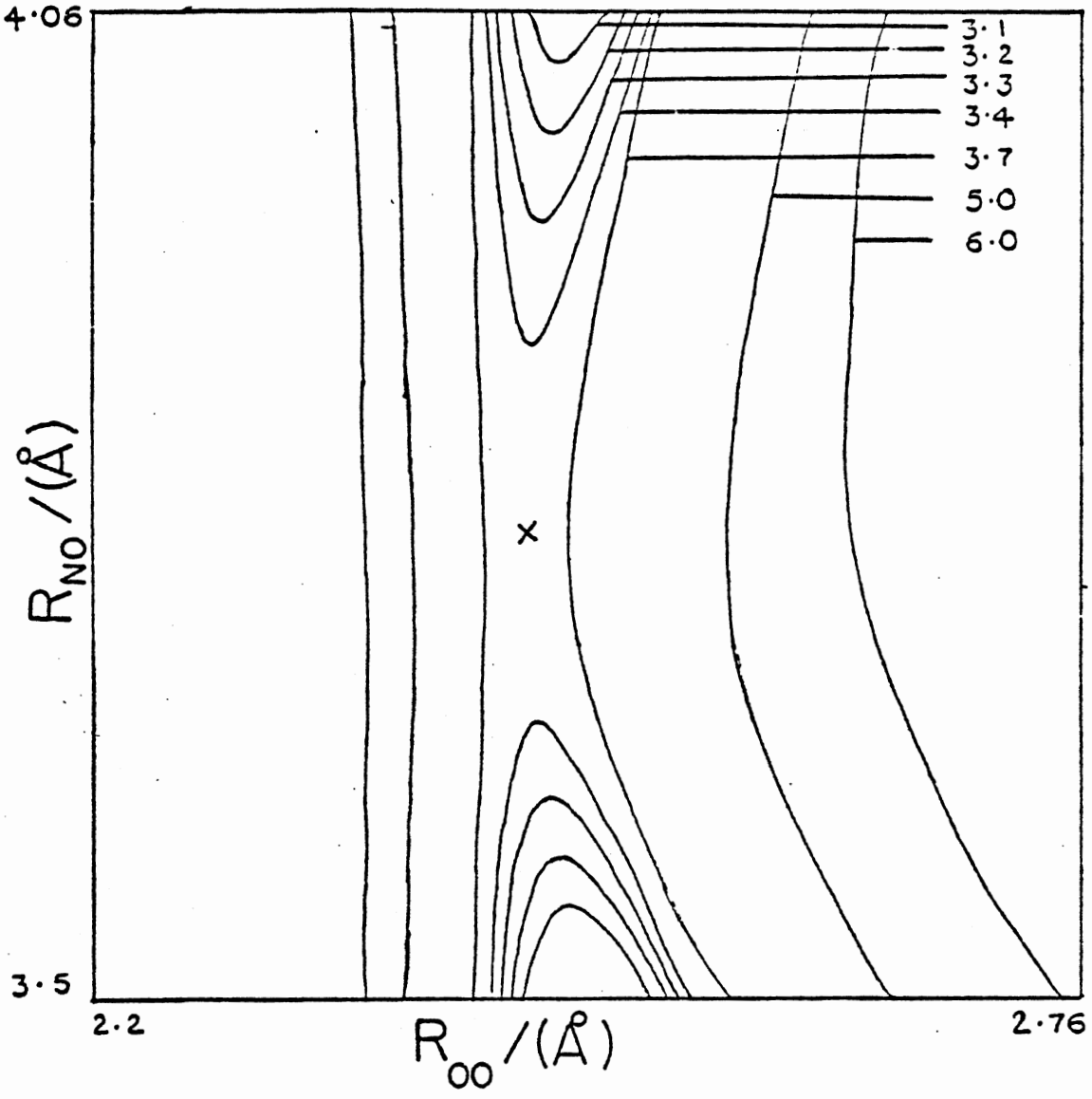

Figure 10. Saddle-Point Region of Surface S5. Contours are in Kcal/mole. X designates the saddle-point. Barrier = 3.5 Kcal/mole.

interpolation between the grid points in this region. These are given in Table XV for surfaces S1 to S5.

TABLE XV

SADDLE-POINT GEOMETRIES

Surface	R_{O-O}/au	R_{N-O}/au	O-O-N/rad	Barrier Kcal/mole
S1	2.99	3.30	1.60	0.71
S2	2.99	3.30	1.90	2.35
S3	2.99	3.30	1.90	3.57
S4	2.99	3.30	1.90	5.4
S5	2.40	3.70	1.90	3.5

The contour lines are almost smooth. The saddle point is indicated with a cross. There is a slight discontinuity exhibited by the contour lines in the product valley. This arises from the polynomial functional form used to vary the dissociation energy of the N-O bond. Other functional forms (exponential, gaussian) were tried for the variation of D_{NO}. They were either found to increase the barrier height by operating over a very large range or introduce an undesirable second minimum in the product valley. Since the observed dynamics are not expected to be altered to a great extent, further investigation along

this line was not attempted.

Surfaces S1 to S4 are almost identical except for the change in barrier height. The saddle point is located in the exit-channel. The minimum reaction path corresponds to the N atom approaching the O_3 molecule such that the O-O-N angle is 110^{o}. From the contour plots, it seems that there would be a very high steric requirement on the system in order for reaction to occur. The surfaces S1 to S4 are comparable to surface IIB2 of Chapman (80) in that the saddle point is located in the exit-channel.

Surface S5 has a barrier height comparable to that of S3 but the saddle-point has been shifted to an earlier position along the reaction path. There is a slight discontinuity introduced into the contour lines. This is due to the difficulty involved in replacing the interaction potentials, V_I, by a (14X14X10) numerical grid of values. However, the prime objective was to obtain a surface with the saddle point located in the entrance channel. The objective has been realised but only with some loss in the smoothness of the contour lines. The minimum reaction path corresponds to an approach angle, O-O-N, of 110^{o}.

Derivatives of the Potential-Energy Surface

In order to carry out the quasiclassical trajectory calculations, derivatives of the potential energy with respect to the coordinates are required. Once the derivatives of the potential with respect to the various bond distances and bond angles have been obtained, it is a relatively simple matter to evaluate the derivatives with respect to the coordinates. The functional form of the potential has been

given previously in Eq (II-1). The potential surface derivatives required to solve the equations of motion are given by

$$\frac{\partial V}{\partial q_i} = \sum_{j=1}^{10} \frac{\partial V}{\partial R_j} \cdot \frac{\partial R_j}{\partial q_i}, \quad i = 1 \text{ to } 15 \tag{II-40}$$

where the R_j are the ten interatomic distances. The $(\partial V/\partial R_j)$ are considered below; the calculation of the derivatives of distances with respect to the coordinates is trivial.

$$\frac{\partial V}{\partial R_1} = \frac{\partial V_{O_3}}{\partial R_1} + \left(\frac{\partial V_I}{\partial R_1} + \frac{\partial V_{att}}{\partial R_1}\right) \Big/ C \tag{II-41}$$

$$\frac{\partial V}{\partial R_2} = \frac{\partial V_{NO_2}}{\partial \theta_1} \cdot \frac{\partial \theta_1}{\partial R_2} + \left(\frac{\partial V_I}{\partial R_2} + \delta_{R_i R_2}\left(\frac{\partial V_{NO_2}}{\partial R_2} + \frac{\partial V_{NO}}{\partial R_2}\right)\right) \Big/ C \tag{II-42}$$

$$\frac{\partial V}{\partial R_3} = \left(\frac{\partial V_I}{\partial R_3} + \frac{\partial V_I}{\partial R_3} + \delta_{R_i R_3}\left(\frac{\partial V_{NO_2}}{\partial R_3} + \frac{\partial V_{NO}}{\partial R_3}\right)\right) \Big/ C + \frac{\partial V_{NO_2}}{\partial \theta_3} \cdot \frac{\partial \theta_3}{\partial R_3} + \frac{\partial V_{att}}{\partial R_3} \tag{II-43}$$

$$\frac{\partial V}{\partial R_4} = \frac{\partial V_{O_3}}{\partial R_4} + \left(\frac{\partial V_I}{\partial R_4} + \frac{\partial V_{att}}{\partial R_4}\right) \Big/ C \tag{II-44}$$

$$\frac{\partial V}{\partial R_5} = \frac{\partial V_{O_3}}{\partial R_5} + \left(\frac{\partial V_{O_2}}{\partial R_5}\right) \Big/ C \tag{II-45}$$

$$\frac{\partial V}{\partial R_6} = \frac{\partial V_{NO_2}}{\partial \theta_2} \cdot \frac{\partial \theta_2}{\partial R_6} + \left(\frac{\partial V_I}{\partial R_6} + \delta_{R_i R_6} \left(\frac{\partial V_{NO_2}}{\partial R_6} + \frac{\partial V_{NO}}{\partial R_6} \right) \right) \Big/ c \qquad \text{(II-46)}$$

$$\frac{\partial V}{\partial R_7} = \frac{\partial V_{NO_2}}{\partial \theta_1} \cdot \frac{\partial \theta_1}{\partial R_7} + \frac{\partial V_{NO_2}}{\partial \theta_2} \cdot \frac{\partial \theta_2}{\partial R_7} + \frac{\partial V_{NO_2}}{\partial \theta_3} \cdot \frac{\partial \theta_3}{\partial R_7} + \left(\frac{\partial V_{NO}}{\partial R_7} \right) \Big/ c \qquad \text{(II-47)}$$

$$\frac{\partial V}{\partial R_8} = \frac{\partial V_{NO_2}}{\partial \theta_1} \cdot \frac{\partial \theta_1}{\partial R_8} + \frac{\partial V_{OO}}{\partial R_8} \qquad \text{(II-48)}$$

$$\frac{\partial V}{\partial R_9} = \frac{\partial V_{NO_2}}{\partial \theta_3} \cdot \frac{\partial \theta_3}{\partial R_9} + \frac{\partial V_{OO}}{\partial R_9} \qquad \text{(II-49)}$$

$$\frac{\partial V}{\partial R_{10}} = \frac{\partial V_{NO_2}}{\partial \theta_2} \cdot \frac{\partial \theta_2}{\partial R_{10}} + \frac{\partial V_{OO}}{\partial R_{10}} \qquad \text{(II-50)}$$

where $c = 0.529177$, $R_i = \text{Min}(R_2, R_3, R_6)$, and $\partial V/\partial R_j$ are in $eV(\mathring{A})^{-1}$.

The various derivatives required to evaluate the $\partial V/\partial R_j$ are now considered.

$$\frac{\partial {}^1E_{AB}}{\partial R_1} = 2\alpha_{O_2} D_{O_2} \{\exp\{-\alpha_{O_2}(R_1 - R_1^0)\} - \exp\{-2\alpha_{O_2}(R_1 - R_1^0)\}\} \qquad \text{(II-51)}$$

and

$$\frac{\partial {}^1E_{\alpha\beta}}{\partial R_i} = \frac{\partial D_{NO}}{\partial R_i} \{\exp\{-2\alpha_{NO}(R_i - R_e)\} - 2\exp\{-\alpha_{NO}(R_i - R_e)\}\}$$

$$+ 2D_{NO}\alpha_{NO}\{\exp\{-\alpha_{NO}(R_i - R_e)\} - \exp\{-2\alpha_{NO}(R_i - R_e)\}\}$$

$$X \left\{1 - \frac{\partial R_e}{\partial R_1}\right\} \quad i = 2, 3 \qquad \text{(II-52)}$$

$\partial D_{NO}/\partial R_i$ and $\partial R_e/\partial R_i$ are given by Eq (II-74) and (II-75), respectively. The derivatives of the triplet-state energies are given by,

$$\frac{\partial {}^3E_{\alpha\beta}}{\partial R_i} = -2\,{}^3D_{\alpha\beta}\beta_i \{\exp\{-\beta_i(R_i - R_i^0)\} + \exp\{-2\beta_i(R_i - R_i^0)\}\}; \quad R_i \leq 3.0 \tag{II-53}$$

$$\frac{\partial {}^3E_{\alpha\beta}}{\partial R_i} = C \exp(-\sigma_i R_i)\{1 - A_i\sigma_i - R_i\sigma_i\} \quad R_i > 3.0 \tag{II-54}$$

$$\frac{\partial Q_{\alpha\beta}}{\partial R_i} = 0.5 \left\{\frac{\partial {}^1E_{\alpha\beta}}{\partial R_i} + \frac{\partial {}^3E_{\alpha\beta}}{\partial R_i}\right\} \tag{II-55}$$

$$\frac{\partial J_{\alpha\beta}}{\partial R_i} = 0.5 \left\{\frac{\partial {}^1E_{\alpha\beta}}{\partial R_i} - \frac{\partial {}^3E_{\alpha\beta}}{\partial R_i}\right\} \tag{II-56}$$

Let,

$$S = \mathrm{Sqrt}\{0.5\{(J_{AB} - J_{BC})^2 + (J_{BC} - J_{CA})^2 + (J_{CA} - J_{AB})^2\}\} \tag{II-57}$$

Then,

$$\frac{\partial V_I}{\partial R_1} = \frac{\partial Q_{AB}}{\partial R_1} - \{\{0.5(2J_{AB} - J_{BC} - J_{CA}) \cdot \frac{\partial J_{AB}}{\partial R_1}\} / S\} \tag{II-58}$$

$$\frac{\partial V_I}{\partial R_2} = \frac{\partial Q_{BC}}{\partial R_2} - \{\{0.5(2J_{BC} - J_{AB} - J_{CA}) \cdot \frac{\partial J_{BC}}{\partial R_2}\} / S\} \tag{II-59}$$

$$\frac{\partial V_I}{\partial R_3} = \frac{\partial Q_{CA}}{\partial R_3} - \{\{0.5(2J_{CA} - J_{AB} - J_{BC}) \cdot \frac{\partial J_{CA}}{\partial R_3}\} / S\} \qquad \text{(II-60)}$$

Similar expressions have been used to obtain the derivatives of $V_I(R_4, R_6, R_3)$. Whenever surface S5 was employed in the trajectory calculations, the derivatives of V_I with respect to R_1, R_2, α_1 and R_4, R_6, α_2 have been obtained by cubic spline interpolation (79). The derivatives with respect to angles were converted to those with respect to distances by making use of the chain rule. The derivatives of the ozone three-body interaction potential with respect to the internuclear distances have been obtained as follows:

Let

$$\begin{aligned} \Delta R_1 &= R_1 - R_0 \\ \Delta R_4 &= R_4 - R_0 \\ \Delta R_5 &= R_5 - R_0 \end{aligned} \qquad \text{(II-61)}$$

and

$$\begin{aligned} Q_1 &= 0.5774(\Delta R_1 + \Delta R_4 + \Delta R_5) \\ Q_2 &= 0.7071(\Delta R_1 - \Delta R_5) \\ Q_3 &= 0.4082(2\Delta R_4 - \Delta R_1 - \Delta R_5) \end{aligned} \qquad \text{(II-62)}$$

$$V_{O_3}(R_1, R_4, R_5) = (P + G)v \qquad \text{(II-63)}$$

where P, G and v have been described earlier. The required derivatives are given by,

$$\frac{\partial V_{O_3}}{\partial R_i} = \left(\frac{\partial P}{\partial R_i} + \frac{\partial G}{\partial R_i}\right)v + (P + G)\frac{\partial v}{\partial R_i}, \quad i = 1, 4 \text{ and } 5 \qquad \text{(II-64)}$$

with

$$\frac{\partial P}{\partial R_j} = \sum_{i=1}^{3} \frac{\partial P}{\partial Q_i} \cdot \frac{\partial Q_i}{\partial R_j}$$

$$\frac{\partial G}{\partial R_j} = \sum_{i=1}^{3} \frac{\partial G}{\partial Q_i} \cdot \frac{\partial Q_i}{\partial R_j}$$

and

$$\frac{\partial V}{\partial R_i} = \frac{\partial v}{\partial Q_1} \cdot \frac{\partial Q_1}{\partial R_i} \qquad \text{(II-65)}$$

The derivatives required to evaluate Equations (II-65) are given by,

$$\frac{\partial P}{\partial Q_1} = 6.5822 + 2(13.9106)Q_1 - 3.1421(Q_2^2 + Q_3^2) \qquad \text{(II-66)}$$

$$\frac{\partial P}{\partial Q_2} = -2(17.1931)Q_2 - 2(3.1421)Q_1Q_2 - 6(2.6323)Q_3Q_2 + 4(13.9659)Q_2(Q_2^2 + Q_3^2) \qquad \text{(II-67)}$$

$$\frac{\partial P}{\partial Q_3} = -2(17.1931)Q_3 - 2(3.1421)Q_1Q_3 + 3(2.6323)Q_3^2 - 3(2.6323)Q_2^2 + 4(13.9659)Q_3(Q_2^2 + Q_3^2) \qquad \text{(II-68)}$$

$$\frac{\partial G}{\partial Q_1} = 0$$

$$\frac{\partial G}{\partial Q_i} = 4.5Q_i \exp\{-7.5(Q_2^2 + Q_3^2)\}, \quad i = 2, 3 \qquad \text{(II-69)}$$

$$\frac{\partial v}{\partial Q_1} = -2.3 \operatorname{sech}^2(2.3Q_1) \qquad \text{(II-70)}$$

and

$$\frac{\partial Q_1}{\partial R_1} = \frac{\partial Q_1}{\partial R_4} = \frac{\partial Q_1}{\partial R_5} = 0.5774$$

$$\frac{\partial Q_2}{\partial R_1} = \frac{-\partial Q_2}{\partial R_5} = 0.7071$$

$$\frac{\partial Q_3}{\partial R_1} = -1/2 \frac{\partial Q_3}{\partial R_4} = \frac{\partial Q_3}{\partial R_5} = -0.4082 \qquad \text{(II-71)}$$

The derivatives of the Morse potentials are given by,

$$\frac{\partial V_{NO}}{\partial R_7} = 2D_{NO}\alpha_{NO}\{\exp(-\alpha_{NO}(R_7 - R_e)) - \exp(-2\alpha_{NO}(R_7 - R_e))\} \qquad \text{(II-72)}$$

$$\frac{\partial V_{NO}}{\partial R_i} = \frac{\partial D_{NO}}{\partial R_i}\{\exp(-2\alpha_{NO}(R_7 - R_e)) - 2\exp(-\alpha_{NO}(R_7 - R_e))\}$$

$$+ 2\alpha_{NO}D_{NO}\{\exp(-2\alpha_{NO}(R_7 - R_e)) - \exp(-\alpha_{NO}(R_7 - R_e))\}\frac{\partial R_e}{\partial R_i}$$

$$R_i = \text{Min}(R_2, R_3, R_6) \tag{II-73}$$

with

$$\frac{\partial D_{NO}}{\partial R_i} = -(a_1 + 2a_2 R_i + 3a_3 R_i^2 + 4a_4 R_i^3)$$

$$2.21 \leq R_i \leq 3.3$$

and

$$\frac{\partial D_{NO}}{\partial R_i} = 0 \text{ otherwise} \tag{II-74}$$

$$\frac{\partial R_e}{\partial R_i} = -5363.026 R_i^4 \exp(-0.0494 R_i^5), \quad 3.02 \leq R_i \leq 3.3$$

$$\frac{\partial R_e}{\partial R_i} = 0 \text{ otherwise} \tag{II-75}$$

The constants a_i (i = 1 to 4) in Eq (II-74) have been given earlier (Eq (II-12)).

$$\frac{\partial V_{O_2}}{\partial R_5} = 2D_{O_2}\alpha_{O_2} \{\exp(-\alpha_{O_2}(R_5 - R_5^0)) - \exp(-2\alpha_{O_2}(R_5 - R_5^0))\} \tag{II-76}$$

$$\frac{\partial V_{NO_2}}{\partial R_i} = k_b^0 (0.95627) \exp(-4.32629(R_i - 2.25754))$$

$$X \{2(0.4585)\Delta\theta_k - 4.32629(\Delta\theta_k)^2\}$$

$$R_i = \text{Min } (R_2, R_3, R_6) \tag{II-77}$$

$$\frac{\partial V_{NO_2}}{\partial \theta_k} = 2k_b^0(0.95627)\ \exp(-4.32629(R_i - 2.2575))(\Delta\theta_k)$$

and

$$\frac{\partial V_{NO_2}}{\partial \theta_{k'}} = 0,\ k' \neq k \qquad \text{(II-78)}$$

where $(\Delta\theta_k) = \theta_k - \theta_e$

$$\frac{\partial V_{OO}}{\partial R_i} = -2(1.8511)R_i\ \exp(-1.8511R_i^2),\quad R_i \leq 3.0\ A^o$$

$$= 0 \text{ otherwise} \qquad \text{(II-79)}$$

$$\frac{\partial V_{att}}{\partial R_i} = 2D_{O_2}\alpha_{O_2}\ \{\exp(-\alpha_{O_2}(R_i - R_i^0)) - \exp(-2\alpha_{O_2}(R_i - R_i^0))\}$$

$$X\ \{\tanh\{2.0(R_3 - R_3^0)\} - 1.0\} \qquad \text{(II-80)}$$

$$\frac{\partial V_{att}}{\partial R_3} = 2D_{O_2}\ \{\exp(-2\alpha_{O_2}(R_i - R_i^0)) - 2\exp(-\alpha_{O_2}(R_i - R_i^0))\}$$

$$X\ \{\text{sech}^2\{2.0(R_3 - R_3^0)\}\};$$

$$R_i = \text{Min}\ (R_1, R_4)$$

The relationship between the distances and the angles and the coordinates and distances are as follows:

$$\alpha_1 = \arccos((R_1^2 + R_2^2 - R_3^2)/2R_1R_2$$

$$\alpha_2 = \arccos((R_4^2 + R_6^2 - R_3^2)/2R_4R_6)$$

$$\theta_1 = \arccos((R_2^2 + R_7^2 - R_8^2)/2R_2R_7)$$

$$\theta_2 = \arccos((R_6^2 + R_7^2 - R_{10}^2)/2R_6R_7)$$

$$\theta_3 = \arccos((R_3^2 + R_7^2 - R_9^2)/2R_3R_7) \qquad \text{(II-81)}$$

and

$$R_1^2 = (x_2 - x_3)^2 + (y_2 - y_3)^2 + (z_2 - z_3)^2$$

$$R_2^2 = (x_2 - x_4)^2 + (y_2 - y_4)^2 + (z_2 - z_4)^2$$

$$R_3^2 = (x_3 - x_4)^2 + (y_3 - y_4)^2 + (z_3 - z_4)^2$$

$$R_4^2 = (x_3 - x_1)^2 + (y_3 - y_1)^2 + (z_3 - z_1)^2$$

$$R_5^2 = (x_1 - x_2)^2 + (y_1 - y_2)^2 + (z_1 - z_2)^2$$

$$R_6^2 = (x_1 - x_4)^2 + (y_1 - y_4)^2 + (z_1 - z_4)^2$$

$$R_7^2 = (x_4 - x_5)^2 + (y_4 - y_5)^2 + (z_4 - z_5)^2$$

$$R_8^2 = (x_5 - x_2)^2 + (y_5 - y_2)^2 + (z_5 - z_2)^2$$

$$R_9^2 = (x_5 - x_3)^2 + (y_5 - y_3)^2 + (z_5 - z_3)^2$$

$$R_{10}^2 = (x_5 - x_1)^2 + (y_5 - y_1)^2 + (z_5 - z_1)^2 \qquad \text{(II-82)}$$

The non-zero derivatives of the angles with respect to the distances are given by,

$$\frac{\partial \alpha_1}{\partial R_1} = (R_2 \cos\alpha_1 - R_1)/R_1 R_2 \sin\alpha_1$$

$$\frac{\partial \alpha_1}{\partial R_2} = (R_1 \cos\alpha_1 - R_2)/R_1 R_2 \sin\alpha_1$$

$$\frac{\partial \alpha_1}{\partial R_3} = R_3/R_1 R_2 \sin\alpha_1$$

$$\frac{\partial \alpha_2}{\partial R_4} = (R_6 \cos\alpha_2 - R_4)/R_4 R_6 \sin\alpha_2$$

$$\frac{\partial \alpha_2}{\partial R_6} = (R_4 \cos\alpha_2 - R_6)/R_4 R_6 \sin\alpha_2$$

$$\frac{\partial \alpha_2}{\partial R_3} = R_3/R_4 R_6 \sin\alpha_2$$

$$\frac{\partial \theta_1}{\partial R_2} = (R_7 \cos\theta_1 - R_2)/R_2 R_7 \sin\theta_1$$

$$\frac{\partial \theta_1}{\partial R_7} = (R_2 \cos\theta_1 - R_7)/R_2 R_7 \sin\theta_1$$

$$\frac{\partial \theta_1}{\partial R_8} = R_8/R_2 R_7 \sin\theta_1$$

$$\frac{\partial \theta_2}{\partial R_6} = (R_7 \cos\theta_2 - R_6)/R_6 R_7 \sin\theta_2$$

$$\frac{\partial\theta_2}{\partial R_7} = (R_6\cos\theta_2 - R_7)/R_6\ R_7\ \sin\theta_2$$

$$\frac{\partial\theta_2}{\partial R_{10}} = R_{10}/R_6\ R_7\ \sin\theta_2$$

$$\frac{\partial\theta_3}{\partial R_3} = (R_7\cos\theta_3 - R_3)/R_3\ R_7\ \sin\theta_3$$

$$\frac{\partial\theta_3}{\partial R_7} = (R_3\cos\theta_3 - R_7)/R_3\ R_7\ \sin\theta_3$$

$$\frac{\partial\theta_3}{\partial R_9} = R_9/R_3\ R_7\ \sin\theta_3 \qquad \text{(II-83)}$$

The derivatives of the total potential with respect to the cartesian coordinates shown in Figure 1 are

$$\frac{\partial V}{\partial x_1} = \frac{\partial V}{\partial R_4}\cdot\frac{\partial R_4}{\partial x_1} + \frac{\partial V}{\partial R_5}\cdot\frac{\partial R_5}{\partial x_1} + \frac{\partial V}{\partial R_6}\cdot\frac{\partial R_6}{\partial x_1} + \frac{\partial V}{\partial R_{10}}\cdot\frac{\partial R_{10}}{\partial x_1}$$

$$\frac{\partial V}{\partial y_1} = \frac{\partial V}{\partial R_4}\cdot\frac{\partial R_4}{\partial y_1} + \frac{\partial V}{\partial R_5}\cdot\frac{\partial R_5}{\partial y_1} + \frac{\partial V}{\partial R_6}\cdot\frac{\partial R_6}{\partial y_1} + \frac{\partial V}{\partial R_{10}}\cdot\frac{\partial R_{10}}{\partial y_1}$$

$$\frac{\partial V}{\partial z_1} = \frac{\partial V}{\partial R_4}\cdot\frac{\partial R_4}{\partial z_1} + \frac{\partial V}{\partial R_5}\cdot\frac{\partial R_5}{\partial z_1} + \frac{\partial V}{\partial R_6}\cdot\frac{\partial R_6}{\partial z_1} + \frac{\partial V}{\partial R_{10}}\cdot\frac{\partial R_{10}}{\partial z_1}$$

$$\frac{\partial V}{\partial x_2} = \frac{\partial V}{\partial R_1}\cdot\frac{\partial R_1}{\partial x_2} + \frac{\partial V}{\partial R_2}\cdot\frac{\partial R_2}{\partial x_2} + \frac{\partial V}{\partial R_5}\cdot\frac{\partial R_5}{\partial x_2} + \frac{\partial V}{\partial R_8}\cdot\frac{\partial R_8}{\partial x_2}$$

$$\frac{\partial V}{\partial y_2} = \frac{\partial V}{\partial R_1} \cdot \frac{\partial R_1}{\partial y_2} + \frac{\partial V}{\partial R_2} \cdot \frac{\partial R_2}{\partial y_2} + \frac{\partial V}{\partial R_5} \cdot \frac{\partial R_5}{\partial y_2} + \frac{\partial V}{\partial R_8} \cdot \frac{\partial R_8}{\partial y_2}$$

$$\frac{\partial V}{\partial z_2} = \frac{\partial V}{\partial R_1} \cdot \frac{\partial R_1}{\partial z_2} + \frac{\partial V}{\partial R_2} \cdot \frac{\partial R_2}{\partial z_2} + \frac{\partial V}{\partial R_5} \cdot \frac{\partial R_5}{\partial z_2} + \frac{\partial V}{\partial R_8} \cdot \frac{\partial R_8}{\partial z_2}$$

$$\frac{\partial V}{\partial x_3} = \frac{\partial V}{\partial R_1} \cdot \frac{\partial R_1}{\partial x_3} + \frac{\partial V}{\partial R_4} \cdot \frac{\partial R_4}{\partial x_3} + \frac{\partial V}{\partial R_3} \cdot \frac{\partial R_3}{\partial x_3} + \frac{\partial V}{\partial R_9} \cdot \frac{\partial R_9}{\partial x_3}$$

$$\frac{\partial V}{\partial y_3} = \frac{\partial V}{\partial R_1} \cdot \frac{\partial R_1}{\partial y_3} + \frac{\partial V}{\partial R_4} \cdot \frac{\partial R_4}{\partial y_3} + \frac{\partial V}{\partial R_3} \cdot \frac{\partial R_3}{\partial y_3} + \frac{\partial V}{\partial R_9} \cdot \frac{\partial R_9}{\partial y_3}$$

$$\frac{\partial V}{\partial z_3} = \frac{\partial V}{\partial R_1} \cdot \frac{\partial R_1}{\partial z_3} + \frac{\partial V}{\partial R_4} \cdot \frac{\partial R_4}{\partial z_3} + \frac{\partial V}{\partial R_3} \cdot \frac{\partial R_3}{\partial z_3} + \frac{\partial V}{\partial R_9} \cdot \frac{\partial R_9}{\partial z_3}$$

$$\frac{\partial V}{\partial x_4} = \frac{\partial V}{\partial R_2} \cdot \frac{\partial R_2}{\partial x_4} + \frac{\partial V}{\partial R_3} \cdot \frac{\partial R_3}{\partial x_4} + \frac{\partial V}{\partial R_6} \cdot \frac{\partial R_6}{\partial x_4} + \frac{\partial V}{\partial R_7} \cdot \frac{\partial R_7}{\partial x_4}$$

$$\frac{\partial V}{\partial y_4} = \frac{\partial V}{\partial R_2} \cdot \frac{\partial R_2}{\partial y_4} + \frac{\partial V}{\partial R_3} \cdot \frac{\partial R_3}{\partial y_4} + \frac{\partial V}{\partial R_6} \cdot \frac{\partial R_6}{\partial y_4} + \frac{\partial V}{\partial R_7} \cdot \frac{\partial R_7}{\partial y_4}$$

$$\frac{\partial V}{\partial z_4} = \frac{\partial V}{\partial R_2} \cdot \frac{\partial R_2}{\partial z_4} + \frac{\partial V}{\partial R_3} \cdot \frac{\partial R_3}{\partial z_4} + \frac{\partial V}{\partial R_6} \cdot \frac{\partial R_6}{\partial z_4} + \frac{\partial V}{\partial R_7} \cdot \frac{\partial R_7}{\partial z_4}$$

$$\frac{\partial V}{\partial x_5} = \frac{\partial V}{\partial R_7} \cdot \frac{\partial R_7}{\partial x_5} + \frac{\partial V}{\partial R_8} \cdot \frac{\partial R_8}{\partial x_5} + \frac{\partial V}{\partial R_9} \cdot \frac{\partial R_9}{\partial x_5} + \frac{\partial V}{\partial R_{10}} \cdot \frac{\partial R_{10}}{\partial x_5}$$

$$\frac{\partial V}{\partial y_5} = \frac{\partial V}{\partial R_7} \cdot \frac{\partial R_7}{\partial y_5} + \frac{\partial V}{\partial R_8} \cdot \frac{\partial R_8}{\partial y_5} + \frac{\partial V}{\partial R_9} \cdot \frac{\partial R_9}{\partial y_5} + \frac{\partial V}{\partial R_{10}} \cdot \frac{\partial R_{10}}{\partial y_5}$$

$$\frac{\partial V}{\partial z_5} = \frac{\partial V}{\partial R_7} \cdot \frac{\partial R_7}{\partial z_5} + \frac{\partial V}{\partial R_8} \cdot \frac{\partial R_8}{\partial z_5} + \frac{\partial V}{\partial R_9} \cdot \frac{\partial R_9}{\partial z_5} + \frac{\partial V}{\partial R_{10}} \cdot \frac{\partial R_{10}}{\partial z_5} \qquad \text{(II-84)}$$

The derivatives of the interatomic distances with respect to the cartesian coordinates are given by,

$$\frac{\partial R_j}{\partial x_i} = \frac{(x_\mu - x_\nu)}{R_j} \qquad \text{(II-85)}$$

where x_μ and x_ν are the x coordinates of atoms μ and ν, $(1 \leq \mu \leq 5)$ and $(1 \leq \nu \leq 5)$ whose interatomic distance is R_j. Similar equations hold for $\partial R_j/\partial y_i$ and $\partial R_j/\partial z_i$.

CHAPTER III

QUASICLASSICAL TRAJECTORY STUDY OF THE EFFECTS OF SURFACE TOPOGRAPHY UPON THE REACTION DYNAMICS OF POLYATOMIC SYSTEMS

Calculational Methods

The quasiclassical trajectory procedure has been described in detail by Porter and Raff (58). In the classical regime, the trajectories of the atoms in colliding molecules may be obtained by the numerical solution of the Hamilton's equations of motion:

$$\dot{q}_i = \frac{\partial H}{\partial p_i} \qquad \text{(III-1)}$$

$$\dot{p}_i = \frac{\partial H}{\partial q_i}, \quad i = 1, 2, \ldots 3N \qquad \text{(III-2)}$$

where the q_i's are the coordinates and p_i's the conjugate momenta of an N-particle system. H is the classical Hamiltonian given by,

$$H = T + V, \qquad \text{(III-3)}$$

where T is the kinetic energy and V the potential energy of the system.

It has been found that cartesian coordinates are the most suitable for treating polyatomic systems (68). In the present case, the positions of the atoms have been described by using the cartesian coordinate

systems shown in Figure 11. The positions of the atoms in the O_3 molecule have been described initially with respect to the space-fixed coordinate system XYZ. The O_3 molecule is initially oriented in the XY plane with the principal axes of inertia coinciding with the space-fixed axes such that the symmetry axis lies along the Y-axis. The center of mass of the O_3 molecule lies at the origin of XYZ. The positions of the atoms in the NO molecule have been described with respect to the space-fixed X'Y'Z'. The axes of X'Y'Z' are parallel to those of XYZ, but the origin of the former lies at the center of mass of NO. The kinetic energy and potential energy of the system in terms of the cartesian coordinates described in Figure 12 are given by

$$T = 1/2 \sum_{i=1}^{3} (1/m_o p_i^2 + 1/m_o\ p_{i+3}^2 + 1/m_o\ p_{i+6}^2 + 1/m_N\ p_{i+9}^2 + 1/m_o\ p_{i+12}^2) \qquad \text{(III-4)}$$

$$V = V(q_1, q_2, \cdots q_{15}) \qquad \text{(III-5)}$$

The potential has been described in Chapter II. The equations of motion are:

$$\dot{q}_i = \frac{p_i}{m_i} \qquad \text{(III-6)}$$

$$\dot{p}_i = -\frac{\partial V}{\partial q_i}, \quad i = 1, 2, \ldots 15 \qquad \text{(III-7)}$$

where $m_i = m_o$ for i = 1 to 9 and 13 to 15; $m_i = m_N$ for i = 10, 11, 12.

If we assume the coupling between the vibrational and rotational

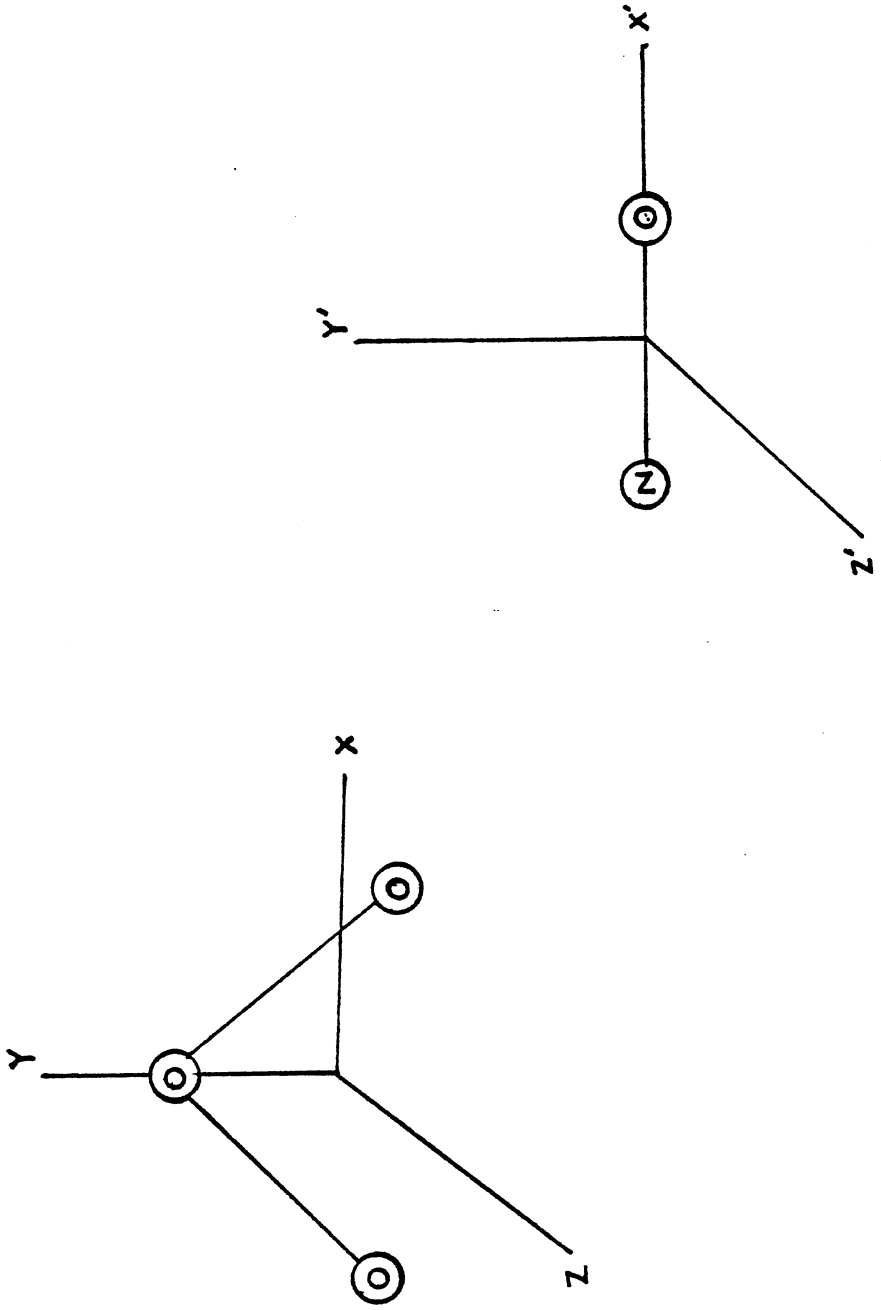

Figure 11. Coordinate Systems for the O_3-NO System

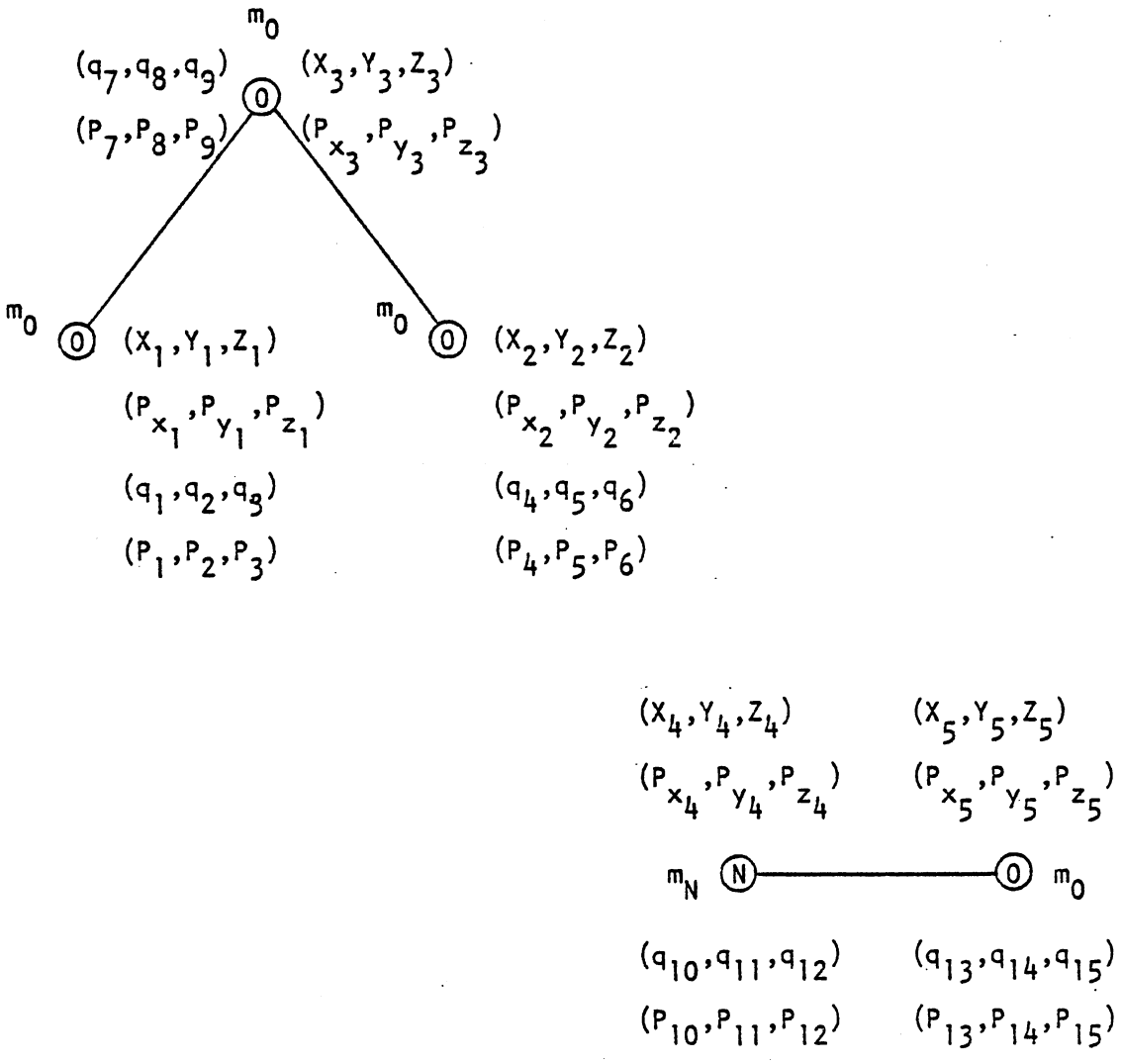

Figure 12. Cartesian Coordinates and Conjugate Momenta for the O_3-NO System

energies of the molecule to be negligible, the kinetic energy of the triatomic molecule may be separated into a rotational part and a vibrational part.

We have assumed that the vibrational motion of a non-linear triatomic molecule can be separated into three modes that are approximations to the normal modes (see Figure 13). Since we are not interested in the energy transfer processes between the modes, an exact separation is not required. The normal coordinates, Q_k, are defined in terms of the components ΔX_α etc., by the relations,

$$\Delta x_\alpha = \sum_{k=1}^{3} l_{\alpha k} Q_k$$

$$\Delta y_\alpha = \sum_{k=1}^{3} m_{\alpha k} Q_k$$

$$\Delta z_\alpha = \sum_{k=1}^{3} n_{\alpha k} Q_k \qquad \text{(III-8)}$$

where ΔX_α are the displacements from equilibrium given by,

$$\Delta x_\alpha = x_\alpha - x_\alpha^e \qquad \text{(III-9)}$$

and the constants $l_{\alpha k}$, $m_{\alpha k}$ and $n_{\alpha k}$ are determined so that,

$$\sum_{\alpha=1}^{3} m_\alpha v_\alpha^2 = \sum_{k=1}^{3} \dot{Q}_k^2 \qquad \text{(III-10)}$$

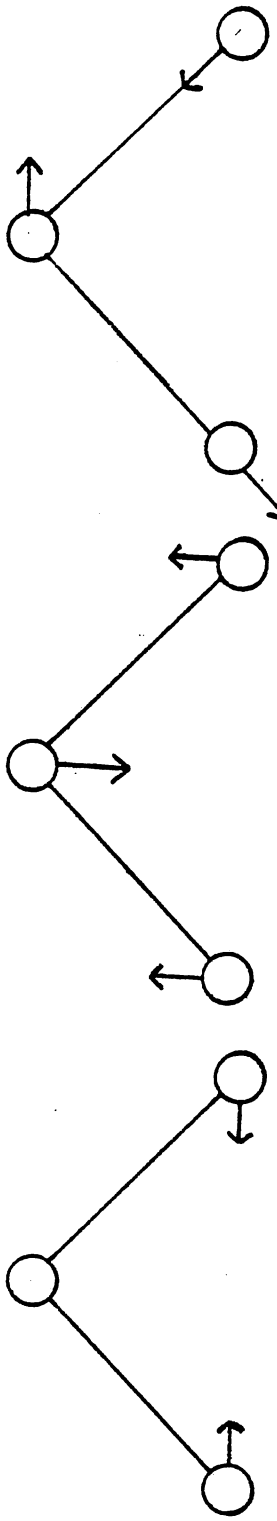

Figure 13. Approximate Normal Modes for O_3

$$V = 1/2 \sum_{k=1}^{3} \lambda_k Q_k^2 \qquad \text{(III-11)}$$

with

$$\lambda_k = 4\pi^2 \nu_k^2 \qquad \text{(III-12)}$$

where ν_k's are the fundamental vibration frequencies of the molecule.

If we assume the O_3 molecule to lie in the X-Y plane, and the NO molecule along the X'-axis, we may derive the following expressions for the cartesian displacement coordinates by making use of Eq (III-8) to (III-10) and the normal modes shown in Figure 13.

$$\Delta x_1 = (1/2m_o)^{1/2} Q_1 - 1/c\ Q_3 \sin\beta/2$$

$$\Delta y_1 = (1/6m_o)^{1/2} Q_2 - 1/c\ Q_3 \cos\beta/2$$

$$\Delta z_1 = 0$$

$$\Delta x_2 = -(1/2m_o)^{1/2} Q_1 - 1/c\ Q_3 \sin\beta/2$$

$$\Delta y_2 = (1/6m_o)^{1/2} Q_2 + 1/c\ Q_3 \cos\beta/2$$

$$\Delta z_2 = 0$$

$$\Delta x_3 = 2/c\ Q_3 \sin\beta/2$$

$$\Delta y_3 = -2(1/6m_o)^{1/2} Q_2$$

$$\Delta z_3 = 0 \qquad \text{(III-13)}$$

where

$$c = (2m_o(1 + 2\sin^2\beta/2))^{\frac{1}{2}} \text{ with}$$

$$\beta = \text{the vertex angle in } O_3$$

$$\Delta x_4 = -(m_o/m_N m_T)^{\frac{1}{2}}\, Q_{NO}$$

$$\Delta x_5 = (m_N/m_O m_T)^{\frac{1}{2}}\, Q_{NO}$$

$$\Delta y_4 = \Delta y_5 = \Delta z_4 = \Delta z_5 = 0 \qquad \text{(III-14)}$$

$$\text{with } m_T = m_o + m_N$$

The kinetic energy, after neglecting the rotational-vibrational interaction, may be written as (81),

$$T_{O_3} = 1/2\ (I_{xx}\omega_x^2 + I_{yy}\omega_y^2 + I_{zz}\omega_z^2 + \sum_{k=1}^{3} \dot{Q}_k^2) \qquad \text{(III-15)}$$

The first three terms represent the rotational kinetic energy and the last term represents the vibrational kinetic energy of the molecule. It should be noted that the terms involving the products of inertia do not enter the rotational kinetic energy expression since the principal axes of inertia of the molecule have been assumed to coincide with the space-fixed axes. The moments of inertia I_{xx}, I_{yy}, I_{zz} are given by,

$$I_{xx} = \sum_{i=1}^{3} m_o(Y_i^2 + Z_i^2)$$

$$I_{yy} = \sum_{i=1}^{3} m_o (X_i^2 + Z_i^2)$$

$$I_{zz} = \sum_{i=1}^{3} m_o (X_i^2 + Y_i^2) \qquad \text{(III-16)}$$

The kinetic energy of the NO molecule is given by,

$$T_{NO} = 1/2 \, (I_{NO} \, (\omega_{1y}^2 + \omega_{1z}^2) + \dot{Q}_{NO}^2) \qquad \text{(III-17)}$$

where I_{NO} is the moment of inertia for NO;

$$I_{NO} = m_N x'^2_4 + m_o \, x'^2_5 \qquad \text{(III-18)}$$

From these expressions for the kinetic energy, both the total angular momentum $\underset{\sim}{M}_{O_3}$ and $\underset{\sim}{M}_{NO}$ and the momenta conjugate to the normal coordinates P_k and P_{NO} can be found:

$$M_x \, (O_3) = \frac{\partial T_{O_3}}{\partial \omega_x} = I_{xx} \omega_x$$

$$M_y \, (O_3) = \frac{\partial T_{O_3}}{\partial \omega_y} = I_{yy} \omega_y$$

$$M_z \, (O_3) = \frac{\partial T_{O_3}}{\partial \omega_z} = I_{zz} \omega_z$$

$$M_x\ (NO) = \frac{\partial T_{NO}}{\partial \omega_{1x}} = 0$$

$$M_y\ (NO) = \frac{\partial T_{NO}}{\partial \omega_{1y}} = I_{NO}\omega_{1y}$$

$$M_z\ (NO) = \frac{\partial T_{NO}}{\partial \omega_{1z}} = I_{NO}\omega_{1z} \qquad \text{(III-19)}$$

and

$$P_k = \frac{\partial T_{O_3}}{\partial \dot{Q}_k} = \dot{Q}_k, \quad k = 1, 2, 3$$

$$P_{NO} = \frac{\partial T_{NO}}{\partial \dot{Q}_{NO}} = \dot{Q}_{NO} \qquad \text{(III-20)}$$

Thus the vibrational and rotational kinetic energies are given by,

$$T_{vib}\ (O_3) = 1/2 \sum_{k=1}^{3} P_k^2$$

$$E_{rot}\ (O_3) = 1/2 \sum_{i=x}^{Z} M_i(O_3)\omega_i$$

$$T_{vib}\ (NO) = 1/2\ P_{NO}^2$$

$$E_{rot}\ (NO) = 1/2\ I_{NO}(\omega_{1y}^2 + \omega_{1z}^2) \qquad \text{(III-21)}$$

The total vibrational energies of the molecules are given by,

$$E_{vib}\ (O_3) = T_{vib}\ (O_3) + V_{O_3} = \sum_{k=1}^{3} E_k \qquad \text{(III-22)}$$

where

$$E_k = 1/2\ (P_k^2 + \lambda_k Q_k^2) \qquad \text{(III-23)}$$

and

$$E_{vib}\ (NO) = T_{vib}\ (NO) + V_{NO}$$

$$= 1/2\ (P_{NO}^2 + \lambda_{NO} Q_{NO}^2) \qquad \text{(III-24)}$$

It should be noted that since the potential energy used is not harmonic, the normal coordinates and their energies can only be approximations to the real behavior of the molecule.

Selection of Initial Conditions

In the quasiclassical trajectory calculations, the initial state of the system is specified by the allowed quantal levels of the molecule. It should be emphasized, however, that once the initial state is determined, the system is treated in a completely classical manner. The initial conditions of each collision trajectory are specified by a set of energy and geometry parameters. The initial state of the trajectory for the ozone-nitric oxide system is defined by the following parameters: for ozone the vibrational and rotational quantum numbers n_1, n_2, n_3, J, K, the vibrational phase angles δ_1, δ_2, δ_3, an angle ψ_1 which defines

the plane of rotation of the molecule, the angles which define the orientation of the molecule ϕ_1, ϕ_2, ϕ_3; for nitric oxide the vibrational quantum number n_4, the rotational quantum number J_{NO}, the vibrational phase angle δ_4, an angle ψ_2 which defines the plane of rotation of the molecule, the angles which define the orientation of the molecule ϕ_1', ϕ_2', ϕ_3'; the impact parameter b, the initial relative velocity vector V_R, and the initial distance R_S between the centers of mass of O_3 and NO. These parameters have been used to obtain the initial cartesian coordinates.

The vibrational energy of ozone has been assumed to be given by,

$$E_{vib}\ (O_3) = \sum_{k=1}^{3} E_k \qquad \text{(III-25)}$$

where

$$E_1 = \omega_2(n_2 + 1/2) + X_{22}(n_2 + 1/2)^2 + 1/2\ X_{12}(n_1 + 1/2)$$
$$(n_2 + 1/2) + 1/2\ X_{23}(n_2 + 1/2)(n_3 + 1/2)$$

$$E_2 = \omega_1(n_1 + 1/2) + X_{11}(n_1 + 1/2)^2 + 1/2\ X_{13}(n_1 + 1/2)$$
$$(n_3 + 1/2) + 1/2\ X_{12}(n_1 + 1/2)(n_2 + 1/2)$$

$$E_3 = \omega_3(n_3 + 1/2) + X_{33}(n_3 + 1/2)^2 + 1/2\ X_{13}(n_1 + 1/2)$$
$$(n_3 + 1/2) + 1/2\ X_{23}(n_2 + 1/2)(n_3 + 1/2) \qquad \text{(III-26)}$$

Since ozone is an asymmetric top, the rotational energy levels cannot be represented by an explicit formula. However, the asymmetry parameter for ozone, defined as

$$\kappa = 2B - A - C/A - C \qquad \text{(III-27)}$$

where A, B and C are the rotational constants, is equal to -0.968 (82). This is very close to the value of -1 for a prolate symmetric top. Hence ozone has been approximated to be a prolate symmetric top. The rotational energies of O_3 have been assumed to be given by,

$$E_{rot}\ (O_3) = 1/2\ (B+C)J(J+1) + (A - 1/2(B+C))K^2 \qquad \text{(III-28)}$$

The constants in Eq (III-26) and Eq (III-28) have been given by Barbe et al. (82) and are given in Table XVI.

The specification of the initial rotational energy of O_3 requires two quantum numbers J and K. These were selected from a Boltzmann distribution of rotational energy levels at the desired temperature, T. The rotational energies were initially computed for various J and K values using Eq (III-28) and were arranged in the order of increasing energy. These ordered levels, each associated with a particular J and K were designated with a single quantum number, M. The initial M value was chosen (58) as the nearest integral solution to the Equation,

$$\xi(M) = Q_M^{-1} \sum_{M'=0}^{M} g_{M'} \exp(-E_{M'}/kT)$$

where

$$Q_M = \sum_{M=0}^{\infty} g_M \exp(-E_M/kT)$$

with

TABLE XVI

SPECTROSCOPIC CONSTANTS OF O_3 AND NO

O_3

Equilibrium geometry[a]

$R = 1.2717\ \text{Å}$
$\beta = 116.57^{o}$

Harmonic frequencies[a]

$\omega_1 = 1103\ cm^{-1}$
$\omega_2 = 701\ cm^{-1}$
$\omega_3 = 1042\ cm^{-1}$

Anharmonic constants[b]

$X_{11} = -4.9\ cm^{-1}$ $X_{12} = -9.1\ cm^{-1}$
$X_{22} = -1.0\ cm^{-1}$ $X_{13} = -34.8\ cm^{-1}$
$X_{33} = -10.6\ cm^{-1}$ $X_{23} = -17.0\ cm^{-1}$

Rotational constants[b,c]

$$X = X_e - \sum_{i=1}^{3} \alpha_i^X (v_i + 1/2),\ X = A, B, C$$

$A_e = 3.55176$	$B_e = 0.44906$	$C_e = 0.39876$
$\alpha_1^A = -2.981$ E-03	$\alpha_1^B = 2.554$ E-03	$\alpha_1^C = 2.319$ E-03
$\alpha_2^A = -5.342$ E-04	$\alpha_2^B = 1.269$ E-03	$\alpha_2^C = 2.307$ E-03
$\alpha_3^A = 5.312$ E-04	$\alpha_3^B = 3.992$ E-03	$\alpha_3^C = 3.613$ E-03

NO[d]

$\omega_e = 1904.03\ cm^{-1}$
$X_{NO} = -13.97\ cm^{-1}$
$B_e = 1.705\ cm^{-1}$
$\alpha_e = 0.0178\ cm^{-1}$

(a) Reference 82.
(b) Reference 82.
(c) Values are in cm^{-1}.
(d) Reference 83.

$$g_M = 2(2J+1) \quad \text{if } K \neq 0$$

$$g_M = (2J+1) \quad \text{if } K = 0 \qquad \text{(III-29)}$$

and $\xi(M)$ is a pseudorandom number selected from a uniform distribution between 0 and 1. The initial M state was then converted to an initial (J,K) pair.

The rotational and vibrational energies of NO have been assumed to be given by,

$$E_{vib}(NO) = \omega_e(n_4 + 1/2) + X_{NO}(n_4 + 1/2)^2$$

$$E_{rot}(NO) = B_e J_{NO}(J_{NO}+1) - \alpha_e(n_4 + 1/2)J_{NO}(J_{NO}+1) \qquad \text{(III-30)}$$

The constants have been defined by Herzberg (83) and are given in Table XVI.

The initial rotational quantum number for NO, J_{NO}, has also been chosen from a thermal Boltzmann distribution. This is achieved by finding the nearest integral solution to the equation,

$$J_{NO} = 1/2(-1 + (1-8I_{NO}kT\ln(1-\xi_J)/\hbar^2)^{\frac{1}{2}}) \qquad \text{(III-31)}$$

where $0 \leq \xi_J \leq 1$.

For a harmonic potential, the time dependence of the normal coordinates is given by,

$$Q_k(t) = \{2E_k/\lambda_k\}^{\frac{1}{2}}\cos(\lambda_k^{\frac{1}{2}}t + \delta_k) \qquad \text{(III-32)}$$

where $\lambda_k = 4\pi^2\nu_k^2$ and δ_k is an arbitrary phase factor, $0 \leq \delta_k \leq 2\pi$. The phase factors are selected randomly from a uniform distribution.

$$\delta_k = 2\pi\xi_k \qquad \text{(III-33)}$$

where ξ_k are pseudorandom numbers uniformly distributed between 0 and 1. The initial momenta conjugate to the normal coordinates are given by,

$$P_k(t=0) = \pm \{2E_k - \lambda_k Q_k^2(t=0)\}^{\frac{1}{2}} \qquad \text{(III-34)}$$

The + sign is used when $0 < \delta_k \leq \pi$ and the - sign is used when $\pi < \delta_k \leq 2\pi$.

The normal coordinates Q_k are converted to the cartesian coordinates as follows:

$$X_1 = (1/2m_o)^{\frac{1}{2}} Q_1 - 1/c\ Q_3 \sin\frac{\beta}{2} - R^e_{O_3} \sin\frac{\beta}{2}$$

$$Y_1 = (1/6m_o)^{\frac{1}{2}} Q_2 - 1/c\ Q_3 \cos\frac{\beta}{2} - 1/3\ R^e_{O_3} \cos\frac{\beta}{2}$$

$$Z_1 = 0$$

$$X_2 = -(1/2m_o)^{\frac{1}{2}} Q_1 - 1/c\ Q_3 \sin\frac{\beta}{2} + R^e_{O_3} \sin\frac{\beta}{2}$$

$$Y_2 = (1/6m_o)^{\frac{1}{2}} Q_2 + 1/c\ Q_3 \cos\frac{\beta}{2} - 1/3\ R^e_{O_3} \cos\frac{\beta}{2}$$

$$Z_2 = 0$$

$$X_3 = 2/c\ Q_3 \sin\frac{\beta}{2}$$

$$Y_3 = -2(1/6m_o)^{\frac{1}{2}} Q_2 + 2/3\ R^e_{O_3} \cos\frac{\beta}{2}$$

$$Z_3 = 0$$

$$X_4' = -(m_o/m_N m_T)^{1/2} Q_{NO} - (m_o/m_T) R_{NO}^e$$

$$Y_4' = 0$$

$$Z_4' = 0$$

$$X_5' = (m_N/m_o m_T)^{1/2} Q_{NO} + (m_N/m_T) R_{NO}^e$$

$$Y_5' = 0$$

$$Z_5' = 0 \qquad \text{(III-35)}$$

where $R_{O_3}^e$ and R_{NO}^e are the equilibrium bond distances in O_3 and NO, respectively. From these cartesian coordinates, the principal moments of inertia of O_3 and NO are calculated. For the O_3 molecule lying in the X-Y plane, with the figure-axis along the X-axis, the total rotational angular momentum, and the X-component are given by,

$$L^2 = J(J+1)\hbar^2$$

and

$$L_X = K\hbar \qquad \text{(III-36)}$$

The angle ψ_1, defining the plane of rotation of the molecule is chosen randomly from a uniform distribution.

$$\psi_1 = 2\pi\xi_5, \quad 0 \leq \xi_5 \leq 1 \qquad \text{(III-37)}$$

Under these conditions, the components of the angular momentum are given by,

$$L_x = K\hbar$$

$$L_y = L \sin\alpha \cos\psi_1$$

$$L_z = L \sin\alpha \sin\psi_1 \qquad \text{(III-38)}$$

where $\alpha = \arccos(L_x/L)$.

The components of the angular velocity are,

$$\omega_x = L_x/I_{xx}$$

$$\omega_y = L_y/I_{yy}$$

$$\omega_z = L_z/I_{zz} \qquad \text{(III-39)}$$

The angular momentum components for the NO molecule assumed to be along the X'-axis are given by,

$$L_{1x'} = 0$$

$$L_{1y'} = (2I_{NO}E_{rot}(NO))^{\frac{1}{2}}\cos\psi_2$$

$$L_{1z'} = (2I_{NO}E_{rot}(NO))^{\frac{1}{2}}\sin\psi_2 \qquad \text{(III-40)}$$

where ψ_2 is the angle specifying the rotational plane of the molecule and is chosen randomly from a uniform distribution.

$$\psi_2 = 2\pi\xi_6, \quad 0 \leq \xi_6 \leq 1 \qquad \text{(III-41)}$$

The components of the angular velocity for the NO molecule are,

$$\omega_{1x} = 0$$

$$\omega_{1y} = L_{1y'}/I_{NO}$$

$$\omega_{1z} = L_{1z'}/I_{NO} \qquad \text{(III-42)}$$

Given the Q_k's and P_k's, the time derivatives of the normal coordinates are easily obtained:

$$\dot{Q}_k = P_k, \quad K = 1, 2, 3$$

$$\dot{Q}_{NO} = P_{NO} \qquad \text{(III-43)}$$

The momenta conjugate to the cartesian coordinates are now given by,

$$P_{x1} = (m_o/2)^{\frac{1}{2}}\dot{Q}_1 - m_o/c \sin\frac{\beta}{2}\dot{Q}_3 - m_o\omega_z Y_1$$

$$P_{y1} = (m_o/6)^{\frac{1}{2}}\dot{Q}_2 - m_o/c \cos\frac{\beta}{2}\dot{Q}_3 + m_o\omega_z X_1$$

$$P_{z1} = m_o(\omega_x Y_1 - \omega_y X_1)$$

$$P_{x2} = -(m_o/2)^{\frac{1}{2}}\dot{Q}_1 - m_o/c \sin\frac{\beta}{2}\dot{Q}_3 - m_o\omega_z Y_2$$

$$P_{y2} = (m_o/6)^{\frac{1}{2}}\dot{Q}_2 + m_o/c \cos\frac{\beta}{2}\dot{Q}_3 + m_o\omega_z X_2$$

$$P_{z2} = m_o(\omega_x Y_2 - \omega_y X_2)$$

$$P_{x3} = 2m_o/c \sin\frac{\beta}{2}\dot{Q}_3 - m_o\omega_z Y_3$$

$$P_{y3} = -2(m_o/6)^{\frac{1}{2}}\dot{Q}_2 + m_o\omega_z X_3$$

$$P_{z3} = m_o(\omega_x Y_3 - \omega_y X_3)$$

$$
\begin{aligned}
P'_{x4} &= -(m_o m_N/m_T)^{\frac{1}{2}}\dot{Q}_{NO} \\
P'_{y4} &= m_N\omega_{1z}X'_4 \\
P'_{z4} &= -m_N\omega_{1y}X'_4 \\
P'_{x5} &= (m_o m_N/m_T)^{\frac{1}{2}}\dot{Q}_{NO} \\
P'_{y5} &= m_o\omega_{1z}X'_5 \\
P'_{z5} &= -m_o\omega_{1y}X'_5
\end{aligned}
\qquad \text{(III-44)}
$$

The O_3 and NO molecules were then randomly oriented in space by rotating about the Y, Z, X and Y', Z', X' axes respectively, through randomly chosen angles.

$$
\begin{bmatrix} X_i \\ Y_i \\ Z_i \end{bmatrix}_f = R_x(\phi_1)R_z(\phi_3)R_y(\phi_2) \begin{bmatrix} X_i \\ Y_i \\ Z_i \end{bmatrix}
$$

$$
\begin{bmatrix} P_{xi} \\ P_{yi} \\ P_{zi} \end{bmatrix}_f = R_x(\phi_1)R_z(\phi_3)R_y(\phi_2) \begin{bmatrix} P_{xi} \\ P_{yi} \\ P_{zi} \end{bmatrix}, \; i = 1, 2, 3 \qquad \text{(III-45)}
$$

Similar transformations have been carried out for the NO molecule with the rotational angles ϕ_i's replaced by ϕ'_i's. The R_x, R_y and R_z functions are the three-dimensional rotation matrices given in Table

XVII. The angles ϕ_i and ϕ_i' were chosen randomly from a uniform distribution.

$$\phi_i = 2\pi\xi$$

$$\phi_i' = 2\pi\xi', \quad 0 \leq \xi, \xi' \leq 1 \tag{III-46}$$

The origin of the space-fixed frame is defined as the center of mass of O_3. The coordinate system X'Y'Z' is at a distance $\underset{\sim}{R}_S$ from the center of mass of O_3 and hence the origin of XYZ. The coordinates of NO are therefore:

$$X_4 = X_4' + (R_S)_x$$

$$Y_4 = Y_4' + (R_S)_y$$

$$Z_4 = Z_4' + (R_S)_z$$

$$X_5 = X_5' + (R_S)_x$$

$$Y_5 = Y_5' + (R_S)_y$$

$$Z_5 = Z_5' + (R_S)_z \tag{III-47}$$

If the impact parameter is b, and if the center of mass of NO is approaching from the -X direction in the XY plane,

$$(R_S)_x = -(R_S^2 - b^2)^{\frac{1}{2}}, \quad (R_S)_y = -b, \quad (R_S)_z = 0$$

The impact parameter is chosen using the linear transformation,

TABLE XVII

ROTATION MATRICES

$$R_y(\phi) = \begin{bmatrix} \cos\phi & 0 & -\sin\phi \\ 0 & 1 & 0 \\ \sin\phi & 0 & \cos\phi \end{bmatrix}$$

$$R_z(\phi) = \begin{bmatrix} \cos\phi & \sin\phi & 0 \\ -\sin\phi & \cos\phi & 0 \\ 0 & 0 & 1 \end{bmatrix}$$

$$R_x(\phi) = \begin{bmatrix} 1 & 1 & 0 \\ 0 & \cos\phi & \sin\phi \\ 0 & -\sin\phi & \cos\phi \end{bmatrix}$$

$$b = b_{max}\xi_b, \qquad \text{(III-48)}$$

where ξ_b is a pseudorandom number uniformly distributed between 0 and 1.

The initial relative velocity vector is assumed to be directed along the X-axis and the center of mass velocity is set to zero. Thus the NO center of mass velocity translates in the X-direction with velocity $(m_{O_3}/m_{O_3} + m_{NO})V_R$, and the O_3 center of mass translates in the -X- direction with velocity $(m_{NO}/m_{O_3} + m_{NO})V_R$ where $m_{O_3} = 3\ m_O$ and $m_{NO} = m_N + m_O$. The relative velocity may be chosen from a thermal Boltzmann distribution if the rate constant is to be computed, or we may run a batch of trajectories with a specified relative velocity if the reaction cross section is to be computed. The former is achieved by choosing V_R to be the solution to the following equation.

$$(\exp(-\mu V_R^2/2kT))(V_R^2 + 2kT/\mu) = (1 - \xi(V_R))X(\exp(-\mu V_M^2/2kT))(V_M^2 + 2kT/\mu) \qquad \text{(III-49)}$$

where μ is the reduced mass of the system given by,

$$\mu = m_{O_3} \cdot m_{NO}/(m_{O_3} + m_{NO}) \qquad \text{(III-50)}$$

and V_M is the threshold velocity, below which the probability of reaction is negligible. $\xi(V_R)$ is a pseudorandom number uniformly distributed between 0 and 1.

The momenta in the space-fixed cartesian coordinates are now given by,

$$p_{x_1} = p_{x_1} - m_o(m_{NO}/m_{O_3} + m_{NO})V_R,\ p_{y_1} = p_{y_1},\ p_{z_1} = p_{z_1}$$

$$p_{x_2} = p_{x_2} - m_o(M_{NO}/m_{O_3} + m_{NO})V_R,\ p_{y_2} = p_{y_2},\ p_{z_2} = p_{z_2}$$

$$p_{x_3} = p_{x_3} - m_o(m_{NO}/m_{O_3} + m_{NO})V_R,\ p_{y_3} = p_{y_3},\ p_{z_3} = p_{z_3}$$

$$p_{x_4} = p_{x_4} + m_N(m_{O_3}/m_{O_3} + m_{NO})V_R,\ p_{y_4} = p_{y_4},\ p_{z_4} = p_{z_4}$$

$$p_{x_5} = p_{x_5} + m_o(m_{O_3}/m_{O_3} + m_{NO})V_R,\ p_{y_5} = p_{y_5},\ p_{z_5} = p_{z_5} \qquad \text{(III-51)}$$

The complete set of initial coordinates and momenta are now defined.

Numerical Integration of the Equations of Motion

The determination of the classical trajectories for the O_3-NO system requires the solution of the thirty coupled first-order differential equations (Hamilton's equations). Once the initial coordinates and momenta have been specified, this can be achieved by numerical methods.

In the present study, the set of coupled differential equations have been solved by using a fifth-order Adams-Bashforth predictor and a sixth-order Adams-Moulton corrector with the fourth-order Runge Kutta as the initiator (97).

The accuracy of the integration routine was monitored by (a) energy conservation, (b) conservation of each component of the total linear and angular momentum, and (c) back integration and step size reduction procedures. A variable step size has been employed in the calculations, in order to decrease the computation time. A step size of 0.04 tu in the non-interaction region and 0.015 tu in the interaction region yielded results with the desired accuracy. The units employed in this

study are given in Table XVIII.

Analysis of Final States

The determination of the results of a given trajectory requires a set of appropriate end tests along with the expression for various energies, scattering angles and bond distances in terms of the cartesian coordinates and momenta.

The trajectory was considered reactive if

$$R_{oo}i > R_S, \quad R_{NO}i < \{(R_e)_{NO} + 0.5\} \text{ au}$$

$$\text{and} \quad R_{OO} < \{(R_e)_{O_2} + 0.5\} \text{ au} \qquad \text{(III-52)}$$

$R_{OO}i$ and R_{OO} refer to the O-O bonds in ozone. The superscript i designates the O atom abstracted by NO. R_{NO} refers to the N-O bond in NO_2 and R_e's are the equilibrium bond distances.

The trajectory was considered non-reactive if

$$R_{NO}i > R_S \quad \text{for } i = 1, 2, 3$$

The final-state dynamic properties of interest are as follows:

If j and k designate the O atoms that form the O_2 molecule, the final velocity of the O_2 center of mass is given by,

$$\underset{\sim}{V}'_{O_2} = 1/m_{O_2} \{ p_{x_j} + p_{x_k}, \; p_{y_j} + p_{y_k}, \; p_{z_j} + p_{z_k} \} \qquad \text{(III-53)}$$

The final relative velocity vector is,

$$\underset{\sim}{V}'_R = (m_{O_2} + m_{NO_2}/m_{NO_2})\underset{\sim}{V}'_{O_2} \qquad \text{(III-54)}$$

TABLE XVIII

UNITS USED IN THE O_3-NO QUASICLASSICAL TRAJECTORY COMPUTER CODE

Quantity	Units	Cgs Equivalent	
distance	angstrom (Å)	1.0	E-08 cm
time	time unit (t.u.)	1.01804287	E-14 s
velocity	velocity unit (v.u.)	0.9822769	E+06 cm/s
energy	electron volt (eV)	1.60219	E-12 erg
mass	atomic mass unit (amu)	1.6604345	E-24 g
momentum	momentum unit	1.631006	E-18 dyne.s
angular momentum	angular momentum unit	1.631006	E-26 erg.s
Planck's constant, $h/2\pi$	0.0646551 eV-tu	1.0545887	E-27 erg.s
Boltzmann constant, k	8.61734×10^{-5} eV/°K	1.380662	E-16 erg/°K
speed of light, c	3.05201×10^{-4} cm/t.u.	2.99792	E+10 cm/s

(a) These units are similar to the molecular units used by Raff et al., J. Chem. Phys. 56, 5998 (1972). The units differ only in the unit of distance.

(b) These values are based on the physical constants recommended by the CODATA Task Group on Fundamental Constants and are taken from Physics Today, Sept. 1974.

The scattering angle H, the angle between the initial and final velocity vectors, is given by,

$$\Theta = (V_R')_x / |V_R| \qquad \text{(III-55)}$$

since the initial relative velocity vector has been assumed to be along the X-axis.

In order to compute the final internal energies of the molecule, the motions of the molecular centers of mass have been subtracted from the cartesian coordinates.

$$p_{x_i} = p_{x_i} + m_i(m_{O_2}/m_{O_2} + m_{NO_2})(V_R')_x$$

$$p_{y_i} = p_{y_i} + m_i(m_{O_2}/m_{O_2} + m_{NO_2})(V_R')_y$$

$$p_{z_i} = p_{z_i} + m_i(m_{O_2}/m_{O_2} + m_{NO_2})(V_R')_z, \; i = 1, 4, 5 \qquad \text{(III-56)}$$

where 1 designates the O atom abstracted from O_3.

$$p_{x_i} = p_{x_i} - m_i(m_{NO_2}/m_{O_2} + m_{NO_2})(V_R')_x$$

$$p_{y_i} = p_{y_i} - m_i(m_{NO_2}/m_{O_2} + m_{NO_2})(V_R')_y$$

$$p_{z_i} = p_{z_i} - m_i(m_{NO_2}/m_{O_2} + m_{NO_2})(V_R')_z, \; i = j, k \qquad \text{(III-57)}$$

The atomic coordinates relative to the respective centers of masses of the product molecules are,

$$X_i = X_i - 1/m_{NO_2}(m_o X_1 + m_N X_4 + m_o X_5)$$

$$Y_i = Y_i - 1/m_{NO_2}(m_o Y_1 + m_N Y_4 + m_o Y_5)$$

$$Z_i = Z_i - 1/m_{NO_2}(m_o Z_1 + m_N Z_4 + m_o Z_5), \; i = 1, 4, 5 \qquad \text{(III-58)}$$

and

$$X_i = X_i - 1/m_{O_2}(m_o X_j + m_o X_k)$$

$$Y_i = Y_i - 1/m_{O_2}(m_o Y_j + m_o Y_k)$$

$$Z_i = Z_i - 1/m_{O_2}(m_o Z_j + m_o Z_k), \; i = j, k \qquad \text{(III-59)}$$

The O_2 molecule is oriented along the X-axis by rotating it about the X-axis by an angle ϕ_1 given by,

$$\phi_1 = \tan^{-1}(Z_j/Y_j) \qquad \text{(III-60)}$$

and then about the Z-axis by an angle ϕ_2 given by,

$$\phi_2 = \tan^{-1}(Y'_j/X'_j) \qquad \text{(III-61)}$$

where Y'_j and X'_j are the coordinates of atom j after the first rotation. The coordinates and momenta are transformed by using the rotational matrices given in Table XVII. The moment of inertia of the O_2 molecule is calculated by using the transformed coordinates.

$$I_{O_2} = m_o X_j^2 + m_o X_k^2 \qquad \text{(III-62)}$$

The moments of inertia and the products of inertia of NO_2 are calculated

as follows:

$$I_{xx} = \sum_i m_i(Y_i^2 + Z_i^2)$$

$$I_{yy} = \sum_i m_i(X_i^2 + Z_i^2)$$

$$I_{zz} = \sum_i m_i(X_i^2 + Y_i^2)$$

$$I_{xy} = \sum_i m_i X_i Y_i$$

$$I_{yz} = \sum_i m_i Y_i Z_i$$

$$I_{xz} = \sum_i m_i X_i Z_i , \quad i = \ell, 4, 5 \qquad \text{(III-63)}$$

The final angular momenta are obtained as follows:

$$M_x(NO_2) = \sum_i (Y_i p_{z_i} - Z_i p_{y_i})$$

$$M_y(NO_2) = \sum_i (Z_i p_{x_i} - X_i p_{z_i})$$

$$M_z(NO_2) = \sum_i (X_i p_{y_i} - Y_i p_{x_i}), \quad i = \ell, 4, 5$$

and

$$M_y(O_2) = \sum_i (Z_i p_{x_i} - X_i p_{z_i})$$

$$M_z(O_2) = \sum_i (X_i p_{y_i} - Y_i p_{x_i}),\ i = j,\ k \qquad \text{(III-64)}$$

The angular velocity components of NO_2 are given by,

$$\begin{bmatrix} \omega_x(NO_2) \\ \omega_y(NO_2) \\ \omega_z(NO_2) \end{bmatrix} = \begin{bmatrix} I_{xx} & -I_{xy} & -I_{xz} \\ -I_{xy} & I_{yy} & -I_{yz} \\ -I_{xz} & -I_{yz} & I_{zz} \end{bmatrix} \begin{bmatrix} M_x(NO_2) \\ M_y(NO_2) \\ M_z(NO_2) \end{bmatrix} \qquad \text{(III-65)}$$

If I is the moment of inertia matrix, then

$$I^{-1} = (1/\det|I|)\ \tilde{I}^t \qquad \text{(III-66)}$$

where $\tilde{I}^t$ is the transpose of the adjoint of I

$$\tilde{I}^t = \begin{bmatrix} I_{yy}I_{zz} - I_{yz}^2 & I_{xy}I_{zz} + I_{xz}I_{yz} & I_{xy}I_{yz} + I_{xz}I_{yy} \\ I_{xy}I_{zz} + I_{xz}I_{yz} & I_{xx}I_{zz} - I_{xz}^2 & I_{xx}I_{yz} + I_{xy}I_{xz} \\ I_{xy}I_{yz} + I_{yy}I_{xz} & I_{xx}I_{yz} + I_{xy}I_{xz} & I_{xx}I_{yy} - I_{xy}^2 \end{bmatrix} \qquad \text{(III-67)}$$

The angular velocity components of O_2 are given by,

$$\omega_y(O_2) = \frac{M_y(O_2)}{I_{O_2}}$$

$$\omega_z(O_2) = \frac{M_z(O_2)}{I_{O_2}} \qquad \text{(III-68)}$$

The total internal energies of the molecules are given by,

$$E_{int}(NO_2) = V_{NO_2} + 1/2 \sum_i \frac{p_{x_i}^2}{m_i} + \frac{p_{y_i}^2}{m_i} + \frac{p_{z_i}^2}{m_i}, \quad i = \ell, 4, 5$$

$$E_{int}(O_2) = V_{O_2} + 1/2 \sum_i \frac{p_{x_i}^2}{m_i} + \frac{p_{y_i}^2}{m_i} + \frac{p_{z_i}^2}{m_i}, \quad i = j, k \qquad \text{(III-69)}$$

where V's are the potential energies of the molecules. The rotational energies of the molecules have been assumed to be given by,

$$E_{rot}(NO_2) = 1/2 \sum_{i=x}^{z} M_i(NO_2)\omega_i(NO_2)$$

$$E_{rot}(O_2) = 1/2\, I_{O_2}\{\omega_y^2(O_2) + \omega_z^2(O_2)\} \qquad \text{(III-70)}$$

The vibrational energies of the molecules have been calculated using the following expressions:

$$E_{vib}(NO_2) = E_{int}(NO_2) - E_{rot}(NO_2)$$

$$E_{vib}(O_2) = E_{int}(O_2) - E_{rot}(O_2) \qquad \text{(III-71)}$$

Statistical Averaging

Any physically observable quantity is an average over a large

number of collision events. In order to obtain a reasonable estimate for the experimentally measurable quantities, the theoretical procedure should consider the various possible collisions. Thus the calculation of the reaction cross sections and rate constant for the reaction requires the evaluation of multi-dimensional integrals. For instance, the rotationally averaged total reaction cross section for the reaction of O_3 with NO may be written as,

$$\sigma(V_R,n_i) = Q_M^{-1} \sum_{M=0}^{\infty} g_M \exp(-E_M/kT)\; Q_{J_{NO}}^{-1} \sum_{J_{NO}=0}^{\infty} g_{J_{NO}} \exp(-E_{J_{NO}}/kT)$$

$$\times \int_0^{2\pi} \frac{d\delta_1}{2\pi} \int_0^{2\pi} \frac{d\delta_2}{2\pi} \int_0^{2\pi} \frac{d\delta_3}{2\pi} \int_0^{2\pi} \frac{d\delta_4}{2\pi} F(\delta_1 \ldots \delta_4) \int_0^{2\pi} \frac{d\psi_1}{2\pi} \int_0^{2\pi} \frac{d\psi_2}{2\pi}$$

$$\times \int_0^{2\pi} \frac{d\phi_1}{2\pi} \int_0^{2\pi} \frac{d\phi_2}{2\pi} \int_0^{2\pi} \frac{d\phi_3}{2\pi} \int_0^{2\pi} \frac{d\phi_1'}{2\pi} \int_0^{2\pi} \frac{d\phi_2'}{2\pi} \int_0^{2\pi} \frac{d\phi_3'}{2\pi}$$

$$\times \int_0^{\infty} 2\pi P(J_{NO},M,\psi_1,\psi_2,\phi_i,\phi_i',b,V_R,n_i) b\,db \qquad \text{(III-72)}$$

where Q's are the rotational partition functions, $F(\delta_1 \ldots \delta_4)$ is the normalized probability density function for the observation of phase angles δ_1 to $\delta_1 + d\delta_1 \ldots \delta_4$ to $\delta_4 + d\delta_4$, and $P(J_{NO},M,\psi_i,\phi_i,\phi_i',b,V_R,n_i)$ is the probability of reaction determined by the quasiclassical trajectory procedure.

These multi-dimensional integrals can be most conveniently carried out by using the Monte Carlo technique. The major advantage of this procedure is that it converges at a rate that is approximately indepen-

dent of the dimensionality of the integral. In this method, the variables of integration are transformed to random numbers on the interval (0,1) as was done in Eq (III-29,31,33,37,41,46,48,49). The Monte Carlo approximant to the integral in Eq (III-72) is given by,

$$\sigma(V_R,n_i) = \frac{2\pi b_{max}^2}{N} \sum_{i=1}^{N} \xi_b^i P^i \qquad \text{(III-73)}$$

where N is the total number of trajectories, ξ_b^i is the random number used to select the impact parameter and P^i is the probability of reaction of the i^{th} trajectory. P^i is 1 if the trajectory is reactive and 0 if it is non-reactive.

The Monte Carlo error is,

$$\varepsilon = \frac{\{ \sum_{i=1}^{N_r} (\xi_b^i)^2 - 1/N\{ \sum_{i=1}^{N_r} \xi_b^i \}^{2 \; \frac{1}{2}} \} X\ 100}{\sum_{i-1}^{N_r} \xi_b^i} \qquad \text{(III-74)}$$

where N_r is the number of reactive trajectories. There is a 68% probability that the actual error in the integral is less than ε.

The rate coefficient may be obtained by using either of the following two procedures: The reaction cross sections can be averaged over a Boltzmann distribution of relative velocities to obtain the rate coefficient as follows:

$$k(T,n_i) = c(2/\pi)^{\frac{1}{2}}(\mu/kT)^{3/2}$$

$$X \int_{V_M}^{\infty} \sigma(V_R,n_i)\exp(-\mu V_R^2/2kT)\ V_R^3\ dV_R \qquad \text{(III-75)}$$

where c is a conversion factor used to obtain the rate coefficient in $cm^3 mole^{-1} sec^{-1}$. V_M is the threshold velocity chosen such that,

$$\sigma(V_R,n_i) = 0 \text{ for } V_R < V_M \qquad \text{(III-76)}$$

The second method of computing the rate coefficient involves evaluating the integral in Eq (III-75) by the Monte Carlo procedure. This is achieved by selecting V_R randomly using Eq (III-49). If N_r reactive trajectories were encountered in a set of N trajectories, the rate coefficient is given by,

$$k(T,n_i) = (2/\pi)^{\frac{1}{2}}(\mu/kT)^{\frac{1}{2}}(V_M^2 + 2kT/\mu)$$

$$X \exp(-\mu V_M^2/2kT).2\pi b_{max}^2 \ X\ 1/N \sum_{i=1}^{N_r} \xi_b^i \qquad \text{(III-79)}$$

with the statistical error determined by Eq (III-74).

Results and Discussion

The collision dynamic studies can be broadly divided into two types:

1. Those in which the prime objective is to provide a model for a particular reactive system, and

2. Those in which the prime objective is the examination of the effect of systematic variation in some parameters governing the reaction dynamics.

The present investigation is an example of the latter.

In the present study, an investigation of the effects of various topological features of the potential-energy surface on the observed reaction dynamics of polyatomic systems has been carried out by employing quasiclassical trajectory procedures. Five different potential-energy surfaces, S1 to S5, have been used in the calculations. Surfaces S1 to S4 differ considerably only in their barrier heights. Surface S5 has a barrier height comparable with S3 but differs in the position of the saddle point.

In order to choose the maximum impact parameter b_{max}, batches of 200 trajectories were run with fixed impact parameters b, and relative velocities V_R. The value of b_{max} was taken to be that value of b for which no reactive trajectories were encountered in a batch of 200. The values of b_{max} thus determined were in the range of 3.4-3.6 Å for the potential-energy surfaces employed in this study.

In order to determine the threshold velocity V_M, batches of 200 trajectories were run at fixed relative velocities V_R, and impact parameters chosen from a uniform distribution (Eq (III-49)). The value of V_M was assumed to be that value of V_R below which no reactive trajectories were encountered in a batch of 200.

In the present study, an initial separation of 8.5 au between the molecules was used. The rotational states were chosen from a Boltzmann distribution at T K. The initial vibrational states of the molecules were assigned specific values. All other variables were chosen from their appropriate distribution functions as described earlier in the chapter.

On surfaces S1 and S2, reactive trajectories were encountered down

to very low relative velocities. Hence the threshold velocity V_M, was taken to be 0.0 on both these surfaces. The rate constants were then computed at two different temperatures by using Eq (III-77) for the ground vibrational state reactants and also for those in which one quanta of energy was introduced through the antisymmetric stretching mode of ozone. Batches of 200 trajectories were run in each case. Six to ten reactions were encountered for the ground vibrational state whereas more than twice as many reactions were encountered for the vibrationally excited case. The activation energies and frequency factors have been calculated by assuming that the Arrhenius equation is a good representation for the temperature dependence of the rate coefficients for this system. The results are presented in Tables XIX and XX. The statistics are poor in the case of ground-state reactants, due to the very low probability of reactive events.

TABLE XIX

ARRHENIUS PARAMETERS FOR THE GROUND STATE REACTANTS

Surface	b_{max}/Å	In A[a]	E_a/Kcal mole
S1	3.5	-24.00	0.86
S2	3.6	-24.48	1.39
S3	3.4	-25.45	2.13
Experiment[b]	---	-27.97	2.33

(a) A values are in cm^3-$molecule^{-1}sec^{-1}$.
(b) Reference 47.

TABLE XX

ARRHENIUS PARAMETERS FOR THE VIBRATIONALLY EXCITED (0010) REACTANTS

Surface	In A'[a]	E_a'/Kcal mole	% Decrease in E_a
S1	-22.72	0.63	27
S2	-23.77	0.32	77
S3	-24.84	0.32	85
Experiment[b]	-28.60	1.03	56

(a) A values are in cm^3-$molecule^{-1}$ sec^{-1}.
(b) Reference 47.

The maximum impact parameter on surface S3 was chosen to be 3.2 Å. The threshold velocity for the ground vibrational state reactants was found to be 0.09 vu. When one quanta of energy was introduced through the antisymmetric stretching mode of ozone, the probability of encountering a reactive event was enhanced considerably and no threshold was observed. The cross sections have been computed as a function of relative velocities at a rotational temperature of 400K. The results are given in Table XXI. Table XXI compares the cross sections obtained with the vibrationally excited O_3 molecules with those obtained when the same total energy is available through relative translation. The results clearly indicate that vibrational energy is much more effective than relative translation, in promoting the reaction.

On surface S4, occurrence of a reactive event was much less probable with ground vibrational state reactants, even at very high

relative translational energies. In order to increase the statistical accuracy, the maximum impact parameter b_{max}, was made to vary with the relative velocity. Calculations have been carried out with ground state and vibrationally excited $O_3(001)$ with V_M = 0.145 vu and the results are given in Table XXII. Less than six reactive trajectories were encountered in a batch of 200. A more detailed investigation was not attempted on this surface, due to the low probability of reactive events.

TABLE XXI

CROSS SECTIONS $(A^o)^2$ OBTAINED ON SURFACE S3

E_R Kcal/mole	E'_R Kcal/mole	$S(E_R)$	
		Ground state vibration + Rel. trans. (E_R)	Excited state vibration + Rel. trans. (E_R')
4.79	1.79	0.0321 ± 0.01	1.54 ± 0.3
8.52	5.52	0.177 ± 0.04	1.08 ± 0.2
16.69	13.69	0.077 ± 0.02	0.80 ± 0.16
19.16	19.16	0.019 ± 0.005	0.70 ± 0.14

In order to investigate the effectiveness of vibrational excitation in promoting the reaction, it is necessary to compare the rate constants obtained on vibrational excitation with those that would be obtained if

the excitation quanta (3.0 Kcal/mole of energy) were distributed statistically among all the reactant degrees of freedom in the collisional center of mass. The equivalent thermal temperature T was determined by inserting the constant volume heat capacities (40) into the equation

$$\int_{T_0}^{T} (c_v^{NO} + c_v^{O_3} - 1.5R)dT' = h\nu_3 \qquad \text{(III-78)}$$

For T_0 = 308K, the ambient temperature in the experimental cell, this yields a value of T = 575K. The increase in thermal rate constant for such a temperature rise is given by,

$$R_1 = \frac{k(575)}{k(308)} \qquad \text{(III-79)}$$

and this is compared with the enhancement obtained on vibrational excitation namely,

$$R_2 = \frac{k'(308)}{k(308)} \qquad \text{(III-80)}$$

TABLE XXII

RATE CONSTANTS COMPUTED ON SURFACE S4

$T/^oK$	Reactant state	$k(T)/cm^3$-molecule^{-1}·sec^{-1}
400	(0000)	2.35×10^{-16}
400	(0010)	1.02×10^{-14}

The computed R_1 and R_2 values for surfaces S1 to S3 are given in Table XXIII. The statistical uncertainty of the results corresponds to a variation of 20-40%. These results clearly indicate that vibration is much more effective than relative translation on these surfaces. This effect becomes more pronounced with increasing barrier height. This type of result is analogous to that which has previously been observed for atom-diatomic exchange reactions (18).

TABLE XXIII

EFFECTIVENESS OF VIBRATION OVER RELATIVE TRANSLATION IN PROMOTING THE REACTION

Surface	Barrier Kcal/mole	$R_1 = k(575)/k(308)^a$	$R_2 = k'(308)/k(308)^a$
S1	0.71	1.92	5.16
S2	2.35	2.84	11.84
S3	3.57	5.02	35.09

(a) Results have a 20-40% statistical error corresponding to one sigma limit.
k(T) - Rate constant with ground state reactants at T K
k'(T) - Rate constant with (0010) reactants at T K where the numbers in parenthesis are the vibrational quantum numbers of O_3 and NO.

Thus for surfaces with a "late" barrier, vibrational excitation seems to be much more effective than relative translation in promoting the reaction. Similar behavior has been observed in the case of

atom-diatomic molecule reactions (18). These findings can be understood by considering the path of a reactive trajectory across the potential-energy surface. Figure 14 shows the course of a typical reactive trajectory on surface S4. The course of the trajectory can be understood by thinking of the path that a rolling marble would take across the surface. In Figure 14 we see that the momentum of a rolling ball travelling transverse to the entry valley of the energy surface tends to carry it over the barrier placed in the exit-valley. The transverse momentum in the entry-valley is converted to parallel momentum along the exit valley. This illustrates the effectiveness of vibrational energy on this class of surfaces (S1 to S4). The results on this class of surfaces can be compared to those on the surface IIB2 of Chapman (80). It has been observed that vibrational energy enhances the probability of reaction on surface IIB2 in which the barrier is located in the exit-channel.

It has also been observed that most of the available energy goes into NO_2 vibration. From Figure 14 it is seen that vibration begins to set in only later in the product valley. In the case of atom-diatomic molecule reactions, when sufficient energy is available through the exothermicity of the reaction, the molecule exhibits vibrational excitation even while entering the product valley (18). This is due to the fact that there is only one vibrational mode in the case of diatomic molecules, whereas in the case of non-linear triatomic molecules there are three vibrational modes. When the NO_2 molecule is formed, the bending mode is excited. The time lag observed in Figure 14 is due to the time taken for coupling between the bending and stretching modes of NO_2 to produce intramolecular energy transfer.

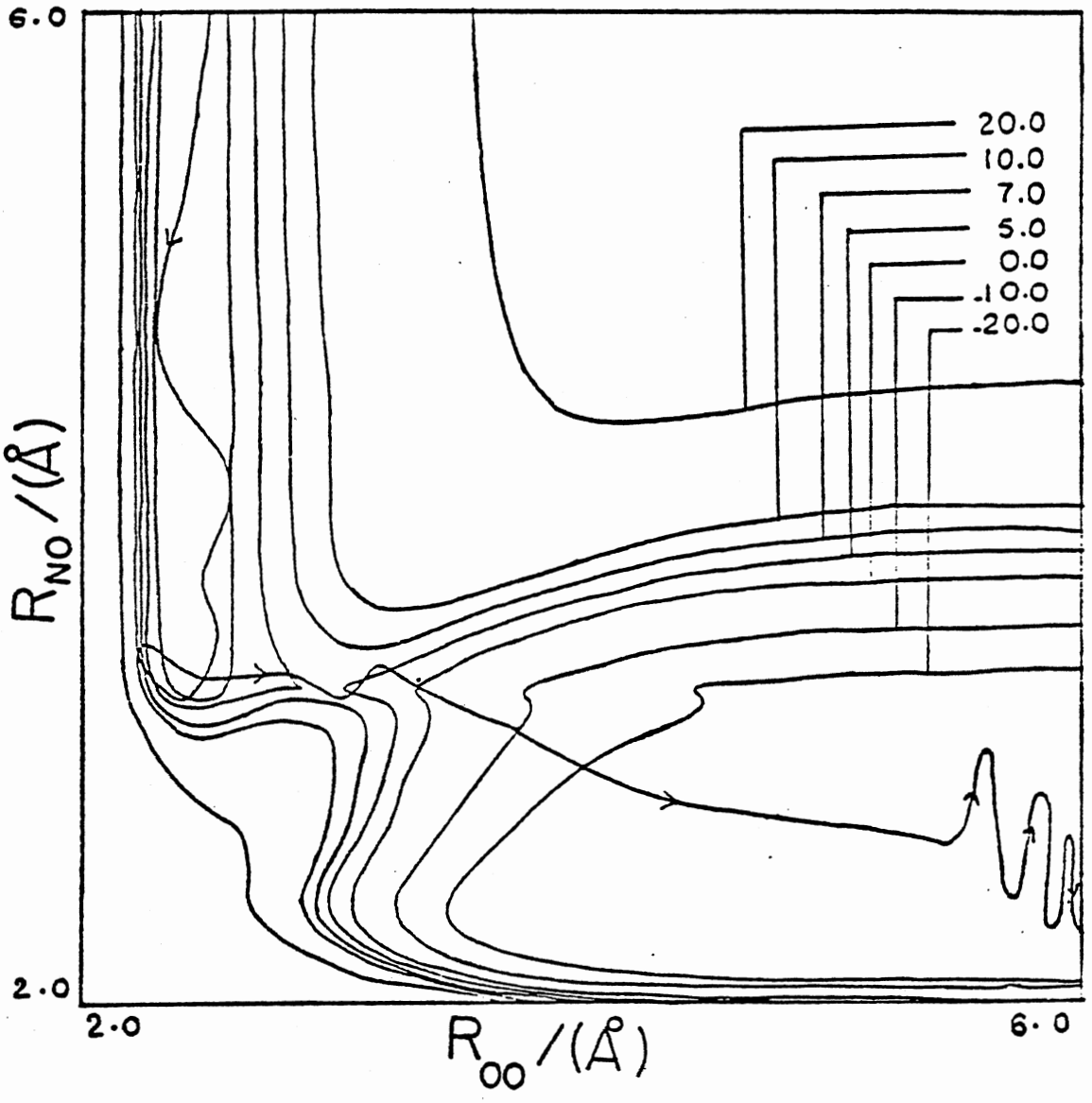

Figure 14. Course of a Reactive Trajectory on Surface S5 for the Ground State Reactants

However, it has been experimentally observed that vibration is only as effective as relative translation in promoting the reaction, for this system. This leads us to predict that the 'actual' surface probably has an 'early' barrier.

On surface S5, cross sections have been evaluated as a function of relative velocities at a rotational temperature of 400 K, for the ground vibrational state reactants and for those in which one quanta of energy was introduced through the antisymmetric stretching mode of ozone. The results given in Table XXIV and Figures 15 and 16 indicate the absence of a threshold velocity on this surface. The same behavior has been observed experimentally by Redpath et al. (52). The zero point energies of the O_3 and NO molecules are 4.07 and 2.72 Kcal/mole respectively. The barrier is about 0.6 Kcal/mole less than the zero point energy of ozone. The absence of a threshold probably implies that most of the zero point energy is available in the reaction coordinate. This enables the system to cross over the barrier even at very low relative translational energies.

In order to evaluate the effectiveness of vibration over relative translation, the cross sections that would be obtained if one quanta of excitation (3 Kcal/mole of energy) were available through relative translation are compared with the cross sections obtained on vibrational excitation in Table XXIV. The results indicate that vibration is as effective as relative translation especially at high relative velocities. At low relative velocities, vibration seems to be slightly more effective than relative translation. However, within the present error limits, these results suggest that vibration and relative translation make comparable contributions to the reaction rate enhancement.

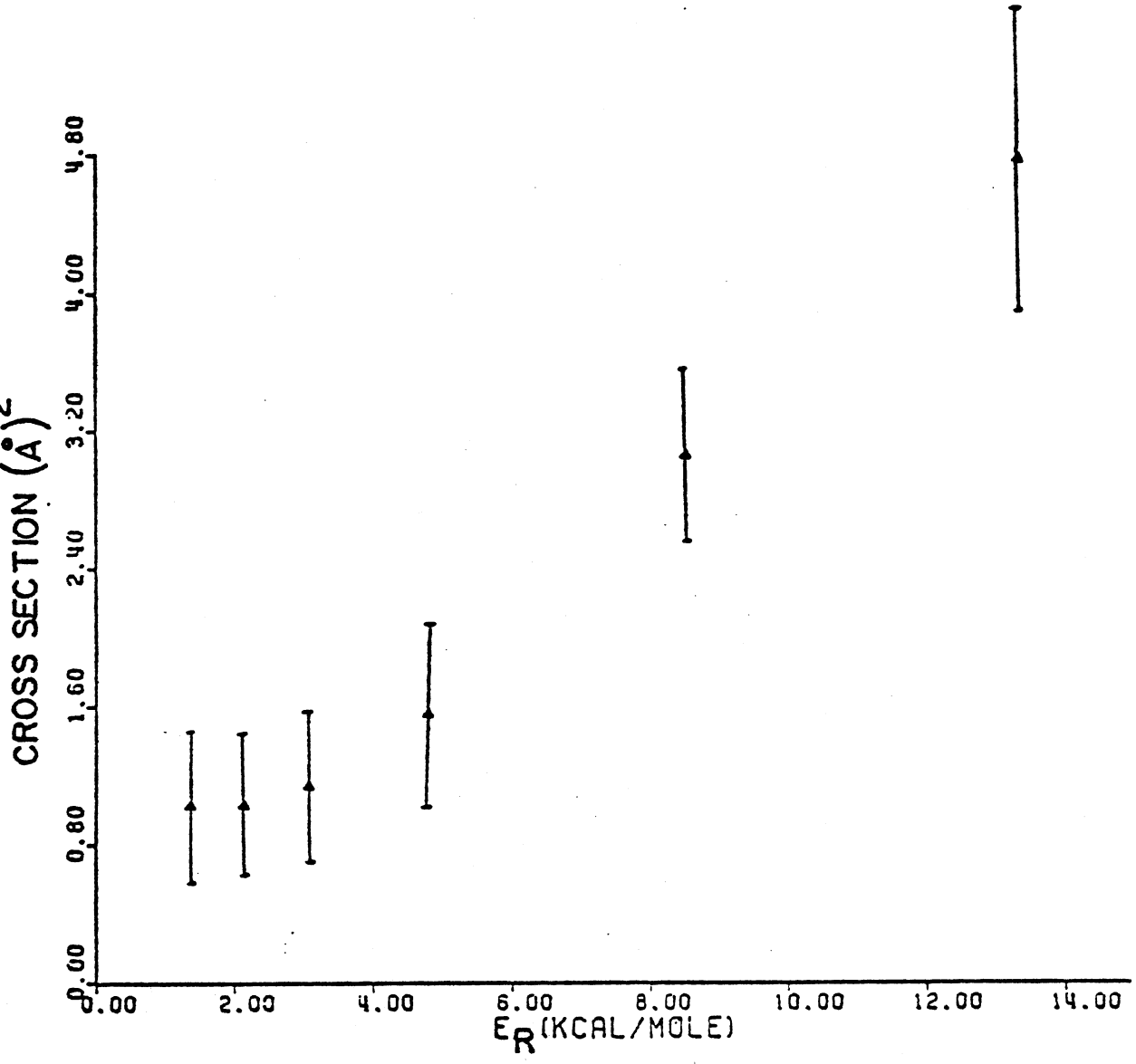

Figure 15. Total Reactive Cross Section Versus Relative Translational Energy on Surface S5 for (0000) State of Reactants

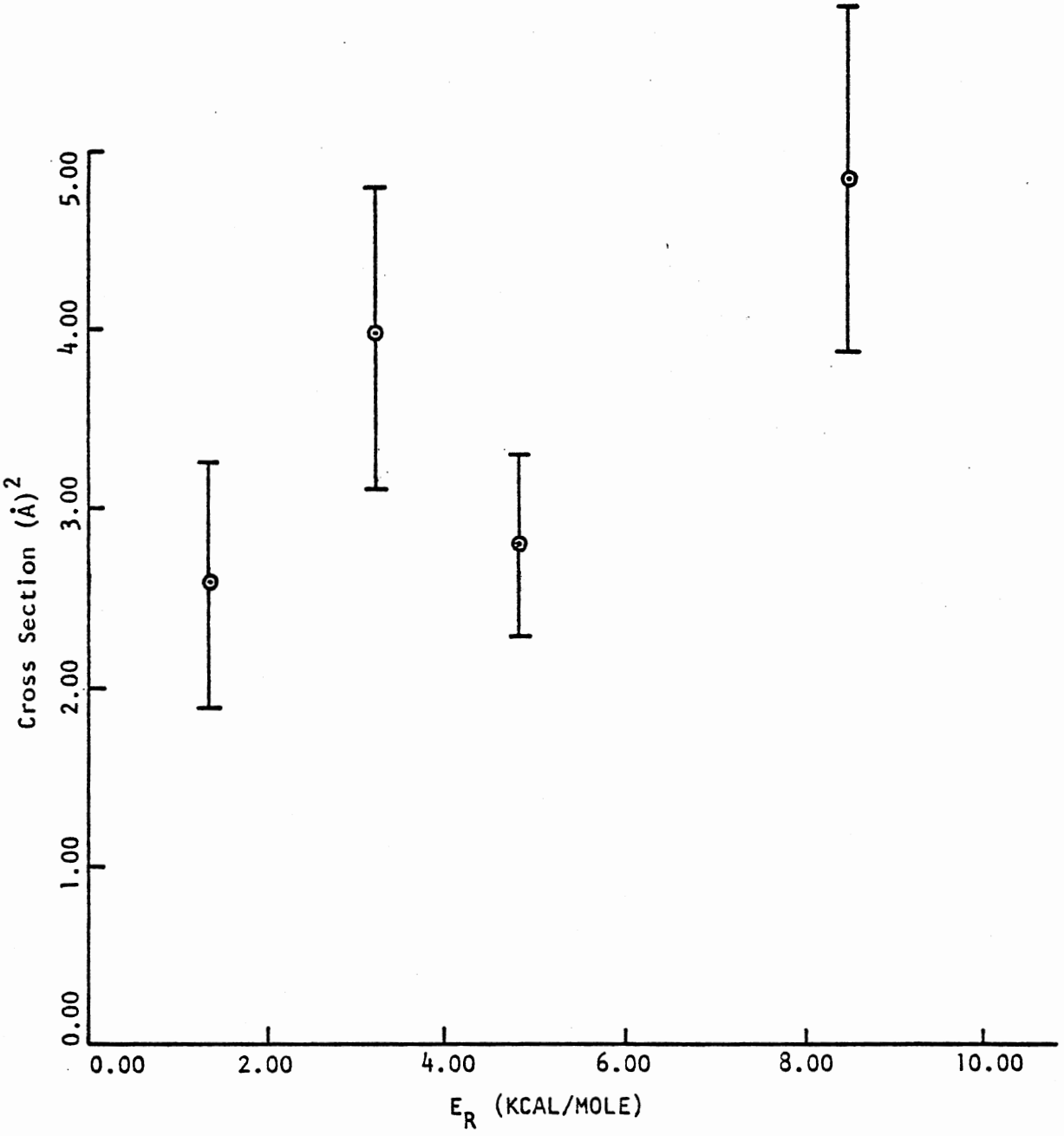

Figure 16. Total Reactive Cross Section Versus Relative Translational Energy on Surface S5 for (0010) State of Reactants

TABLE XXIV

CROSS SECTIONS $(\mathring{A})^2$ OBTAINED ON SURFACE S5

E_R Kcal/mole	E_R' Kcal/mole	$S(E_R)$ ground state vibration + rel. trans. (E_R)	$S(E_R)$ excited state vibration + rel. trans. (E_R')
4.36	1.36	1.44 ± 0.58	2.59 ± 0.76
5.13	2.13	1.75 ± 0.7	3.15 ± 0.9
6.06	3.06	1.96 ± 0.78	3.95 ± 0.9
7.79	4.79	2.73 ± 1.09	2.82 ± 0.76
11.5	8.5	4.32 ± 1.73	4.91 ± 1.02

The rate constants have been evaluated by averaging over a Boltzmann distribution of relative velocities at T K. We have assumed that the rotational contributions do not alter the results significantly and have carried out the calculations at a rotational temperature of 400 K. ln k is plotted vs 1/T in Figures 17 and 18 for the ground state and the vibrationally excited (0010) reactants. It should be noted that the rate constants calculated are larger than the experimental values by two orders of magnitude. The potential-energy surface formulation is probably inadequate to represent the system exactly. Since the reaction involves several electronic states, it might be necessary to assume a surface hopping model rather than carrying out calculations on a single potential-energy surface. However, no threshold was observed and a finite signal was measured even at the lowest collision

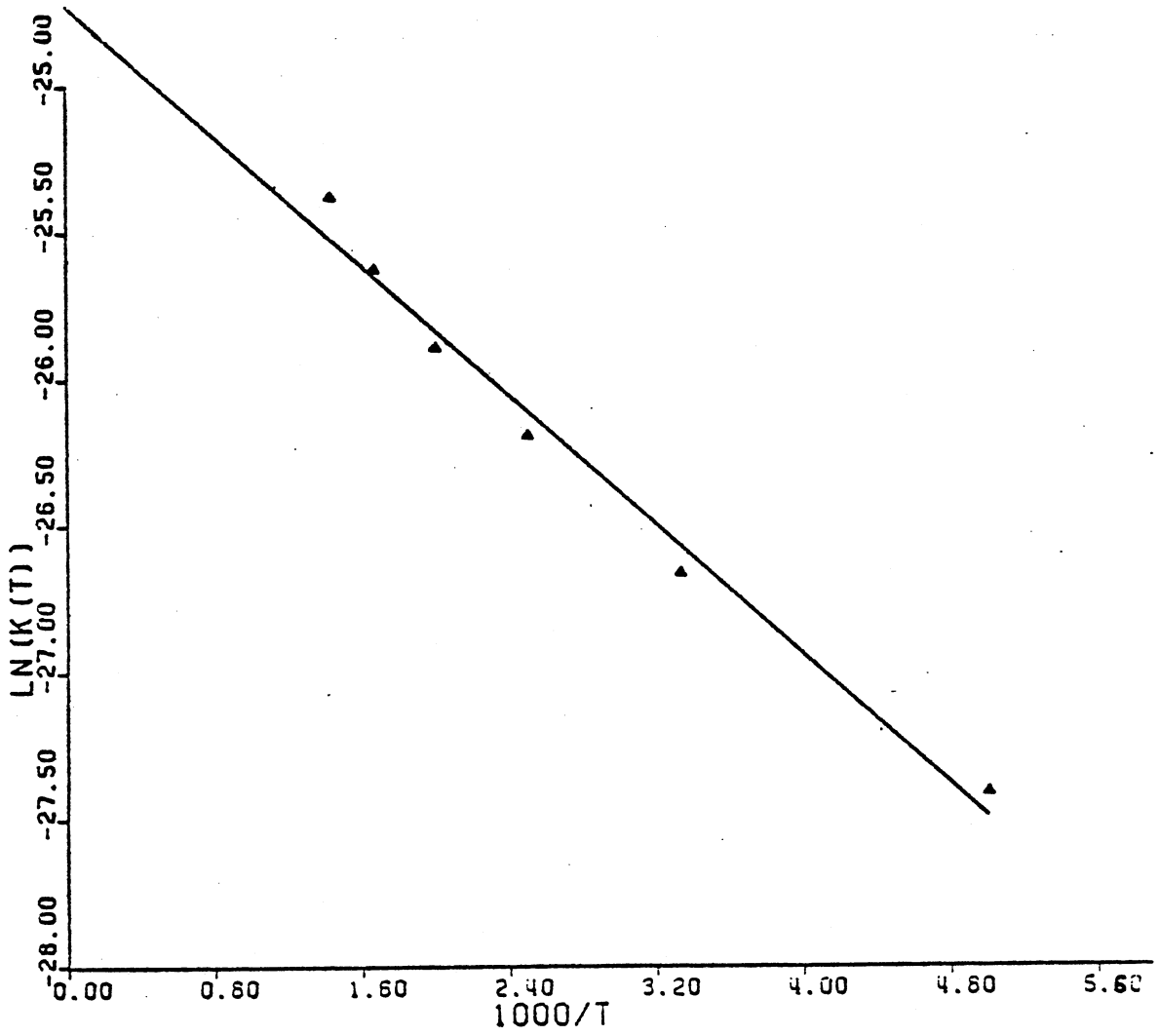

Figure 17. Arrhenius Fit to the Rate Constants for the O_3-NO System Obtained on Surface S5 for the (0000) State of Reactants. k(T) is in units of cm^3/molecule-sec. E_a= 1174.9 cal/mole. ln A = -24.75; A is in units of cm^3/molecule-sec.

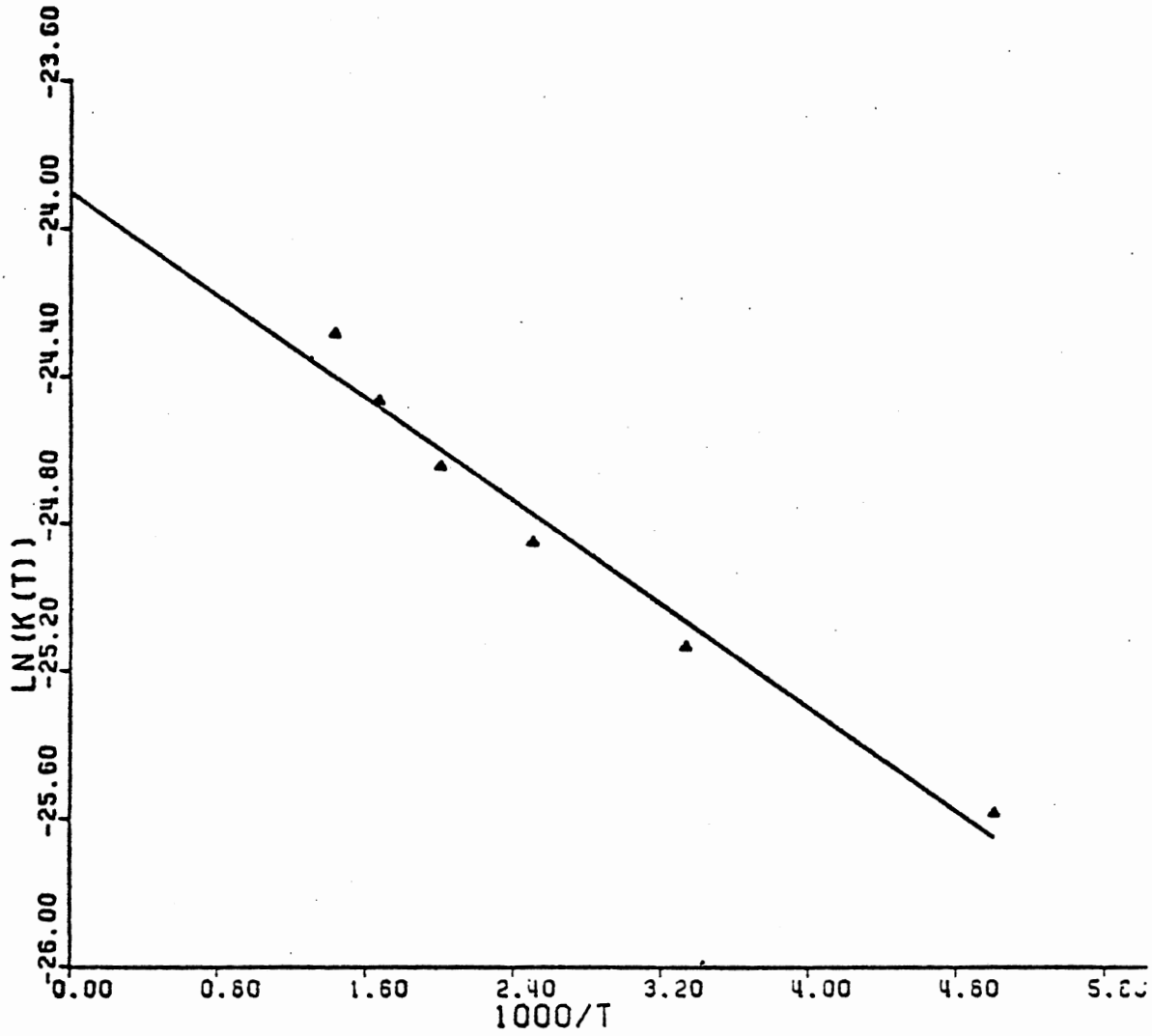

Figure 18. Arrhenius Fit to the Rate Constants for the O_3-NO System Obtained on Surface S5 for the (0010) State of Reactants. k(T) is in units of cm^3/molecule-sec. E'_a = 740.16 cal/mole; ln A' = -23.91; A' is in units of cm^3/molecule-sec.

energy (1 Kcal/mole) in the molecular beam experiments of Redpath et al. (52). In the flow tube experiments conducted by Hui et al. (47), an activation energy of 2.3 Kcal/mole was measured for this reaction. We are unable to rationalize these observations at this point.

In order to investigate the importance of other vibrational modes of ozone and NO in enhancing the reaction rate, rate constants have been computed using Eq (III-77) with one quanta of energy in each of these modes. Tables XXV and XXVI give the results for the reactants in the various initial vibrational states designated by $(n_1 n_2 n_3 n_4)$, where n_1, n_2 and n_3 are the quantum numbers corresponding to the bending, symmetric stretching and antisymmetric stretching modes of O_3 respectively, and n_4 is the vibrational quantum number of NO. Since one quanta of energy in the bending mode is less than one quanta of energy in the stretching modes, calculations have also been carried out with 1.5 quanta of energy in the bending mode in order to make the comparisons meaningful. The results seem to indicate that the bending mode is slightly more effective in enhancing the reaction than the stretching modes. This difference is probably insignificant in view of the present error limits and we may expect all three modes to make comparable contributions to the reaction rate enhancement. Vibrational excitation of NO does not result in any observable enhancement of the reaction rate. This probably indicates that the reaction proceeds through a direct mechanism rather than going through a complex formation, at least on these surfaces. It is reasonable to expect this, since the present surface formulations are not associated with a well at the saddle point which would favor a complex formation. The trajectories were direct and no evidence for the formation of even a transient complex was

observed. This is made clear by Figures 19 and 20 where the distances of the bonds involved in the reaction are plotted as a function of time for two randomly chosen reactive trajectories.

TABLE XXV

COMPARISON OF THERMAL RATE CONSTANTS AND THOSE OBTAINED WITH VIBRATIONALLY EXCITED NO

T K	$k(T) \times 10^{11}$ cm^3-molecule^{-1} sec^{-1}	
	(0000)	(0001)
300	0.26 ± 0.05	--
400	0.42 ± 0.1	0.39 ± 0.2
500	0.57 ± 0.11	0.79 ± 0.37
600	0.74 ± 0.2	1.01 ± 0.4
700	0.95 ± 0.22	--

The absence of a mode specific behavior can be either due to the formation of a collision complex or due to very rapid V-V intermode coupling. The formation of a collision complex is ruled out since vibrational excitation of NO does not cause an appreciable enhancement of the reaction rate. The V-V coupling of the ν_1 and ν_3 modes was found to be very rapid (84). Since the frequencies of the ν_1 and ν_3 modes are nearly equal (1103 cm and 1042 cm, respectively), it was

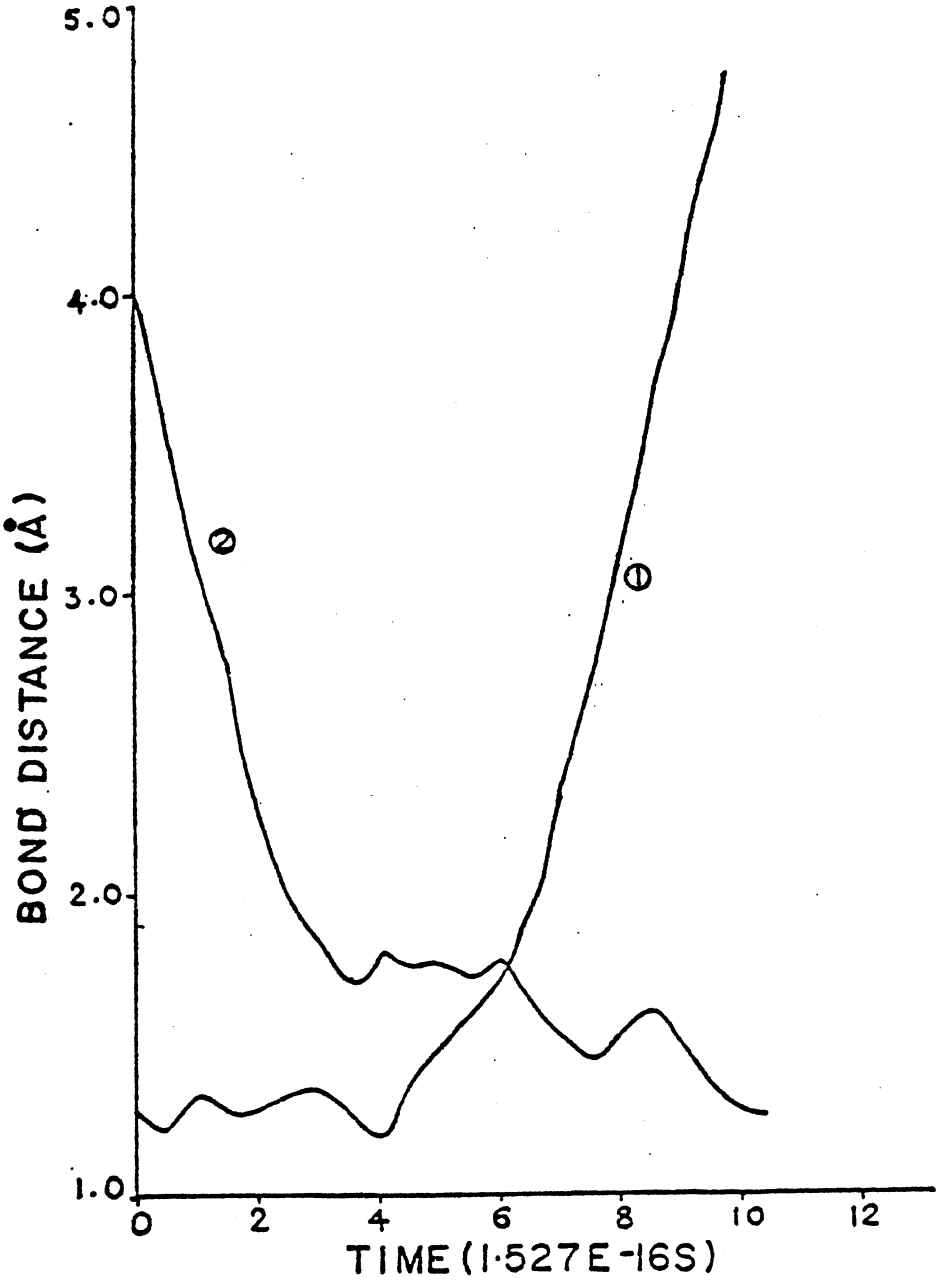

Figure 19. $O\text{-}O^i$ and $O^i\text{-}N$ Bond Distances as a Function of Time for a Reactive Trajectory on Surface S5 for the (0000) State of Reactants. Superscript i designates the O atom abstracted from O_3. (1) $R_{O\text{-}O}{}^i$; (2) $R_{N\text{-}O}{}^i$.

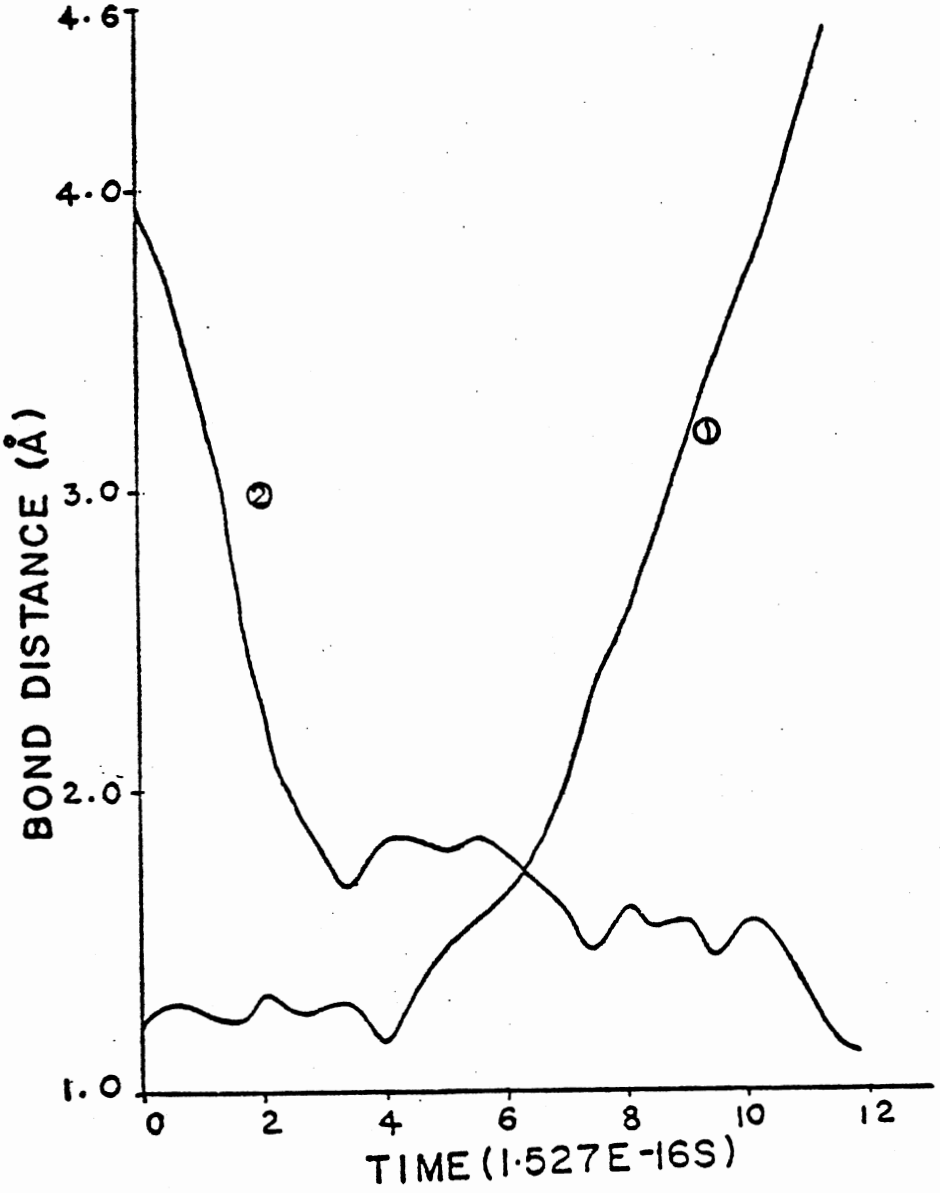

Figure 20. $O\text{-}O^{i}$ and $O^{i}\text{-}N$ Bond Distances as a Function of Time for a Reactive Trajectory on Surface S5 for the (0010) State of Reactants. Superscript i designates the O atom abstracted from O_3. (1) $R_{O\text{-}O^{i}}$; (2) $R_{N\text{-}O^{i}}$.

observed that in a very short time interval following the laser excitation of the ν_3 mode, the ν_1 and ν_3 modes undergo rapid intermode and intramode V-V exchange to establish a quasisteady Boltzmann-like vibrational distribution in the vibrational manifold of each mode (84). The V-V exchange with the ν_2 mode appears to occur on a somewhat longer time scale. The average vibrational energy defect for single quantum exchange from the ν_1 and ν_3 modes to the ν_2 mode is only about 370 cm^{-1} compared with about 1073 cm^{-1} for the V-T relaxation of the ν_1 and ν_3 modes. Hence, the V-V coupling between the ν_2 and (ν_1 and ν_3) modes is expected to be faster than the V-T relaxation of the ν_1 and ν_3 modes. The rate constant for the V-V exchange with the ν_2 mode has been observed to be an order of magnitude smaller than the rate constant for the coupling between ν_1 and ν_3 modes (lower limit for the magnitude of the rate constants for such near-resonant intermode coupling processes is 1.6×10^5 sec^{-1} $torr^{-1}$ at 298 K) (84).

The V-V coupling processes in ozone have been investigated by subdividing the vibrational energy of ozone into the energies of the individual normal modes as the reaction proceeds.

$$E_k = 1/2(P_k^2 + \lambda_k Q_k^2), \quad k = 1,2,3$$

However, this procedure is only approximate since the ozone potential is not harmonic and the normal mode energies develop large fluctuations. The normal mode energies have been computed for a few time intervals before reaction (when the reactants still exist as O_3 + NO). The combination of normal mode energies which yield approximately the same total energy as at t = 0 have been chosen to be the energies before the commencement of reaction.

TABLE XXVI

RATE CONSTANTS OBTAINED WITH VIBRATIONALLY EXCITED OZONE (n_1 n_2 n_3) ON SURFACE S5

T/K	k(T) x 10^{11} cm^3-$molecule^{-1}$ sec^{-1}		
	(0100)	(1.5000)	(0010)
300	--	--	1.21 ± 0.36
400	--	1.57 ± 0.4	1.61 ± 0.5
500	1.08 ± 0.39	2.52 ± 0.6	1.98 ± 0.6
600	1.75 ± 0.51	--	2.37 ± 0.7
700	2.60 ± 0.6	--	2.84 ± 0.8

The initial normal mode energies and the normal mode energies before the commencement of reaction are shown in Table XXVII for three different initial states of reactants.

It was observed that there is sufficient coupling of the normal modes as the reaction proceeds. Thus it is not possible to characterize one mode as directed along the reaction coordinate. This rapid coupling between the normal modes accounts for the absence of a mode specific behavior in this system.

We have also examined certain average properties of the products. Table XXVIII gives the values of the fraction of the available energy, partitioned into the product modes for various initial states of reactants on surface S5. Table XXIX compares these values on the different surfaces employed.

TABLE XXVII

ANALYSIS OF NORMAL MODE ENERGIES OF OZONE

Initial State	Normal mode energies					
	At t = 0			Before reaction		
	E_1	E_2	E_3	E_1	E_2	E_3
(100)	0.132	0.069	0.066	0.070	0.09	0.09
(010)	0.044	0.208	0.066	0.107	0.138	0.08
(001)	0.044	0.069	0.197	0.121	0.124	0.138

(a) Energies are in eV.

TABLE XXVIII

FRACTION (%) OF THE AVAILABLE ENERGY DEPOSITED IN THE PRODUCT MOLECULES ON SURFACE S5 AT T = 400K

Initial state of reactants	% Energy			
	$(NO_2)_{vib}$	$(NO_2)_{rot}$	$(O_2)_{vib}$	$(O_2)_{rot}$
(0000)	37.8	16.1	5.1	8.0
(0100)	35.3	15.3	6.9	13.4
(1000)	44.7	12.8	5.2	8.5
(0010)	40.8	15.2	6.1	6.4
(0001)	42.9	16.9	3.6	10.0

TABLE XXIX

FRACTION (%) OF THE AVAILABLE ENERGY DEPOSITED IN THE PRODUCT MOLECULES AT T = 400K

Surface	Initial state of reactants	% Energy			
		$(NO_2)_{vib}$	$(NO_2)_{rot}$	$(O_2)_{vib}$	$(O_2)_{rot}$
S3	(0010)	39.1	20.4	2.4	10.7
S4	(0010)	44.5	12.7	3.2	11.1
S5	(0010)	40.8	15.2	6.1	6.4

In the case of atom-diatomic molecule reactions, it has been observed that the major part of the available energy appears as vibration in the molecular product on those surfaces with the barrier located in the entry valley. On those surfaces with the barrier located in the exit valley, only a small part of the available energy appears as product vibration (18). The results obtained for the polyatomic system differs from those for the atom-diatomic molecule reactions. The results clearly indicate that most of the available energy goes into NO_2 vibration. The partitioning does not show a strong dependence on surface topography or reagent energy distribution. Consequently, it would appear that measurements of energy partitioning have little information content related to potential surface topography in this system.

The mean scattering angle has been calculated by using the expression,

$$< \theta >_{O_2} = \sum_{i=1}^{N} \xi_i^b \theta_i / N, \qquad \text{(III-79)}$$

where ξ_i^b is the random number used in selecting the impact parameter for the i^{th} trajectory, θ_i is the scattering angle for the i^{th} trajectory and the sum extends over all the reactive trajectories. The mean scattering angle of the NO_2 product can then be obtained from,

$$< \theta >_{NO_2} = 2\pi - < \theta >_{O_2}$$

Table XXX lists the values of the mean scattering angles for the various impact parameter ranges. It is observed that the scattering angle decreases with increasing impact parameters. However, at all impact parameters the NO_2 molecule is scattered into the backward hemisphere with respect to the incoming NO molecule. The mean scattering angle for the NO_2 product was calculated to be 157^o. The average scattering angle for the NO_2 product has also been computed for the surfaces S1 to S5 for the (0010) vibrational state of the reactants at a temperature of 400 K. These data are given in Table XXXI. It is seen that irrespective of the topography of the potential-energy surface, the NO_2 product is scattered into the backward hemisphere with respect to the direction of the incident NO molecule. Similar behavior has been observed for the atom-diatomic molecule reactions (18). It has been observed that at low reagent energy, irrespective of the position of the saddle point, the molecular product is scattered backwards. The fact that the NO_2 product is scattered into the backward hemisphere on these surfaces probably implies that the reaction occurs via an

abstraction mechanism. The NO molecule approaches the ozone molecule at an approach angle, OON, greater than 100^{o}, abstracts one of the end oxygen atoms in ozone and rebounds back to form the products $NO_2 + O_2$. Smaller approach angles are found to be less favorable due to energy considerations.

TABLE XXX

SCATTERING DISTRIBUTION OF THE PRODUCT MOLECULES FOR THE GROUND STATE REACTANTS ON SURFACE S5

b/Å	$\langle\theta_i\rangle_{O_2}$ /deg	$\langle\theta_i\rangle_{NO_2}$ /deg
0 - 0.5	3.2	176.8
0.5 - 1.0	11.6	168.4
1.0 - 1.5	29.4	150.6
1.5 - 2.0	40.2	139.8
2.0 - 3.5	63.2	116.8

$\langle\theta\rangle_{NO_2} = 157^{o}$

$\langle\theta\rangle_{NO_2} = 23^{o}$

The scattering angle has also been computed for the initial reactant states (0000), (0010) and (0030) on surface S5 at T = 400 K. The results are given in Table XXXII. The NO_2 product is scattered into the backward hemisphere irrespective of the initial state of

reactants. The scattering angle is observed to decrease slightly with increasing energy. This difference is probably insignificant in view of the present error limits.

TABLE XXXI

AVERAGE SCATTERING ANGLES ON SURFACES S1, S2, S3 and S5

Surface	N_R	N_{tot}	$\langle\theta\rangle_{NO_2}$
S1	10	50	126
S2	19	200	143
S3	12	200	142
S5	15	200	143

Initial reactant state is (0010); T = 400 K.
N_R is the number of reactive trajectories.
N_{tot} is the total number of trajectories.

TABLE XXXII

SCATTERING ANGLES FOR VARIOUS INITIAL STATES OF REACTANTS ON SURFACE S5

Initial state	$\langle\theta\rangle_{NO_2}$/deg
(0000)	157
(0010)	143
(0030)	128

Similar calculations have been reported recently by Chapman (80). Chapman has attempted to exaggerate the possible effects by carrying out calculations at significantly higher energies than are present in the experimental studies but was unable to obtain good statistical accuracy. However, it has been reported that vibrational energy was more effective on those surfaces in which the barrier was located in the product valley, but no studies of the systematic variation in barrier height or barrier position within a set of surfaces was carried out. The present investigation has attempted a systematic analysis of the importance of the various topological features in determining the reaction dynamics in a polyatomic system. The results of the present calculations show agreement in a qualitative sense with those of Chapman (80).

Conclusions

The present study has investigated the effects and importance of some surface topological features in determining the reaction dynamics in polyatomic systems. It has been found that the position of the saddle-point plays a role very similar to that in the case of atom-diatomic molecule reactions. However, the energy partitioning in the product modes differs from that observed in the atom-diatomic molecule case. Thus we see that the behavior of the atom-diatomic molecule reactions may be used to predict the outcome of larger systems only with difficulty. It has also been observed that the NO_2 product is scattered in the backward hemisphere with respect to the direction of the incident NO molecule. This probably implies that the reaction proceeds via an abstraction mechanism.

The absence of a mode-specific behavior does not necessarily imply that the reaction proceeds via formation of a collision complex. It is observed that the intermode V-V coupling occurs in a time interval much shorter compared to the collision time; thus the reaction exhibits no mode-specific behavior.

The partitioning of available energy among the product modes is found to be independent of the surface topography and also the initial state of reactants. Similar behavior is also observed for the average scattering angle. Thus it seems impossible to obtain information about the detailed topographical features of the potential-energy surface from a measurement of these quantities. The incorporation of the experimental data into such a multi-dimensional hypersurface is obviously a very difficult task.

CHAPTER IV

POTENTIAL-ENERGY SURFACE FOR THE HF + Ar RIGID ROTOR SYSTEM

Two different potential-energy surfaces have been employed in the present study, a pairwise Lennard-Jones (12, 6) potential and an *ab initio* spline fitted SCF surface (SAI) augmented by a Van der Waals attractive term to compensate for the lack of configuration mixing in the SCF wavefunction.

Spline Fitted *Ab Initio* Surface (SAI)

An unrestricted potential-energy surface formulation would require the calculation of the *ab initio* energies as a function of three variables, R, r and Γ (see Figure 21). The dimensionality of the problem can be reduced from three to two by approximating the HF molecule to be a rigid rotor. This approximation considerably simplifies the problem and is expected to be a valid approximation due to the following reasons:

1. At ordinary temperatures, only the ground vibrational state is appreciably populated. Thus the vibrational amplitude is minimal, and the variation in R is therefore small.

2. Rotationally inelastic scattering is mainly affected by the variables r and Γ, the distance of the He atom from the center of mass of the HF molecule, and the angle which the He atom makes with the HF bond axis, respectively (see Figure 21).

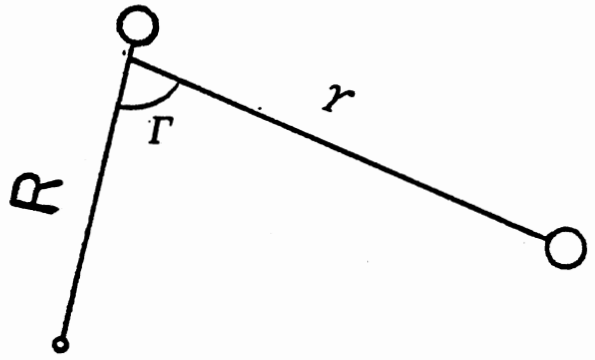

Figure 21. The HF-Ar Rigid Rotor System

The most accurate ab initio calculation is the one which incorporates configuration interaction (CI). In such calculations, a proper account of the electronic interaction is made by correlating the motion of all the electrons, so that the position of one depends on the instantaneous position of the other, rather than on the average position of the other electrons. The major disadvantage of a CI calculation is the enormous amount of computer time required for treating even very simple systems. Since the correlation error is considerably smaller in the case of closed-shell systems, an LCAO-MO-SCF (Linear Combination Of Atomic Orbitals-Molecular Orbitals-Self Consistent Field) approximation in the Hartree-Fock limit is expected to yield results with reasonable accuracy for these systems.

The LCAO-MO-SCF energies for the HF-Ar rigid rotor system have been evaluated using gaussian-70 (85). The basis sets were taken directly from those provided by the program. In all cases, the HF molecule was fixed at its equilibrium geometry (R_{HF} = 0.9171 Å).

The basis sets employed for both Ar and HF consisted of Slater-type orbitals (STO's) approximated by expansions of gaussian type orbitals. The valence shells of H and F were represented by two STO's: one approximated by a three-term gaussian and the other by a single gaussian (31G). The inner shells of F and all the orbitals of Ar were represented by STO's approximated by a six-term gaussian expansion. The extended basis set was chosen after carrying out certain preliminary calculations with minimal basis sets and various extended basis sets. The comparison shown in Table XXXIII indicates that the 6-31G basis for HF and a (STO-6G) basis for AR yields energies lower than those obtained with minimal basis sets and other extended basis sets, with only a

slight increase in computational time. Hence, the more accurate (6-31G) extended basis set for HF and a (STO-6G) basis set for Ar were chosen.

TABLE XXXIII

COMPARISON OF TIMES AND ACCURACIES OF THE DIFFERENT BASIS SETS FOR ARGON AND HF

Basis		$E_{r=2\text{Å}}$ (au)[b]	E_{∞} (au)[c]	ΔE (eV)	Time[d] (sec)
Hf	Ar				
STO-6G	STO-6G	-624.48419	-624.55410	1.92976	22.74
4-31G	STO-4G	-623.99840	-623.92722	1.93697	15.83
	STO-5G	-624.71911	-624.64783	1.93963	19.36
	STO-6G	-624.94149	-624.87018	1.94053	23.11
5-31G	STO-4G	-624.07480	-624.00322	1.94790	17.15
	STO-5G	-624.79551	-624.72382	1.95068	19.92
	STO-6G	-625.01789	-624.94617	1.95163	23.76
6-31G	STO-4G	-624.09455	-624.02287	1.95056	17.67
	STO-5G	-624.81526	-624.74347	1.95340	20.52
	STO-6G	-625.03764	-624.96582	1.95433	24.58

(a) Basis employed was the one provided by the Gaussian-70 program.

(b) Energies correspond to the configuration with $\Gamma = 90^{\circ}$ (Ar perpendicular to the HF bond axis).

(c) E_{∞} corresponds to the interaction energy for r = 25 Å and $\Gamma = 90^{\circ}$.

(d) The time tabulated is that required to calculate E (r = 2.0 Å).

The ab initio energies have been evaluated at various r and Γ values and are given in Table XXXIV. The results were interpolated by using a cubic spline interpolation technique (79) which enabled us to determine the potential energy as a function of r and Γ.

The ab initio surface thus evaluated does not include configuration interaction. The dispersion forces which operate between systems at large distances are a result of a small, but significant, correlative interaction of the motions of the electrons in the two systems. Thus, the polarization of the two systems resulting from this long range correlative effect and the accompanying small change in energy are not properly represented in the Hartree-Fock description of the combined system. In order to compensate for the lack of configuration mixing in the SCF wavefunction, the spline fitted ab initio surface has been augmented by a Van der Walls attractive term.

$$V_{SAI} = V_{SCF} + V_{CI} \qquad \text{(IV-1)}$$

with

$$V_{CI} = -4.0\ \varepsilon_o\ (\sigma_o/r)^6 \qquad \text{(IV-2)}$$

where r is the distance of the He atom from the center of mass of the HF molecule. ε_o and σ_o are the L-J parameters for the HF-Ar interaction. ε_o was taken to be the geometric mean of the ε values for HF and Ar and σ_o was taken to be the arithmetic mean of the σ values for the collision partners, i.e.,

$$\varepsilon_o = (\varepsilon_{HF} \cdot \varepsilon_{Ar})^{\frac{1}{2}} \qquad \text{(IV-3)}$$

TABLE XXXIV

AB INITIO INTERMOLECULAR POTENTIAL FOR THE RIGID ROTOR HF-Ar SYSTEM. ENERGIES ARE MEASURED IN eV FROM THE ENERGY OF HF AND Ar AT INFINITE SEPARATION.
r IS IN Å

r	$\Gamma = 0^\circ$	$\Gamma = 5^\circ$	$\Gamma = 10^\circ$	$\Gamma = 15^\circ$	$\Gamma = 20^\circ$	$\Gamma = 30^\circ$
1.4	78.2680	75.5422	68.3664	58.9929	49.5655	34.9561
1.6	30.3621	29.5884	27.4819	24.5710	21.4495	16.1652
1.8	12.1116	11.8673	11.1923	10.2341	9.1678	7.2399
2.0	4.7662	4.6860	4.4618	4.1364	3.7634	3.0528
2.2	1.6823	1.6566	1.5826	1.4739	1.3473	1.1006
2.4	0.3547	0.3478	0.3282	0.2999	0.2678	0.2098
2.6	-0.1980	-0.1976	-0.1963	-0.1934	-0.1879	-0.1673
2.8	-0.3876	-0.3847	-0.3759	-0.3616	-0.3422	-0.2915
3.0	-0.4043	-0.4007	-0.3900	-0.3728	-0.3500	-0.2925
3.2	-0.3428	-0.3393	-0.3293	-0.3132	-0.2921	-0.2394
3.4	-0.2551	-0.2523	-0.2441	-0.2309	-0.2137	-0.1715
3.7	-0.1351	-0.1334	-0.1284	-0.1205	-0.1102	-0.0857
4.0	-0.0588	-0.0580	-0.0555	-0.0517	-0.0468	-0.0353
4.3	-0.0217	-0.0213	-0.0204	-0.0188	-0.0169	-0.0124
4.7	-0.0048	-0.0047	-0.0045	-0.0041	-0.0037	-0.0027
5.0	-0.0015	-0.0015	-0.0014	-0.0013	-0.0012	-0.0010
6.0	-0.0004	-0.0004	-0.0004	-0.0004	-0.0003	-0.0003
7.0	-0.0003	-0.0003	-0.0003	-0.0003	-0.0003	-0.0003
8.0	-0.0003	-0.0003	-0.0003	-0.0003	-0.0003	-0.0003
10.0	-0.0002	-0.0002	-0.0002	-0.0002	-0.0002	-0.0002
11.0	0.0000	0.0000	0.0000	0.0000	0.0000	0.0000

TABLE XXXIV (Continued)

r	$\Gamma = 40^{\circ}$	$\Gamma = 50^{\circ}$	$\Gamma = 60^{\circ}$	$\Gamma = 70^{\circ}$	$\Gamma = 80^{\circ}$	$\Gamma = 85^{\circ}$
1.4	26.8623	23.0220	21.2724	20.4269	19.9826	19.8512
1.6	12.9065	11.1965	10.3416	9.9170	9.7244	9.6851
1.8	5.9287	5.1667	4.7509	4.5385	4.4539	4.4450
2.0	2.5331	2.2124	2.0340	1.9504	1.9317	1.9393
2.2	0.9173	0.8073	0.7548	0.7439	0.7618	0.7777
2.4	0.1761	0.1687	0.1818	0.2091	0.2443	0.2629
2.6	-0.1340	-0.0924	-0.0473	-0.0026	0.0379	0.0557
2.8	-0.2317	-0.1704	-0.1138	-0.0655	-0.0277	-0.0127
3.0	-0.2275	-0.1644	-0.1099	-0.0672	-0.0365	-0.0252
3.2	-0.1814	-0.1272	-0.0827	-0.0499	-0.0280	-0.0204
3.4	-0.1263	-0.0855	-0.0536	-0.0313	-0.0173	-0.0126
3.7	-0.0605	-0.0390	-0.0232	-0.0130	-0.0069	-0.0050
4.0	-0.0240	-0.0149	-0.0086	-0.0047	-0.0026	-0.0019
4.3	-0.0083	-0.0050	-0.0029	-0.0016	-0.0010	-0.0008
4.7	-0.0018	-0.0012	-0.0008	-0.0006	-0.0005	-0.0004
5.0	-0.0007	-0.0006	-0.0005	-0.0004	-0.0004	-0.0004
6.0	-0.0003	-0.0003	-0.0004	-0.0004	-0.0004	-0.0003
7.0	-0.0003	-0.0003	-0.0003	-0.0003	-0.0003	-0.0003
8.0	-0.0003	-0.0003	-0.0003	-0.0003	-0.0003	-0.0003
10.0	-0.0002	-0.0002	-0.0002	-0.0002	-0.0002	-0.0002
11.0	0.0000	0.0000	0.0000	0.0000	0.0000	0.0000

TABLE XXXIV (Continued)

r	$\Gamma = 90^{\circ}$	$\Gamma = 100^{\circ}$	$\Gamma = 110^{\circ}$	$\Gamma = 120^{\circ}$	$\Gamma = 130^{\circ}$
1.4	19.7663	19.7046	19.7312	19.7793	19.7995
1.5	9.6729	9.7005	9.7500	9.7738	9.7459
1.8	4.4517	4.4922	4.5377	4.5585	4.5396
2.0	1.9542	1.9944	2.0299	2.0449	2.0327
2.2	0.7958	0.8325	0.8601	0.8711	0.8639
2.4	0.2809	0.3121	0.3329	0.3414	0.3378
2.6	0.0715	0.0962	0.1114	0.1177	0.1163
2.8	-0.0002	0.0180	0.0285	0.0329	0.0328
3.0	-0.0162	-0.0039	0.0029	0.0058	0.0062
3.2	-0.0145	-0.0068	-0.0027	-0.0009	-0.0005
3.4	-0.0091	-0.0046	-0.0024	-0.0013	-0.0010
3.7	-0.0037	-0.0020	-0.0012	-0.0008	-0.0008
4.0	-0.0015	-0.0009	-0.0007	-0.0006	-0.0005
4.3	-0.0006	-0.0005	-0.0004	-0.0004	-0.0004
4.7	-0.0004	-0.0004	-0.0004	-0.0004	-0.0004
5.0	-0.0004	-0.0004	-0.0004	-0.0004	-0.0004
6.0	-0.0003	-0.0004	-0.0003	-0.0003	-0.0004
7.0	-0.0003	-0.0003	-0.0003	-0.0003	-0.0003
8.0	-0.0003	-0.0003	-0.0003	-0.0003	-0.0003
10.0	-0.0002	-0.0002	-0.0002	-0.0002	-0.0002
11.0	0.0000	0.0000	0.0000	0.0000	0.0000

TABLE XXXIV (Continued)

r	$\Gamma = 140^{o}$	$\Gamma = 150^{o}$	$\Gamma = 160^{o}$	$\Gamma = 170^{o}$	$\Gamma = 180^{o}$
1.4	19.7711	19.7032	19.6222	19.5585	19.5345
1.6	9.6664	9.5566	9.4473	9.3679	9.3390
1.8	4.4833	4.4053	4.3277	4.2712	4.2507
2.0	1.9963	1.9464	1.8967	1.8606	1.8475
2.2	0.8415	0.8108	0.7804	0.7585	0.7505
2.4	0.3248	0.3070	0.2893	0.2765	0.2719
2.6	0.1095	0.0999	0.0902	0.0833	0.0808
2.8	0.0296	0.0249	0.0202	0.0168	0.0155
3.0	0.0050	0.0029	0.0008	-0.0007	-0.0013
3.2	-0.0008	-0.0015	-0.0024	-0.0030	-0.0032
3.4	-0.0011	-0.0013	-0.0017	-0.0019	-0.0020
3.7	-0.0008	-0.0008	-0.0009	-0.0009	-0.0009
4.0	-0.0005	-0.0005	-0.0005	-0.0005	-0.0005
4.3	-0.0004	-0.0004	-0.0004	-0.0004	-0.0004
4.7	-0.0004	-0.0004	-0.0004	-0.0004	-0.0004
5.0	-0.0004	-0.0004	-0.0004	-0.0004	-0.0004
6.0	-0.0003	-0.0004	-0.0003	-0.0004	-0.0003
7.0	-0.0003	-0.0003	-0.0003	-0.0003	-0.0003
8.0	-0.0003	-0.0003	-0.0003	-0.0003	-0.0003
10.0	-0.0002	-0.0002	-0.0002	-0.0002	-0.0002
11.0	0.0000	0.0000	0.0000	0.0000	0.0000

$$\sigma_o = (\sigma_{HF} + \sigma_{Ar})/2 \qquad \text{(IV-4)}$$

This gives σ_o = 3.278 Å and ε_o/k = 198.9146 deg.

Lennard Jones Potential-Energy Surface

The LJ (12, 6) pairwise potential is given by

$$V_{LJ} = V_{Ar-H}(R_1) + V_{Ar-F}(R_2) \qquad \text{(IV-5)}$$

where each term has the form

$$V_i(R_i) = 4.0\ \varepsilon_i((\sigma_1/R_i)^{12} - (\sigma_i/R_i)^6) \qquad \text{(IV-6)}$$

The σ parameters for the Ar-H and Ar-F interaction and the ε parameter for the Ar-H interaction were obtained from the NASA compilation (86) of LJ parameters and the use of arithmetic and geometric mean combining rules for the mixed interactions. The ε and σ parameters for the H atom in the HF molecule were taken to be the geometric and arithmetic means, respectively, of the tabulated values for isolated H and He. The σ parameter for F in HF was taken to be that for Ne. The ε value for F was chosen such that the well depth of the resulting potential approached the estimated well depth of 0.017 eV (86) for the HF-Ar interaction. The mixed interaction parameters required were then obtained from

$$\begin{aligned} \sigma_{Ar-H} &= (\sigma_H + \sigma_{Ar})/2 \\ \sigma_{Ar-F} &= (\sigma_F + \sigma_{Ar})/2 \\ \varepsilon_{Ar-H} &= (\varepsilon_{Ar}\varepsilon_H)^{1/2} \end{aligned} \qquad \text{(IV-7)}$$

The values of all parameters are given in Table XXXV. The intermolecular

potential obtained by using the LJ (12, 6) pairwise potential are plotted vs r for $\Gamma = 90^{o}$ in Figure 22.

TABLE XXXV

LENNARD-JONES PARAMETERS

Interaction	ε_i/k (deg)[a]	σ (A^{o})
H-Ar	48.2862	3.01875
F-Ar	138.8522	3.086
HF-Ar	198.9146	3.278

(a) k is the Boltzmann constant.

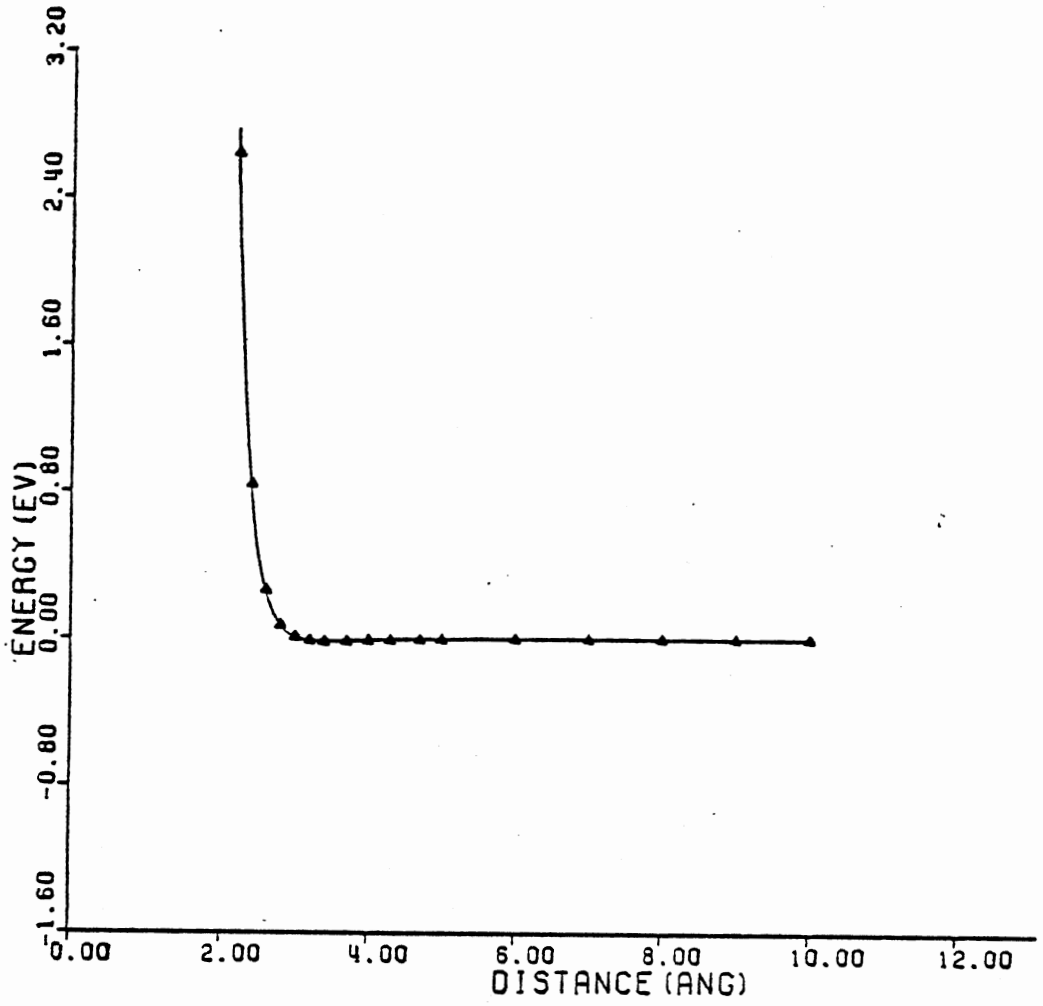

Figure 22. Plot of ln V Versus r for $\Gamma = 90^{o}$

CHAPTER V

STUDY OF THE ROTATIONALLY INELASTIC SCATTERING IN THE HF-Ar RIGID ROTOR SYSTEM USING THE INFINITE ORDER SUDDEN APPROXIMATION METHOD

Calculational Methods

In recent years, a number of quantum mechanical sudden approximations have been employed for molecular scattering calculations (87-91). Some of these are very simple and yet work well at normal collision energies. The Infinite Order Sudden Approximation (IOSA) belongs to this category. The simplicity and accuracy of the IOSA method make it very suitable for routine analysis of experimental data. A simple, direct derivation of the IOS equations for the rotationally inelastic scattering accompanying a rigid rotor-atom collision has been given by Parker and Pack (62). The application of the IOSA method to the rigid rotor HF + Ar system follows very closely the treatment of the CO_2-He rigid rotor system by Parker and Pack (62) and by Agrawal and Raff (63). Hence, only the important results will be given here.

The Hamiltonian for the system (see Figure 21) may be written as

$$H = -\hbar^2/2\mu r \frac{\partial^2}{\partial r^2} \cdot r + \frac{L_{op}^2}{2\mu r^2} + \frac{J_{op}^2}{2\mu_{BC} R^2} + V(r,\Gamma) \qquad \text{(V-1)}$$

where L^2_{op} is the operator corresponding to the square of the orbital angular momentum representing the rotation of atom A about the BC center-of-mass and J^2_{op} is the operator corresponding to the square of the molecular angular momentum representing the rotation of the BC molecule. μ_{BC} is the reduced mass of the molecule BC; μ is the reduced mass of the system given by

$$\mu = m_A \cdot m_{BC}/(m_A + m_{BC}) \tag{V-2}$$

The Schrodinger equation for the system is

$$(E-H)\psi = 0 \tag{V-3}$$

The wavefunction for the system may be expanded as

$$\psi^{JMj1} = \sum_{j"} \sum_{1"} r^{-1} G^{JMj1}_{j"1"}(r) Y^{JM}_{j"1"}(\hat{R},\hat{r}) \tag{V-4}$$

where the J and M are the total angular momentum quantum numbers; j" and 1" are quantum numbers corresponding to the eigenvalues of the operators J^2_{op} and L^2_{op}, respectively.

$Y^{JM}_{j"1"}(\hat{R},\hat{r})$ can be expressed in terms of the initial state wavefunctions by making use of the Clebsch-Gordan theorem.

$$Y^{JM}_{j"1"}(\hat{R},\hat{r}) = \sum_{m_j=-j}^{+j} \sum_{m_1=-1}^{+1} C(j"1"J;m_j,m_1,M)\, Y_{jm_j}(\hat{R}) Y_{1m_1}(\hat{r}) \tag{V-5}$$

Substitution of Eq (V-4) into Eq (V-3) followed by multiplication by $Y^{JM*}_{j'1'}(\hat{R},\hat{r})$ and integration over all space yields the following radial

equation

$$\{d^2/dr^2 + k_{j'}^2 - l'(l'+1)/r^2\}G_{j'l'}^{JMjl}(r) =$$

$$2\mu/\hbar^2 \times \sum_{j''} \sum_{l''} \langle JMj'l' \mid V \mid JMj''l'' \rangle G_{j''l''}^{JMjl}(r) \qquad \text{(V-6)}$$

where

$$k_{j'}^2 = \{E - \hbar^2 j'(j'+1)/2I_o\}2\mu/\hbar^2 \qquad \text{(V-7)}$$

Eq (V-6) is an infinite set of coupled equations for $G_{j'l'}^{JMjl}(\hat{r})$. It is very difficult to solve this set of equations, especially when a large number of coupled equations must be included in order to obtain converged cross sections.

The IOSA method simplifies the problem by replacing the angular momentum operators in the Hamiltonian by eigenvalue forms, namely,

$$L^2 = \hbar^2 \bar{l}(\bar{l}+1) \qquad \text{(V-8)}$$

and

$$J^2 = \hbar^2 \bar{j}(\bar{j}+1) \qquad \text{(V-9)}$$

where $\bar{l}$ and $\bar{j}$ are suitable constants.

This approximation simplifies the problem enormously. The resulting radial equation is

$$\{d^2/dr^2 + k_{\bar{j}}^2 - \bar{l}(\bar{l}+1)/r^2\}g^{\bar{j}\bar{l}}(r,\Gamma) = 2\mu/\hbar^2 \, V(r,\Gamma) \, g^{\bar{j}\bar{l}}(r,\Gamma) \qquad \text{(V-10)}$$

The matrix element of the g functions,

$$\tilde{G}^{JMj1}_{j'1'} = \langle JMj'1' \mid g^{\bar{j}\bar{1}}(r,\Gamma) \mid JMj1 \rangle \qquad \text{(V-11)}$$

are approximate solutions of Eq (V-6). It can be shown that $\tilde{G}^{JMj1}_{j'1'}$ satisfy the set of equations

$$\{d^2/dr^2 + k_{\bar{j}}^2 - \bar{1}(\bar{1}+1)/r^2\} \; \tilde{G}^{JMj1}_{j'1'}(r) =$$

$$2\mu/\hbar^2 \sum_{j''} \sum_{1''} \langle j'1'JM \mid V \mid j''1''JM \rangle \tilde{G}^{JMj1}_{j''1''}(r) \qquad \text{(V-12)}$$

These are identical with Eq (V-6) except that $k_{j'}$ has been replaced by $k_{\bar{j}}$ and 1' by $\bar{1}$ on the left hand side of the equation. By the definition of $k_{j'}$ given by Eq (V-7), it may be inferred that the IOS equations will be valid whenever the kinetic energy is large compared to the rotational energy spacing.

In order to evaluate the scattering amplitude and the cross section, a choice has to be made for $\bar{j}$ and $\bar{1}$. In our calculations, $\bar{j}$ was chosen to be the initial rotational quantum number, j, and $\bar{1}$ was chosen to be the final orbital quantum number. With this choice, the radial equations were solved to obtain the phase shifts, η_1, and then the various cross sections were evaluated by using the following expressions due to Parker and Pack (62).

State-to-State Cross Sections

$$\sigma(j' \leftarrow j) = \frac{k_o^2}{k_j^2} \sum_{j''} C^2(jj''j';000)\sigma(j'' \leftarrow 0) \qquad \text{(V-13)}$$

where

$$\sigma(j'' \leftarrow 0) = \pi/(2j''+1)k_o^2 \sum_{l'} (2l'+1) \left| t_{j''}^{\bar{k}_j l'} \right|^2 \qquad \text{(V-14)}$$

with

$$t_{j''}^{\bar{k}_j l'} = (j''+1/2) \int_{-1}^{+1} \{1 - \exp\{2i\eta_l^{\bar{k}_j}(\Gamma)\}\} P_{j''}(\cos\Gamma) d\cos\Gamma \qquad \text{(V-15)}$$

The expression for the state-to-state cross sections derived by the IOSA method (Eq (V-13)) is independent of the exit-channel velocity. Consequently, the above IOSA method yields significant cross sections even for those transitions closed by energy conservation constraints. In order to eliminate this undesirable feature, the IOSA equations were modified by Agrawal and Raff by including an explicit exit-channel velocity dependence (66) into the expression for the scattering cross section.

The IOSA expression for the scattering amplitude is

$$f(j'm_j' \leftarrow jm \mid \hat{r}) = i(\pi/k_j k_{j'})^{\frac{1}{2}} \sum_{JMll'm_{l'}} (-1)^{1-\bar{l}} (2l+1)^{\frac{1}{2}}$$

$$XC(jlJ;m_j 0M) C(j'l'J;m_j, m_{l'}, M)$$

$$X \langle JMj'l' \mid T^{\bar{j}\bar{l}}(\Gamma) \mid JMjl \rangle Y_{l'm_{l'}}(r) \qquad \text{(V-16)}$$

Under the modified IOSA method, this becomes,

$$f(j'm_{j'} \leftarrow jm \mid \hat{r}) = i(\pi/k_j k_{\bar{j}})^{\frac{1}{2}} \sum_{JM11'm_{1'}} (-1)^{1-\bar{1}} (21+1)^{\frac{1}{2}}$$

$$XC(j1J;m_j OM)C(j'1'J;m_{j'},m_{1'},M)$$

$$X < JMj'1' \mid T^{\bar{j}\bar{1}}(\Gamma) \mid JMj1 > Y_{1'm_{1'}}(\hat{r}) \qquad \text{(V-17)}$$

The modified expression for the scattering cross section is

$$\sigma(j' \leftarrow j) = (k_{j'}/k_{\bar{j}})(k_o^2/k_j^2) \sum_{j''} C^2(jj''j';000)\sigma(j'' \leftarrow 0) \qquad \text{(V-18)}$$

which is explicitly dependent upon the exit-channel velocity, $k_{j'}$.

This modification is very simple. It simply involves multiplying the scattering amplitude obtained by the IOSA method by $k_{\bar{j}}^{-\frac{1}{2}} k_{j'}^{\frac{1}{2}}$. Since the cross sections are directly proportional to the square of the amplitude, the expressions for the cross sections derived by the IOSA method are modified by multiplying by $k_{\bar{j}}^{-1} k_{j'}$.

As can be seen from Eq (V-13) - (V-15), the calculation of the state-to-state cross sections is very simple once the phase shifts are evaluated. Thus, the major portion of the calculation resides in the computation of the phase shifts, η_1.

The WKB phase shift formula employed to compute the required η_1 is

$$\eta_1 = \lim_{R \to \infty} \{ \int_{r_i'}^{R} \{k^2 - (1+1/2)^2/r^2 - U\}^{\frac{1}{2}} dr - kR + (1+1/2)\pi/2 \} \qquad \text{(V-19)}$$

where

$$k^2 = 2\mu E/\hbar^2 \qquad \text{(V-20)}$$

$$U = 2\mu V/\hbar^2 \qquad \text{(V-21)}$$

k is the wave number, V the potential energy and r_i the classical turning point.

The N-point Gauss-Mehler approximation to this integral is given by (92),

$$\eta_l(E) \approx kr_i \sum_{j=1}^{N} w_j f(x_j) + (l + 1/2 - kr_i)\pi/2 \qquad \text{(V-22)}$$

where the points x_j and the weights appropriate to the weighting function $(1 - x^2)^{\frac{1}{2}}$ are given by Kopal (92) as,

$$x_j = \cos\{\pi j/(2N+1)\}$$

$$\text{and } w_j = (1 - x_j^2)\pi/(2N+1) \qquad \text{(V-23)}$$

This enables a very rapid calculation of the phase shifts. The integral in Eq (V-15) was evaluated numerically by using the Gaussian quadrature.

The total number of phase shifts required depends upon the initial relative translational energy. The phase shifts, $\eta_l(\Gamma)$, are to be evaluated for various l values ranging from 0 to l_{max} where,

$$l_{max} \approx ka$$

$$\text{and } \lim_{l \to l_{max}} \eta_l(\Gamma) \longrightarrow 0 \qquad \text{(V-24)}$$

a is the range over which the interaction potential is appreciable and k is the wave vector given by,

$$k = (2\mu E)^{\frac{1}{2}}/\hbar \qquad \text{(V-25)}$$

In the present case, calculations have been carried out at three different initial translational energies, namely T_i = 4, 9, and 15 Kcal/mole on the LJ(12,6) surface. The number of phase shifts evaluated at these energies were 300, 500 and 600, respectively. Figure 23 shows a plot of $\eta_1(\Gamma)$ vs l for the LJ(12,6) surface at T_i = 9 Kcal/mole for $\Gamma = 100^{\circ}$. Calculations have been carried out at T_i = 4 Kcal/mole on the ab initio surface and the number of phase shifts evaluated was 200. The phase shifts, $\eta_1(\Gamma)$, are plotted vs l in Figure 24 for $\Gamma = 100^{\circ}$.

Results and Discussion

State-to-state cross sections have been calculated for the initial rotational states j = 0, 1 and 2 at three different initial translational energies using the IOSAM method on the pairwise LJ(12,6) potential surface. These are given in Tables XXXVI to XXXVIII. Figures 25 and 26 show a comparison of IOSAM results for both the LJ(12,6) and ab initio surfaces with the experimental data reported by Barnes, et al (67) for initial states j = 1 and 2, respectively, at a relative translational energy of 4 Kcal/mole. Since the experiment yields only relative cross sections, the figures give the results in terms of cross section ratios. For the j = 1 calculations, the $(\sigma(j' \leftarrow 1)/\sigma(3 \leftarrow 1))$ ratios are given. For the j = 2 calculations, the values of $(\sigma(j' \leftarrow 2)/\sigma(4 \leftarrow 2))$ are plotted.

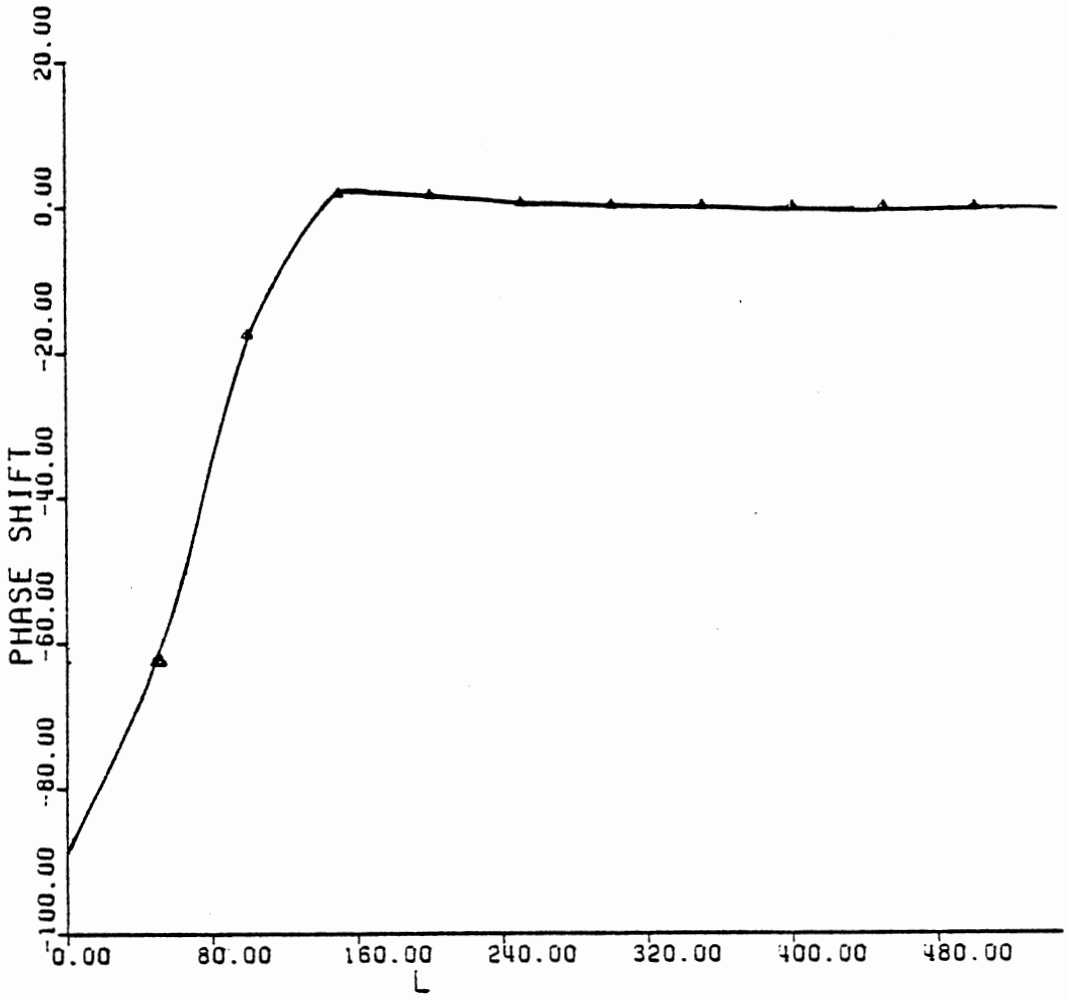

Figure 23. HF-Ar Phase Shifts (in Radians) on the LJ(12,6) Surface for $\Gamma = 100^{o}$ Versus Partial Wave. T_i = 9 Kcal/mole.

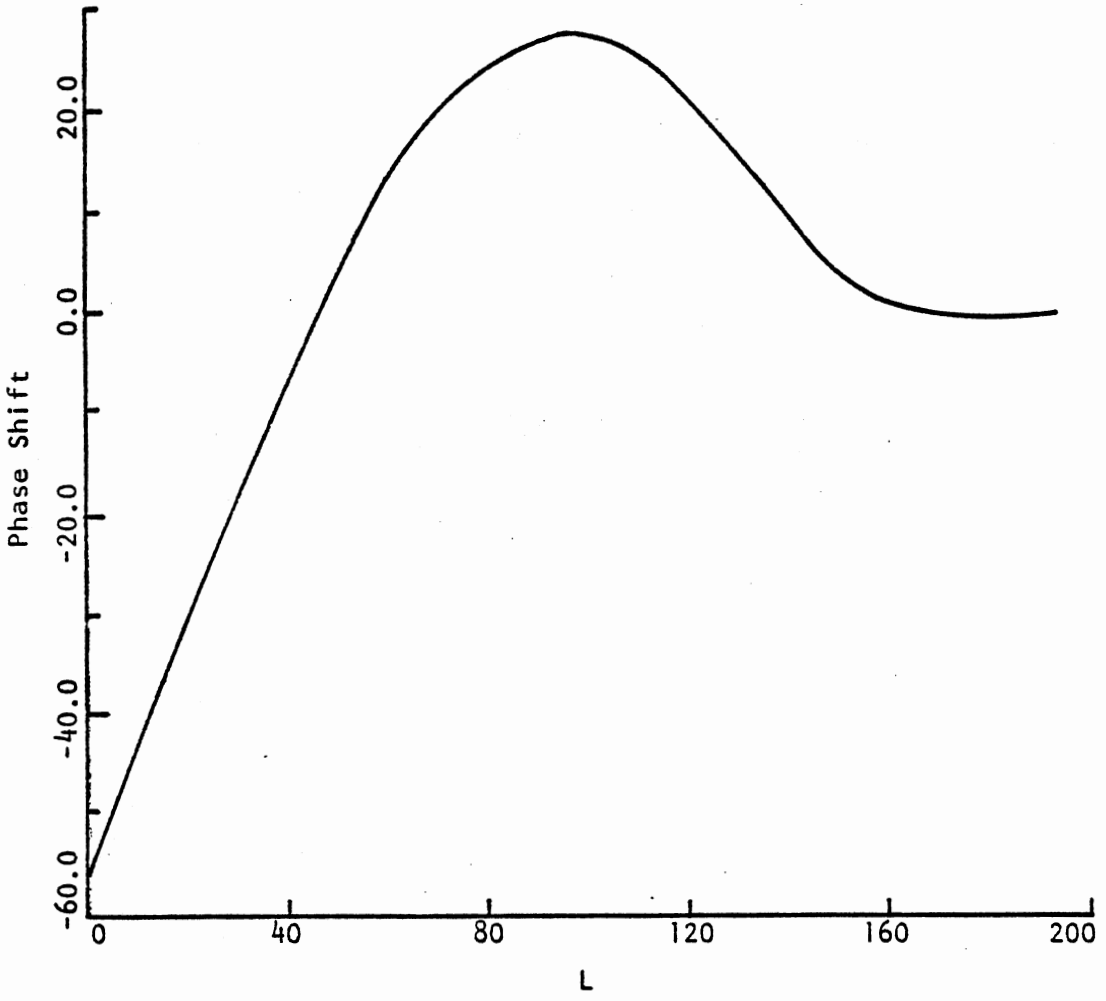

Figure 24. HF-Ar Phase Shifts (in Radians) on the SAI Surface for Γ = 100° Versus Partial Wave; T_i = Kcal/mole

TABLE XXXVI

IOSAM RESULTS FOR THE STATE-TO-STATE INTEGRAL CROSS SECTIONS ON THE LJ(12,6) POTENTIAL SURFACE[a]

j'	T_i = 4 Kcal/mole		
	$\sigma(j' \leftarrow 0)$	$\sigma(j' \leftarrow 1)$	$\sigma(j' \leftarrow 2)$
0	-	3.4606	1.3845
1	10.0754	-	5.1519
2	6.3262	8.0869	-
3	3.2137	4.3676	7.2361
4	1.4274	2.3750	3.7423
5	1.2266	1.1201	1.9855
6	0.6896	0.9068	0.9238
7	0.4569	0.4526	0.6538
8	0.0	0.0	0.1089
9	0.0	0.0	0.0

(a) Cross sections are in units of $(\text{Å})^2$.

T_i = 4 Kcal/mole.

TABLE XXXVII

IOSAM RESULTS FOR THE STATE-TO-STATE INTEGRAL CROSS SECTIONS ON THE LJ(12,6) POTENTIAL SURFACE[a]

j'	$\sigma(j' \leftarrow 0)$	$\sigma(j' \leftarrow 1)$	$\sigma(j' \leftarrow 2)$
0	-	2.3922	1.1762
1	7.0817	-	3.8219
2	5.6506	6.2026	-
3	3.4336	3.9792	5.6913
4	1.3794	2.7301	3.4750
5	1.7018	1.1373	2.3257
6	0.8050	1.3157	1.0108
7	0.8457	0.6881	1.0986
8	0.5316	0.6609	0.6114
9	0.4476	0.4525	0.5579
10	0.3374	0.3531	0.3694
11	0.2142	0.2236	0.2518

(a) Cross sections are in units of $(\text{Å})^2$.

T_i = 9 Kcal/mole.

TABLE XXXVIII

IOSAM RESULTS FOR THE STATE-TO-STATE INTEGRAL CROSS SECTIONS ON THE LJ(12,6) POTENTIAL SURFACE[a]

j'	$\sigma(j' \leftarrow 0)$	$\sigma(j' \leftarrow 1)$	$\sigma(j' \leftarrow 2)$
0	-	1.9988	1.1225
1	5.9488	-	3.3624
2	5.4798	5.5153	-
3	3.5929	3.8793	5.1181
4	1.3623	2.9159	3.4002
5	1.9042	1.1278	2.4604
6	0.8060	1.4302	1.0082
7	0.8554	0.6985	1.2065
8	0.5615	0.6901	0.6466
9	0.4989	0.5158	0.6234
10	0.4533	0.4547	0.4588
11	0.3952	0.3838	0.3878

(a) Cross sections are in units of $(\text{Å})^2$.

T_i = 15 Kcal/mole.

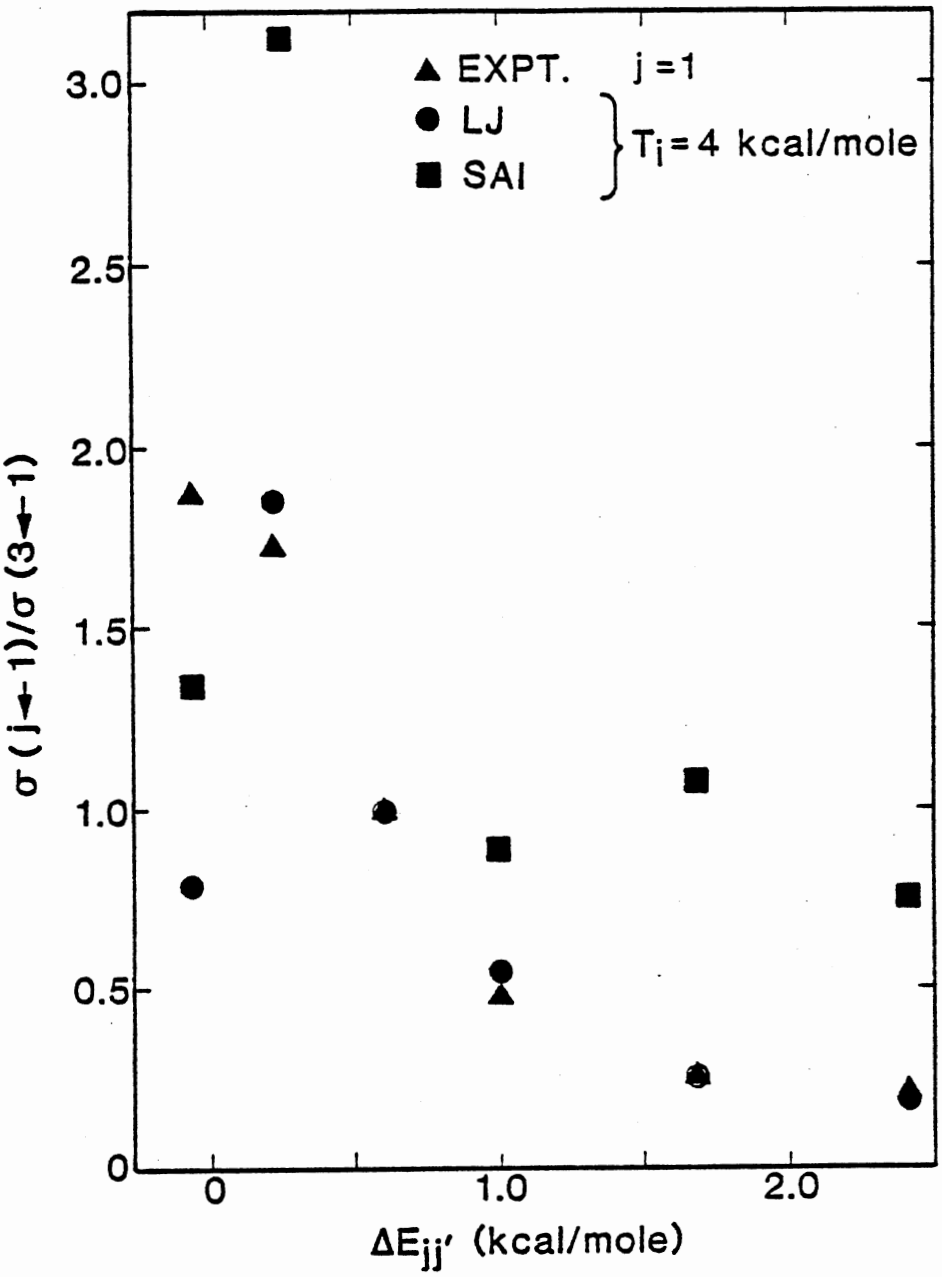

Figure 25. Comparison of Computed IOSAM Cross Section Ratios $\{\sigma(j'-1)/\sigma(3-1)\}$ with Experimental Ratios at T_i = 4 Kcal/mole. (●) and (■) are the IOSAM results on the LJ(12,6) and SAI surfaces, respectively. (▲) are the experimental data of Barnes et al. (Reference 67).

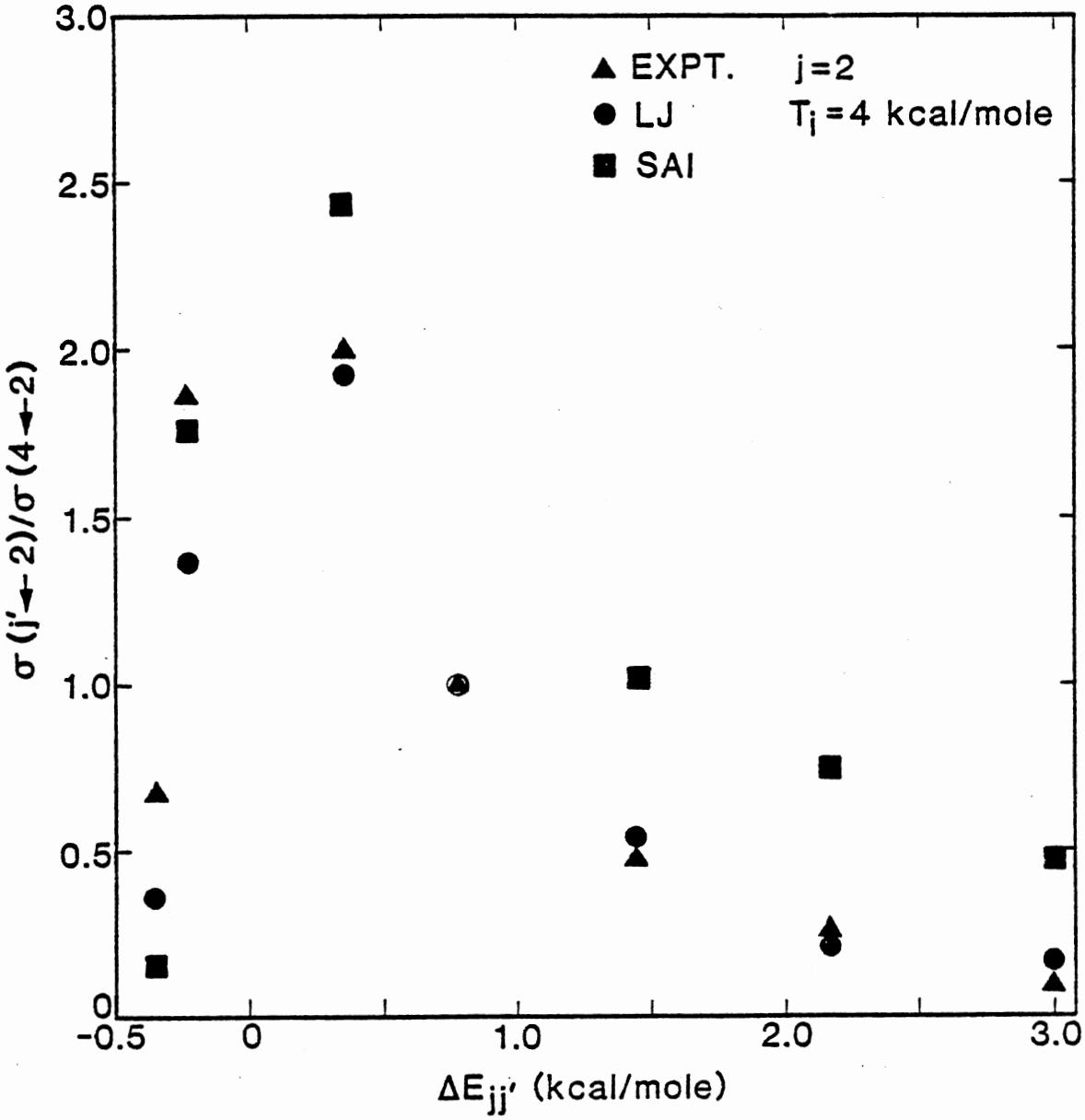

Figure 26. Comparison of Computed IOSAM Cross Section Ratios {σ(j'-2)/σ(4-2)} with Experimental Ratios at T_i = 4 Kcal/mole. (●) and (■) are the IOSAM results on the LJ(12,6) and SAI surfaces, respectively. (▲) are the experimental data (Reference 67).

As seen from the figures, the computed state-to-state T↔R cross sections on the LJ(12,6) surface for transitions with $j' > j$ are in excellent accord with the experimental results. For transitions with $j' < j$, the degree of agreement is significantly reduced. In general, the infinite-order sudden calculations tend to underestimate the cross sections for the de-excitation processes. Overall, the cross sections scale as an inverse power of $\Delta E_{jj'}$, in accord with a recently proposed expression suggested by Brunner, Driver, Smith and Pritchard (93),

$$\sigma(j' \leftarrow j) = (2j'+1)(T_f/T_i)^{\frac{1}{2}} \mid \Delta E_{jj'} \mid^{-\Gamma} \qquad \text{(V-26)}$$

where T_i and T_f are the initial and final relative translational energies.

The results obtained on the ab initio surface are found to be in generally poor agreement with the experimental data for all transitions. This is surprising in view of the fact that a similar surface formulation yielded results in good agreement with experiment for the (He,CO_2) system (63). The probable reasons for the discrepancy are:

1. The asymmetry of the (Ar,HF) system is incompatible with the assumption that the attractive interaction operates between the centers-of-mass.

2. The calculations at the SCF level are inadequate in spite of the closed-shell nature of this system.

Barnes et al, (67) found the relative T↔R cross sections to be almost insensitive to the relative translational energy, T_i, over the range 4 Kcal/mole $\leq T_i \leq$ 16.0 Kcal/mole. Figure 27 shows the IOSAM cross sections computed on the LJ(12,6) surface at T_i = 4, 9 and 15 Kcal/mole. The line represents the experimental results of Barnes et al

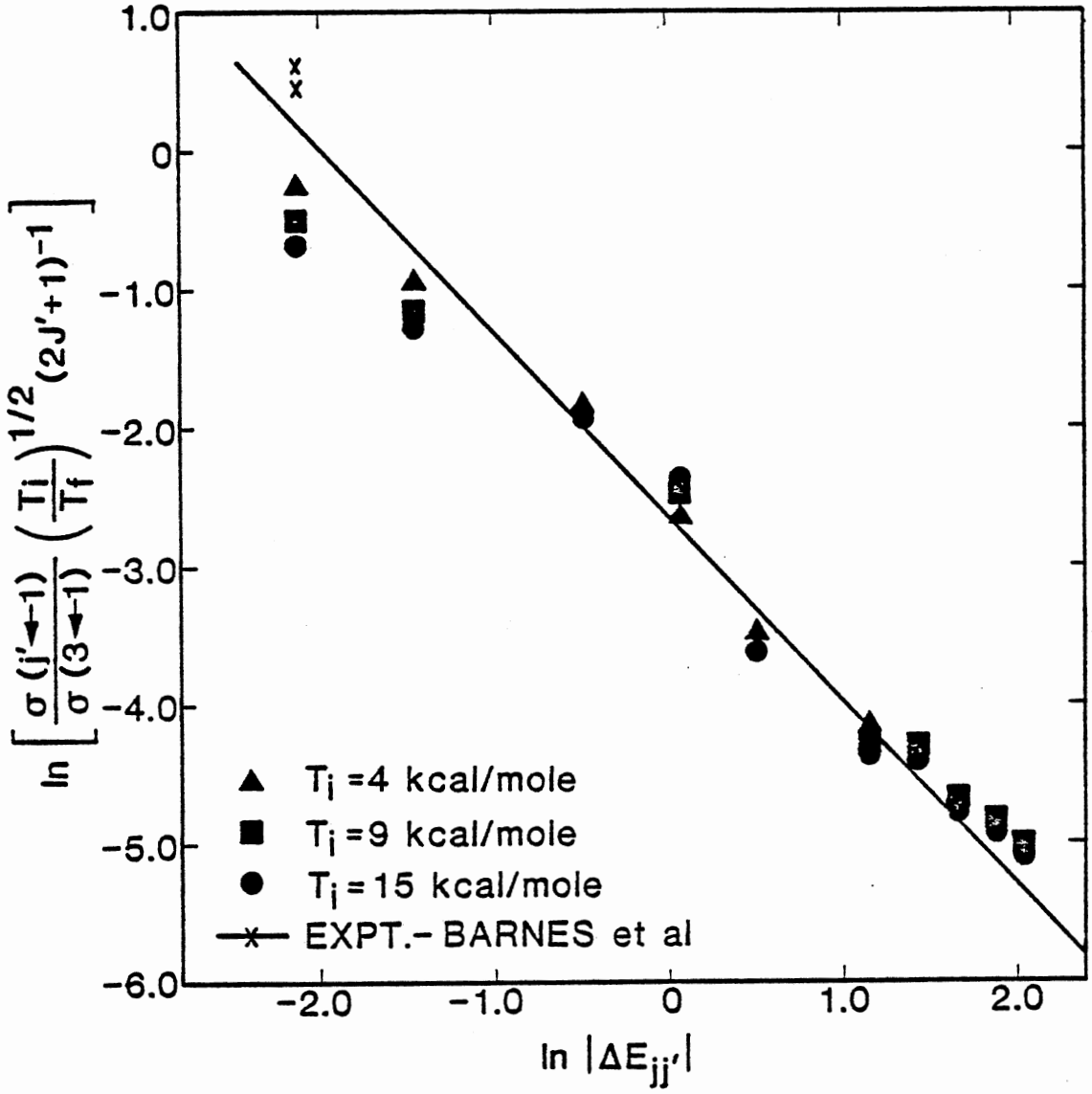

Figure 27. Log-log Plot of $\{\frac{\sigma(j'-1)}{\sigma(3-1)}\left(\frac{T_i}{T_f}\right)^{\frac{1}{2}}(2j'+1)^{-1}\}$ Versus $|\Delta E_{jj'}|$ on the LJ(12,6) Surface. Cross sections have been computed by the IOSAM procedure. (▲) T_i = 4 Kcal/mole. (■) T_i = 9 Kcal/mole. (●) T_i = 15 Kcal/mole.

(67). The Pritchard correlation is obeyed very well at each energy, and the overall agreement between theory and experiment is reasonably good.

The state-to-state cross sections have also been evaluated as a function of the well depth, using the pairwise LJ(12,6) potential. The results for the initial states j = 1, 2 at an initial relative translational energy of 4 Kcal/mole are given in Tables XXXIX and XL. It is seen that an increase in the well-depth, decreases the cross sections for those transitions with $\Delta j = \pm 1$ and increases the cross sections for those transitions with $\Delta j = \pm 2$. The cross sections corresponding to larger Δj transitions are almost unaffected by the change in the well-depth.

The total inelastic cross sections for the initial states j = 0, 1, 2 have been evaluated as a function of the relative translational energy on the LJ(12,6) potential-energy surface. These are given in Table XLI. It is seen that the total inelastic cross sections decrease with increasing energy, and that at each energy, they are almost independent of the j-state. Similar behavior was observed in the (CO_2-He) system (63). The total inelastic cross section includes significant contributions from many state-to-state processes. The summation over all such transitions tends to average out the dependence of σ_{total} on j. Suzukawa, et al (94) have also observed a similar behavior in the quasiclassical trajectory calculations of the CO_2-Kr system. In this classical case, this behavior was explained as being due to the fact that the rotational periods are much larger than the collision times.

Total inelastic cross sections have also been evaluated as a function of the well-depth for T_i = 4 Kcal/mole and the initial states j = 0, 1 and 2. These results are given in Table XLII. The total

TABLE XXXIX

IOSAM RESULTS FOR THE STATE-TO-STATE INTEGRAL CROSS SECTIONS AS A FUNCTION OF THE WELL-DEPTH OF THE POTENTIAL SURFACE[a]

j'	ε = 0.007 eV	ε = 0.01 eV	ε = 0.016 eV
	σ(j'←-1)	σ(j'←-1)	σ(j'←-1)
0	4.3285	3.9120	3.4606
1	-	-	-
2	9.7577	9.1691	8.0869
3	2.8811	3.3920	4.3676
4	2.2763	2.6357	2.3750
5	1.2097	1.0293	1.1201
6	0.7816	0.8948	0.9068
7	0.5010	0.4676	0.4526

(a) Cross sections are in units of $(\text{Å})^2$.

T_i = 4 Kcal/mole

Initial j-state = 1

TABLE XL

IOSAM RESULTS FOR THE STATE-TO-STATE INTEGRAL CROSS SECTIONS AS A FUNCTION OF THE WELL-DEPTH OF THE POTENTIAL SURFACE[a]

j'	ε = 0.007 eV	ε = 0.01 eV	ε = 0.016 eV
	(j' ← 2)	(j' ← 2)	(j' ← 2)
0	0.8096	1.0518	1.3845
1	6.2763	5.8413	5.1519
2	-	-	-
3	8.6282	8.1363	7.2361
4	2.5450	2.9659	3.7423
5	1.9154	2.1758	1.9855
6	0.9920	0.8676	0.9238
7	0.5771	0.6472	0.6538
8	0.1174	0.1111	0.1089

(a) Cross sections are in units of $(\text{Å})^2$.

T_i = 4 Kcal/mole

Initial j-state = 2

TABLE XLI

TOTAL INELASTIC INTEGRAL CROSS SECTION ON THE LJ(12,6) SURFACE[a]

j	Energy (Kcal/mole)		
	4.0	9.0	15.0
0	23.4158	22.4321	21.8584
1	20.7697	20.1352	19.6103
2	21.1868	20.3899	19.7950

(a) Cross sections are in units of $(\mathring{A})^2$.
Initial j-states = 0, 1, and 2

TABLE XLII

TOTAL INELASTIC INTEGRAL CROSS SECTION AS A FUNCTION OF THE WELL-DEPTH OF THE POTENTIAL[a]

j	Well-depth (eV)		
	0.007	0.01	0.016
0	23.2575	23.4931	23.4158
1	21.7360	21.5005	20.7697
2	21.8010	21.7972	21.1868

(a) Cross sections are in units of $(\mathring{A})^2$.
T_i = 4 Kcal/mole
Initial j-states = 0, 1 and 2

inelastic cross sections are seen to be almost independent of the well-depth. Thus, it is unlikely that the evaluation or measurement of total cross sections will enable such topographical details of the surface to be accurately determined.

Figures 28 and 29 show a comparison of cross section ratios computed by the IOSA and IOSAM procedures on the LJ(12,6) surface with the experimental ratios obtained by Barnes, et al (67) at T_i = 4 Kcal/mole. For virtually all transitions, the computed IOSAM cross sections are found to be in better accord with the experimental data than is the case for the IOSA results. This is particularly true for transitions associated with large positive Δj.

Table XLIII gives a similar comparison of IOSA and IOSAM results on the ab initio surface. Although the degree of agreement between theory and experiment is significantly less for the ab initio surface than for the LJ(12,6) formulation, the IOSAM results are still found to be in better agreement with experiment. This enables us to conclude that the improvement in IOSA results achieved by the inclusion of an explicit exit-channel velocity dependence into the scattering cross section is a general feature of the theory that is independent of the detailed topography of the potential-energy surface.

Conclusions

Our study of the rotationally inelastic scattering processes in the HF-Ar system illustrates that the IOSAM method should be the method of choice for the routine analysis of experimental data. Several interesting points have emerged from this study.

A simple LJ(12,6) pairwise potential formulation is capable of

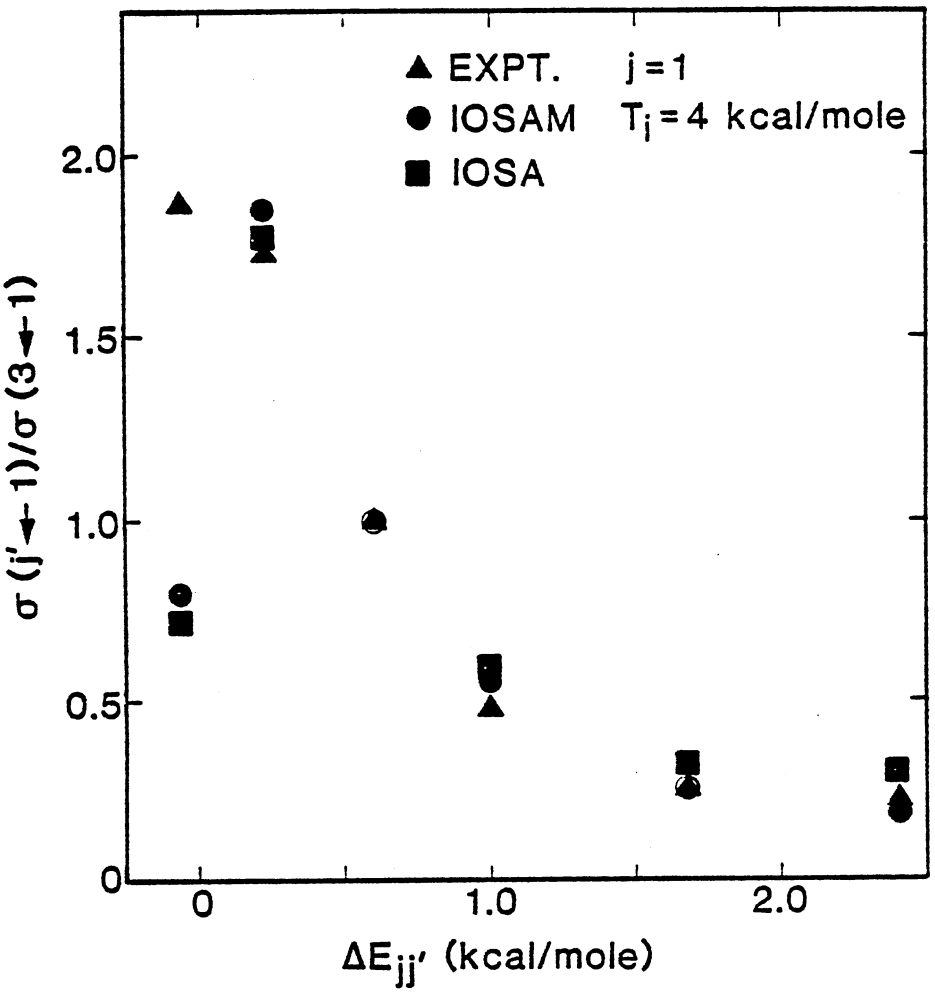

Figure 28. Comparison of IOSAM and IOSA Cross Section Ratios $\{\sigma(j'-1)/\sigma(3-1)\}$ on the LJ(12,6) Surface to the Measured Ratios at T_i = 4 Kcal/mole.

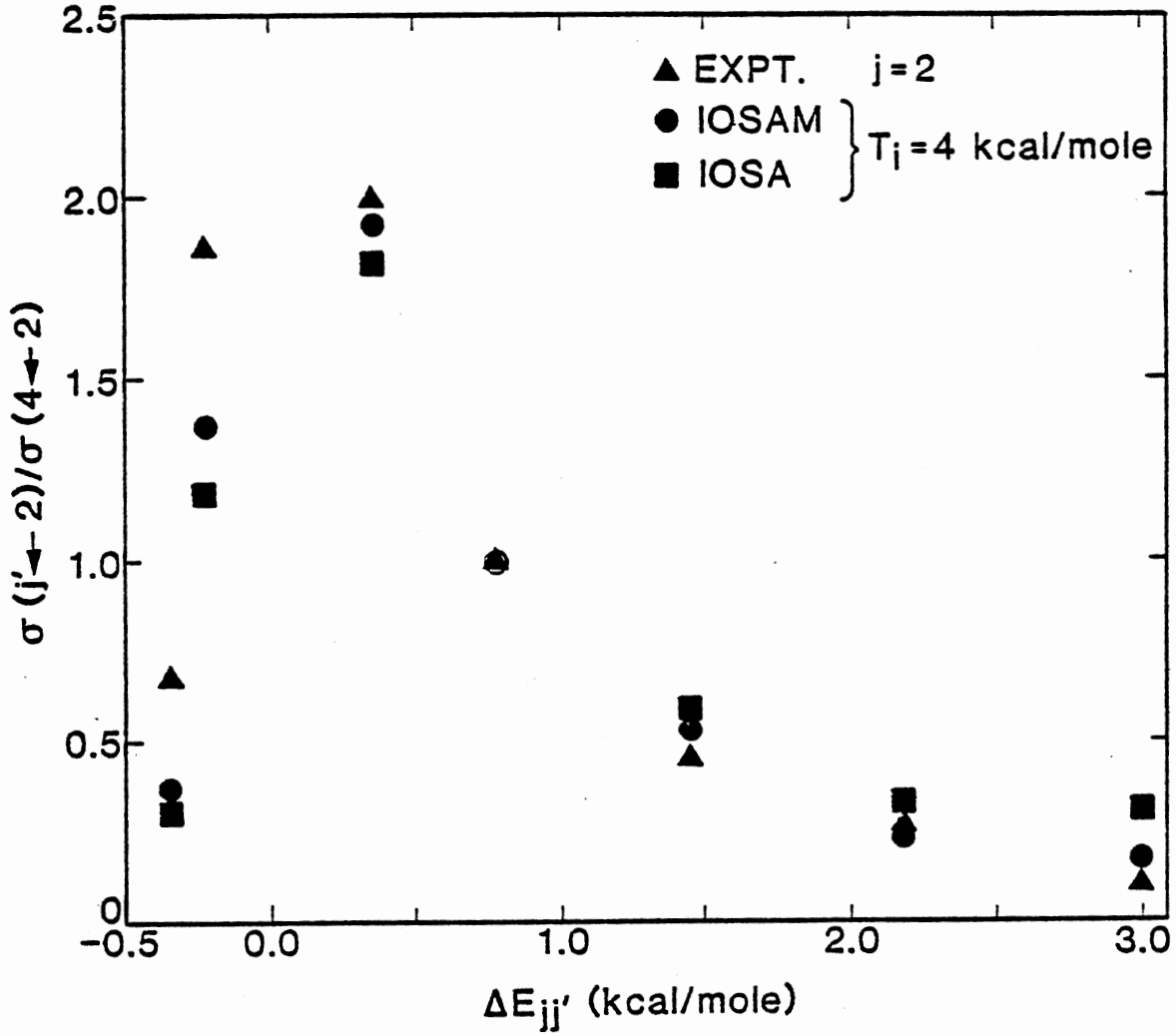

Figure 29. Comparison of IOSAM and IOSA Cross Section Ratios $\{\sigma(j' - 2)/\sigma(4 - 2)\}$ on the LJ(12,6) Surface to the Measured Ratios at T_i = 4 Kcal/mole.

TABLE XLIII

COMPARISON OF IOSAM AND IOSA CROSS SECTION RATIOS $\{\sigma(J' \leftarrow 2)/\sigma(4 \leftarrow 2)\}$ ON THE SAI SURFACE TO THE MEASURED RATIOS

j'	IOSA	IOSAM	Experiment Reference 67
0	0.135	0.1588	0.680
1	1.542	1.786	1.866
3	2.271	2.437	2.000
4	1.000	1.000	1.000
5	1.185	1.067	0.453
6	0.985	0.753	0.267
7	0.849	0.479	0.106

yielding results in reasonable agreement with experiment. The cross sections were found to scale as an inverse power of the energy transferred from relative translation to the HF rotation, $\Delta E_{jj'}$, in accordance with the expression proposed by Brunner, Driver, Smith and Pritchard (93). Surprisingly, results obtained on the SAI surface are in relatively poor agreement with experiment.

The total integral cross sections for the initial j-states 0, 1 and 2 were observed to decrease with increasing relative translational energy. At a given energy, the variation of the total inelastic cross section with the initial j-state is very small. The state-to-state integral cross sections and the total inelastic cross sections have been calculated as a function of the well-depth of the potential at T_i = 4 Kcal/mole. The state-to-state integral cross sections change appreciably with changing well-depth, whereas, the total inelastic cross sections are almost invariant with well-depth. This enables us to conclude that it is unlikely that the evaluation of total inelastic cross sections will enable such topographical details of the surface to be accurately determined.

The IOSA and IOSAM results have been compared with the experimentally measured cross section ratios. It was observed that the IOSAM results are in significantly better agreement with experiment than the IOSA results, for both the LJ(12,6) and the SAI surfaces. This indicates that the modification of the IOSA method by including an explicit exit-channel velocity dependence into the scattering cross section yields significant improvement in the calculated results, irrespective of the topography of the potential-energy surface employed.

BIBLIOGRAPHY

(1) D. R. Yarkony, S. V. O'Neil and H. F. Schaefer, J. Chem. Phys. 60, 855 (1974).

(2) N. Sathyamurthy and L. M. Raff, J. Chem. Phys. 66, 2191 (1977).

(3) C. Stroud and L. M. Raff, J. Chem. Phys. 72, 5479 (1980).

(4) N. Sathyamurthy and L. M. Raff, J. Chem. Phys. 63, 464 (1975).

(5) P. M. Agrawal and L. M. Raff, J. Chem. Phys., to be published.

(6) E. A. Hylleraas, Z. Physik. 48, 469 (1928).

(7) Z. Gershgorn and I. Shavitt, Int. J. Quant. Chem. 2, 751 (1968).

(8) R. N. Porter and L. M. Raff, J. Chem. Phys. 50, 5216 (1969).

(9) L. M. Raff, J. Chem. Phys. 60, 2220 (1974).

(10) H. Eyring and M. Polanyi, Z. Physik. Chem. (leipzig), B12, 279 (1931).

(11) J. O. Hirschfelder, H. Eyring and B. Topley, J. Chem. Phys. 4, 170 (1936).

(12) (a) F. T. Wall, L. A. Hiller and J. Mazur, J. Chem. Phys. 29, 255 (1958); (b) F. T. Wall, L. A. Hiller and J. Mazur, J. Chem. Phys. 35, 1284 (1961).

(13) (a) R. N. Porter, Ann. Rev. of Phys. Chem. 25, 317 (1964); (b) M. Karplus and L. M. Raff, J. Chem. Phys. 41, 1267 (1964); (c) N. C. Blais and D. L. Bunker, J. Chem. Phys. 41, 2377 (1964).

(14) (a) D. L. Bunker, W. L. Hase, J. Chem. Phys. 59, 4621 (1973); (b) H. H. Harris, D. L. Bunker, Chem Phys. Lett. 11, 433 (1971).

(15) (a) R. F. Heidner and I. V. V. Kasper, Chem. Phys. Lett. 15, 179 (1972); (b) L. B. Sims, L. R. Dosser and P. S. Wilson, Chem. Phys. Lett. 32, 150 (1975).

(16) D. J. Douglas, J. C. Polanyl and J. J. Sloan, J. Chem. Phys. 59, 6679 (1973).

(17) (a) T. J. Odirone, P. R. Brooks and J. V. V. Kasper, J. Chem. Phys. 55, 1980 (1971); (b) S. R. Levine, R. G. Mac Donald and C. B. Moore, J. Chem. Phys. 63, 4735 (1975); (c) Z. Karny, B. Katz and A. Szcke, Chem. Phys. Lett. 35, 100 (1978); (d) R. G. Mac Donald and C. B. Moore, J. Chem. Phys. 68, 513 (1978).

(18) (a) N. N. Hijazi and K. J. Laidler, J. Chem. Phys. 58, 349 (1973); (b) J. C. Polanyi and W. H. Wong, J. Chem. Phys. 51, 1439 (1969); (c) B. A. Hodgson and J. C. Polanyi, J. Chem. Phys. 55, 4745 (1971).

(19) S. Chapman and D. L. Bunker, J. Chem. Phys. 62, 2890 (1975).

(20) J. C. Polanyi and N. Sathyamurthy, Chem. Phys. 33, 287 (1978).

(21) J. W. Duff and D. G. Truhlar, J. Chem. Phys. 62, 2477 (1975).

(22) N. Sathyamurthy, J. W. Duff, C. Stroud and L. M. Raff, J. Chem. Phys. 67, 3563 (1977).

(23) C. Stephenson and S. M. Freund, J. Chem. Phys. 65, 4303 (1976).

(24) (a) R. G. Manning, W. Braun and M. J. Kurylo, J. Chem. Phys. 65, 2609 (1976); (b) M. Kneba, H. G. Wagner, and J. Wolfrum, Ber. Max-Planck-Inst. Stromungsforschung 23, 1 (1976); (c) M. Kneba and J. Wolfrum, Ann. Rev. Phys. Chem. 31, 47 (1980).

(25) C. Riley, R. Shatas and V. Arkle, Abstract #132, Physical Division, 175th ACS National Meeting, Anaheim, California, March 1978.

(26) C. T. Ting and R. E. Weston, Jr., J. Phys. Chem. 77, 2257 (1973).

(27) C. W. Tsao and J. W. Root, unpublished work.

(28) D. L. Bunker and D. Pattengill, J. Chem. Phys. 53, 3041 (1970).

(29) T. Valencich and D. L. Bunker, Chem. Phys. Lett. 15, 521 (1972).

(30) T. Valencich and D. L. Bunker, J. Chem. Phys. 61, 21 (1974).

(31) L. M. Raff, unpublished results.

(32) (a) F. M. Lussier, C. Reiser, C. Jensen and J. I. Steinfeld, paper #206, Physical Division, 175th ACS National Meeting, Anaheim, California, March, 1978; (b) F. M. Lussier, J. I. Steinfeld and T. F. Deutsch, Chem. Phys. Lett. 58(2), 277 (1978).

(33) R. J. Cross, Jr., contributed paper, Conference on Dynamics of Molecular Collisions, Asilomar, California, June, 1978.

(34) M. A. A. Clyne, B. A. Thrush and R. P. Wayne, Trans. Faraday Soc. 60, 359 (1964).

(35) P. N. Clough and B. A. Thrush, Trans. Faraday Soc. 63, 915 (1967).

(36) P. N. Clough and B. A. Thrush, Trans. Faraday Soc. 65, 23 (1969).

(37) M. F. Golde and F. Kaufmann, Chem. Phys. Lett. 29, 480 (1974).

(38) M. Gauthier and D. R. Snelling, Chem. Phys. Lett. 20, 178 (1973).

(39) R. J. Gordon and M. C. Lin, Chem. Phys. Lett. 22, 262 (1973).

(40) R. J. Gordon and M. C. Lin, J. Chem. Phys. 64, 1058 (1976).

(41) J. Moy, E. Bar-Ziv and R. J. Gordon, J. Chem. Phys. 66, 5439 (1977).

(42) E. Bar-Ziv, J. Moy and R. J. Gordon, J. Chem. Phys. 68, 1013 (1978).

(43) M. J. Kurylo, W. Braun, A. Kaldor, S. M. Freund and R. P. Wayne, J. Photochem. 3, 71 (1974).

(44) W. Braun, M. J. Kurylo, A. Kaldor and R. P. Wayne, J. Chem. Phys. 61, 461 (1974).

(45) M. J. Kurylo, W. Braun, C. N. Xuan and A. Kaldor, J. Chem. Phys. 62, 2065 (1975).

(46) S. M. Freund and J. C. Stephenson, Chem. Phys. Lett. 41, 157 (1976).

(47) K. K. Hui and T. A. Cool, J. Chem. Phys. 68, 1022 (1978).

(48) K. K. Hui, D. T. Rosen and T. A. Cool, Chem. Phys. Lett. 32, 141 (1975).

(49) D. Vanden Ende and S. Stolte, Chem. Phys. 45, 55 (1980).

(50) D. Vanden Ende and S. Stolte, J. Chem. Phys., to be published.

(51) (a) A. Redpath and M. Menzinger, Can. J. Chem. 49, 3063 (1971); (b) A. Redpath and M. Menzinger, J. Chem. Phys. 62, 1987 (1975).

(52) A. Redpath, M. Menzinger and T. Carrington, Chem. Phys. 27, 409 (1978).

(53) J. J. Valentini, J. B. Cross and G. H. Kwei, unpublished results.

(54) C. Kahler, M. Kowalczyk and Y. T. Lee, unpublished results.

(55) P. Brooks and S. Anderson, J. Chem. Phys., to be published.

(56) (a) F. Engelke, R. K. Sander and R. N. Zare, J. Chem. Phys. 65, 1146 (1976); (b) I. R. Slagle, J. R. Gilbert and D. Gutman, J. Chem. Phys. 61, 704 (1974).

(57) R. D. Levine and R. B. Bernstein, Molecular Reaction Dynamics (Oxford University Press, London, 1974).

(58) (a) M. Karplus, R. N. Porter and R. D. Sharma, J. Chem. Phys. 43, 3259 (1965); (b) R. N. Porter and L. M. Raff, "Classical Trajectory Studies of Molecular Collisions", Dynamics of Molecular Collisions, Part B; University of California, Berkeley (1976), Chapter 1.

(59) T. L. Cottrell and J. C. Mc Coubrey, "Molecular Energy Transfer in Gases", Butterworth and Co. Ltd., London, 1961.

(60) A. R. Blythe, A. E. Grosser and R. B. Bernstein, J. Chem. Phys. 41, 1917 (1964).

(61) A. M. Arthurs and A. Dalgarno, Proc. R. Soc. (London), Ser. A256, 540 (1960).

(62) G. A. Parker and R. T. Pack, J. Chem. Phys. 68, 1585 (1978).

(63) P. M. Agrawal and L. M. Raff, J. Chem. Phys., to be published.

(64) C. L. Stroud and L. M. Raff, J. Chem. Phys. 72, 5479 (1980).

(65) H. P. Butz, R. Feltgen, H. Pauly and H. Vehmeyer, Z. Phys. 70, 247 (1971).

(66) P. M. Agrawal and L. M. Raff, J. Chem. Phys. 74(6), 3292 (1981).

(67) J. A. Barnes, M. Keil, R. E. Kutina and J. C. Polanyi, J. Chem. Phys. 72(6), 6306 (1980).

(68) L. M. Raff, J. Chem. Phys. 60, 2220 (1974).

(69) L. M. Raff, L. Stivers, R. N. Porter, D. L. Thompson and L. B. Sims, J. Chem. Phys. 52, 3449 (1970).

(70) C. F. Jackel and E. R. Davidson, J. Chem. Phys. 65, 2941 (1976).

(71) Paul A. Debosh, Ph.D. Thesis, Carnegie-Mellon University, 1969.

(72) H. A. Pohl, R. Rein and K. Appel, J. Chem. Phys. 41, 3385 (1964).

(73) H. A. Pohl and L. M. Raff, Intern. J. Quantum Chem. 1, 577 (1967).

(74) R. S. Mulliken, C. A. Reike, D. Orloff and H. Orloff, J. Chem. Phys. 17, 1248 (1949).

(75) W. Kolos and L. Woiniewicz, J. Chem. Phys. 43, 2429 (1965).

(76) (a) J. N. Murrel and S. Farantos, Mol. Phys. 34, 1185 (1977); (b) J. N. Murrel, K. S. Sorbie and A. J. C. Varandas, Mol. Phys. 32, 1359 (1976); (c) K. S. Sorbie and J. N. Murrel, Mol. Phys. 29, 1387 (1975).

(77) R. J. Whitehead and N. C. Handy, J. Mol. Spec. 55, 356 (1975).

(78) J. L. Hardwick and J. C. D. Brand, Can. J. Phys. 54, 80 (1976).

(79) (a) N. Sathyamurthy and L. M. Raff, J. Chem. Phys. 63, 464 (1975); (b) N. Sathyamurthy and L. M. Raff, "Spline Package, Program 322", Quantum Chemistry Program Exchange, Indiana University (1976).

(80) S. Chapman, J. Chem. Phys. 74(2), 1001 (1981).

(81) E. B. Wilson, Jr., J. C. Decius and P. Cross, "Molecular Vibrations", Dover Publications Inc., New York, 1980, p. 273.

(82) A. Barbe, C. Secroun and P. Jouve, J. Mol. Spec. 49, 171 (1974).

(83) G. Herzberg, "Spectra of Diatomic Molecules", (Van Nostrand, New York, 1950), p. 558.

(84) D. I. Rosen and T. A. Cool, J. Chem. Phys. 62, 466 (1975).

(85) W. J. Hehre, W. A. Lathan, R. Ditchfield, M. D. Newton and J. A. Pople, Gaussian 70, Program 236, Quantum Chemistry Program Exchange, Indiana University (1974).

(86) R. A. Svehla, NASA Tech. Rep. TRR-132 (1962).

(87) S. I. Drozdov, Zh. Exp. Teor. Fiz. 28, 734 (1955) (English Translation: Sov. Phys. JETP 1, 591 (1955)).

(88) D. M. Chase, Phys. Rev. 104, 838 (1956).

(89) R. D. Levine, Chem. Phys. Lett. 4, 211 (1969); J. Chem. Phys. 54, 997 (1971).

(90) R. T. Pack, J. Chem. Phys. 60, 633 (1974).

(91) T. P. Tsien and R. T. Pack, Chem. Phys. Lett. 6, 54 (1970).

(92) Z. Kopal, Numerical Analysis, Wiley, New York, 1961, second edition, p. 381.

(93) (a) T. A. Brunner, R. D. Driver, N. Smith and D. E. Pritchard, Phys. Rev. Lett. 41, 856 (1978); (b) D. E. Pritchard, N. Smith, R. D. Driver and T. A. Brunner, J. Chem. Phys. 70, 2115 (1979); (c) T. A. Brunner, R. D. Driver, N. Smith and

D. E. Pritchard, J. Chem. Phys. 70, 4155 (1979); (d) M. Waigner, I. Al-Agil, T. A. Brunner, A. W. Karp, N. Smith and D. E. Pritchard, J. Chem. Phys. 71, 1977 (1979).

(94) H. H. Suzukawa, Jr., M. Wolfsberg and D. L. Thompson, J. Chem. Phys. 68(2), 455 (1978).

(95) E. W. Thulstrup and Y. Ohrn, J. Chem. Phys. 57, 3716 (1972).

(96) H. O. Pritchard and H. A. Skinner, Chem. Rev. 55, 745 (1955).

(97) A. Ralston and P. Rabinowitz, "A First Course in Numerical Analysis", McGraw-Hill Book Company, 1978.

APPENDIX

DESCRIPTION OF BASIS FUNCTIONS EMPLOYED IN THE LCAO-MO-SCF CALCULATIONS FOR THE HF-Ar SYSTEM

An extended 6-31G basis set was employed in the calculations. The valence shells of the atoms were described by the sum of two terms, one being a three gaussian expansion and the other a single gaussian expansion. The inner shells were described by a six gaussian expansion.

For hydrogen, the functions may be written as

$$\psi'_{1s}(\vec{r}) = \sum_{k=1}^{3} c'_{1s,k} f_s (\alpha'_k, \vec{r}) \qquad \text{(A-1)}$$

$$\psi''_{1s}(\vec{r}) = c_{1s} f_s (\alpha''_k, \vec{r}) \qquad \text{(A-2)}$$

For fluorine, the functions may be written as

$$\psi_{1s}(\vec{r}) = \sum_{k=1}^{6} c_{1s,k} f_s (\alpha_{1k}, \vec{r}) \qquad \text{(A-3)}$$

$$\psi'_{2s}(\vec{r}) = \sum_{k=1}^{3} c'_{2s,k} f_s (\alpha'_{2k}, \vec{r}) \qquad \text{(A-4)}$$

$$\psi'_{2p_x}(\vec{r}) = \sum_{k=1}^{3} c'_{2p,k}\, f_{p_x}(\alpha'_{2k}, \vec{r}) \qquad \text{(A-5)}$$

$$\psi''_{2s}(\vec{r}) = c_{2s}\, f_s\,(\alpha''_{2k}, \vec{r}) \qquad \text{(A-6)}$$

$$\psi''_{2p_x}(\vec{r}) = c_{2p}\, f_{p_x}\,(\alpha''_{2k}, \vec{r}) \qquad \text{(A-7)}$$

and similarly for the p_y and p_z orbitals.

For Argon, the functions may be written as

$$\psi_{1s}(\vec{r}) = \sum_{k=1}^{6} c_{1s,k}\, f_s\,(\alpha_{1k}, \vec{r}) \qquad \text{(A-8)}$$

$$\psi_{2s}(\vec{r}) = \sum_{k=1}^{6} c_{2s,k}\, f_s\,(\alpha_{2k}, \vec{r}) \qquad \text{(A-9)}$$

$$\psi_{2p_x}(\vec{r}) = \sum_{k=1}^{6} c_{2p,k}\, f_{p_x}(\alpha_{2k}, \vec{r}) \qquad \text{(A-10)}$$

Similarly for the 3s and 3p orbitals. The f's are Gaussian functions defined as

$$f_s(\alpha, \vec{r}) = (2\alpha/\pi)^{3/4} \exp(-\alpha r^2) \qquad \text{(A-11)}$$

$$f_{p_x}(\alpha, \vec{r}) = (128\alpha^5/\pi^3)^{1/4} \times \exp(-\alpha r^2) \qquad \text{(A-12)}$$

The values of c's and α's are given in Table XLV and are due to Pople and coworkers (85).

TABLE XLIV

BASIS SET COMPONENTS

Atom	Orbital Type	Exponent (α)	s Coef. (c_s)	p Coef. (c_p)
Hydrogen	1s	0.187311E02	0.334946E-01	0.0
		0.282539E01	0.234727E+00	0.0
		0.640121E00	0.813757E+00	0.0
	1s'	0.161278E00	0.100000E+01	0.0
Fluorine	1s	0.700171E04	0.181962E-02	0.0
		0.105137E04	0.139161E-01	0.0
		0.239286E03	0.684053E-01	0.0
		0.673974E02	0.233186E+00	0.0
		0.215799E02	0.471267E+00	0.0
		0.740310E01	0.356619E+00	0.0
	2sp	0.208479E02	-0.108507E+00	0.716287E-01
		0.480831E01	-0.146452E+00	0.345912E+00
		0.134407E01	0.112869E+01	0.722470E00
	2sp'	0.358151E00	0.100000E+01	0.100000E01
Argon	1s	0.699467E04	0.916360E-02	0.0
		0.128246E04	0.493615E-01	0.0
		0.358787E03	0.168538E+01	0.0
		0.123253E03	0.370563E+00	0.0
		0.478628E02	0.416492E+00	0.0
		0.197125E02	0.130334E+00	0.0

TABLE XLIV (Continued)

2sp	0.486299E03	-0.132528E-01	0.375970E-02
	0.926886E02	-0.469917E-01	0.376794E-01
	0.288076E02	-0.337854E-01	0.173897E+00
	0.110833E02	0.250242E+00	0.418036E+00
	0.481349E01	0.595117E+00	0.425860E+00
	0.220637E01	0.240706E+00	0.101708E+00
3sp	0.167219E02	-0.794312E-02	-0.713936E-02
	0.447828E01	-0.710026E-01	-0.182928E-01
	0.167940E01	-0.178503E+00	0.762162E-01
	0.751731E00	0.151064E+00	0.414510E+00
	0.371993E00	0.735491E+00	0.488962E+00
	0.191713E00	0.276059E+00	0.105882E+00

VITA[2]

Rajalakshmi Viswanathan

Candidate for the Degree of

Doctor of Philosophy

Thesis: I. INVESTIGATION OF THE EFFECTS OF SURFACE TOPOLOGY UPON THE REACTION DYNAMICS OF POLYATOMIC SYSTEMS: THE $O_3 + NO \rightarrow O_2 + NO_2^{\ddagger}$ REACTION

II. QUANTUM MECHANICAL STUDY OF ROTATIONALLY INELASTIC SCATTERING IN THE HF-Ar SYSTEM

Major Field: Chemistry

Biographical:

Personal Data: Born in India, on December 13, 1956.

Education: Graduated from I.C.F. High School, India in June 1972; received the Bachelor of Science degree in Chemistry from the University of Madras, India, in June 1976; received the Master of Science degree in chemistry from the University of Madras, India in June 1978; recipient of the gold medals awarded by the University of Madras, India for outstanding performance in both the B.S. and M.S. University examinations; joined Oklahoma State University in January 1979; completed requirements for the Doctor of Philosophy degree at Oklahoma State University in December, 1981.

Professional Experience: Graduate Teaching Assistant, Oklahoma State University, Spring 1979; National Science Foundation Research Assistant, Oklahoma State University, 1979-1981.

Membership in Honorary and Professional Societies: Member of Phi Lambda Upsilon, Honorary Chemical Society.